Composite carbon membranes for the desalination of water

By

Jessica Chamier

Thesis presented in partial fulfilment of the requirements for the degree of

Master of Science (Chemistry)

at the

University of Stellenbosch

Promoter

Prof. AM Crouch

Stellenbosch

March 2007

I, the undersigned, hereby declare that the work contained in this thesis is my own original work and that I have not previously in its entirety, or in part, submitted it at any university for a degree.

Signature: …….. Date: ……

Abstract

Electrodialysis is a method of water desalination which involves the separation of TDS through an ion-exchange membrane under a potential gradient. In this study it was attempted to reverse engineer the composite carbon ion-exchange membrane used in a prototype plant and electrochemically evaluate a prototype desalination cell. The influence of applied potential on the capacitance of the various electrode surfaces and possible electrode reactions was investigated. A model was also suggested to describe the conductivity through the membrane.

The composition of composite carbon membranes were determined by compositional analysis using various analytical tools. Elemental analysis, done with PIXE and EDS, showed that the membranes contained chloride, fluoride, oxygen, carbon, and possibly hydrogen. With LC-MS and IR it was established that the membranes consisted of two polymers with no carbonyl or aromatic functional groups. After further thermal analysis the following possible compounds remained: hexafluoropropylene tetrafluoroethylene copolymer, polychlorotrifluoroethylene (PCTFE), polyoxyethylene oxide (PEO) and polyethylene glycol (PEG). This assessment is in good agreement with the contents of US patent 4,153, 661, which describes the composite membrane.

Cyclic voltammetry (CV) and linear sweep voltammetry (LSV) were carried out using various carbon electrodes to study the possible reactions in electrolyte solutions and the formation of the diffusion double layer on the electrode surface. The size of the diffusion double layer, or rather the capacitance, was found to be related to the surface oxidation of the various electrodes. The surface roughness of the various electrodes was confirmed with SEM and AFM. Electrode reactions, which influence the size of the double layer, were the oxidation of nitrite, the oxidation of sulphate to peroxydisulphate, the oxidation of chloride and the reduction of chlorine gas.

A custom cell was built to evaluate the conductivity of various anions through the composite carbon membrane. An adsorption model based on the Michealis-Menten model was used to describe the first 30 min of the conductivity experiments. After sufficient ions have been transported across the membrane a potential gradient occurs and the Michealis-Menten Model no longer applies. It is suggested that the ion-exchange membrane is basic, and has a stronger affinity for sulphate than for chloride and nitrate.

EIS were carried out at high frequencies to determine the electrical properties of the membrane-electrode –electrolyte cell design. The high surface roughness of the membrane caused its almost pure capacitor behaviour. The behaviour of the electrode was described by a Warburg impedance for non-homogeneous surfaces. Impedance studies confirmed the higher selectivity for sulphate transport across the membrane and the relative sizes of the diffusion double layer.

Opsomming

Elektrodialiese is ‘n metode van water desalineering wat die skeiding van TOS met ‘n ion uitruilings membrane, onder die invloed van ‘n potentiale gradient, behels. In hierdie studie is daar gepoog om die ion uitruiling membraan in ‘n prototiepe eenheid te tru-ingineer en om ‘n prototype eenheid elektrochemies te evalueer. Die invloed van ‘n toegepaste potential op die kapasitansie van die elektrode oppervlakte en moontlike elektrode reaksies is ondersoek. ‘n Model vir die konduktiwiteit deur die membraan is ook voorgestel.

Die komposisie van ‘n koolstof saamgestelde membrane is bepaal deur komposisionele analiese met verskeie analitiese tegnieke. Die bestandele van die membraan is bepaal deur ‘n proses van eliminasie. Elementêre analiese met PIXE en EDS het bepaal dat die hoof elemente chloried, fluoried, koolstof, suurstof en waterstof is. Met LC-MS en IR is bepaal dat die membraan uit twee polimere bestaan en dat daar geen karboniel of aromatiese funksionele groepe teenwoordig is nie. Na Termiese analiese is die kortlys vir bestandele in die membrane as volg:
hexafluoropropylene tetrafluoroethylene copolymer, Polychlorotrifluoroethylene (PCTFE), Polyoxyethylene oksied (PEO) and Polyethylene glycol (PEG).
Hierdie gevolgtrekkings is in goeie ooreenstemming met patent 4,153,661 waarvan die membrane vervaardig is. Een van die doelwitte van die studie was om die samestelling van die membraan te bepaal met die oog op tru-engineering.

CV en LSV is uitgevoer met ‘n verskeidenheid van koolstof elektrodes om die moontlike reaksies in die elektroliet oplossings te bestudeer sowel as die formasie van die diffusie dubbel laag op die elektrode oppervlak. Die grote van die diffusie dubbel laag is gevind om direk verband te hou met die oppervlak oksidasie van die elektrodes en die oppervlak grofheid. The oppervlak grofheid is bevestig met SEM en AFM.
Elektrode reaksies wat die grote van die diffusie laag beinvloed is die oksidasie van nitriet, sulfaat en chloried en die reduksie van chloor gas.

‘n Sel is gebou om die leiding van die verskeie anione deur die membraan te bestudeer. ‘n Adsorpsie, model gebaseer op die Michealis Menten model, is gebruik om die eerste 30 minute van die leidings eksperiment te beskryf. Nadat genoegsame ione deur die membraan vervoer is, begin

‘n potentiële gradient en die Michealis Menten Model is nie meer van toepassing nie. Dit is aangevoer dat die membraan alkalies is en ‘n hoër affiniteit vir SO_4^- toon.

EIS is uitgevoer onder hoë frekwensies om die elektriese eienskappe van die membraan – elektrode-elektroliet sel-opstel te bepaal. Die hoë oppervlak grofheid van die membraan het sy kapasitor gedrag bepaal en die elektrode is met ‘n Warburg impedansie vir nie-homogene opervlaktes beskryf. Impedansie studies het die hoër selektiwiteit vir sulfaat deur die membraan bevestig sowel as die relatiewe grotes van die gevormde diffusie lae.

Acknowledgements

- I wish to express my sincere appreciation to my promoter, Prof. AM Crouch, for his assistance, encouragement and financial support throughout the project.
- I would like to acknowledge the financial assistance of the CSIR, Pretoria.
- The assistance of Dr PGL Baker of the University of the Western Cape with the impedance studies is acknowledged.

Abbreviations

AFM	- Atomic force microscopy
CDI	- Capacitive deionization
CIER	- Chlorine electrode reaction
CPE	- Constant phase elements
CSIR	- Council for scientific and industrial research
CV	- Cyclic voltammetry
DBL	- Diffusion boundary layer
DDE	- Diamond doped electrode
DSC	- Differential scanning calorimeter
ED	- Electrodialysis
EDR	- Electrodialysis reversal
EDX	- Energy dispersive X-ray analysis
EIS	- Electrochemical impedance studies
EPPGE	- Edge plane pyrolytic graphite electrode
FTIR	- Fourier transform infrared
GC	- Glassy carbon
GCE	- Glassy carbon electrode
HPLC	- High performance liquid chromatography
IEM	- Ion exchange membrane
LSV	- Linear sweep voltammetry
LC-MS	- Liquid Chromatography – mass spectroscopy
NF	- Nanofiltration
OHP	- Helmholtz plane
ORR	- Oxygen reduction reaction
PEP	- Hexafluoropropylene tetrafluoroethylene copolymer
PIXE	- Particle induced X-ray emission
PCTFE	- Polychlorotrifluoroethylene
PTFE	- Polytetrafluoroethylene
RO	- Reverse Osmosis
SCE	- Saturated calomel electrode
SEM	- Scanning electron microscopy
STM	- Scanning tunnelling microscopy

Tc	- Crystallization temperature
TDS	- Total dissolved solids
Tg	- Glass transition temperature
TGA	- Thermogravimetric analysis
Tm	- Melting temperature

List of contents

List of figures

List of Tables

Chapter 1

Introduction and objectives

1.1 The need for desalination and membrane processes

Thomas Jefferson published the first technical report describing the process of desalination in 1791 and since then the process has been present throughout history. The historical significance of desalination is not surprising since 97 percent of the water on earth is in the oceans. Desalination is the process of removing dissolved solids from brine or seawater. Brine is water saturated with or containing large amounts of a salt, especially sodium chloride. Desalination has been brought to the forefront in the last half of the 20th century because fresh water has become a precious commodity in many parts of the world. A number of reasons can be given to explain the recent shortages of water, including growth of the population, wasteful use of water, pollution of available water resources, and climatic changes related to global warming.

The key element for all societies is a sufficient supply of fresh water. It is a fundamental requirement for most aspects of life. Fresh water is needed in agriculture, as drinking water, and as process water in various industries [1]. Although desalination has been available for the past forty years, it is still far too expensive to make it a viable solution for developing countries. North Africa, for example, is facing serious water supply shortages due to limited water resources and rapidly increasing water demands [2]. Until recently, the application of seawater desalination on a large scale has been primarily limited to the arid regions of the world that have a cheap supply of energy, such as in the Middle East.

There are three basic categories of water purification technologies that are used for desalination; distillation processes (thermal technologies), membrane technologies and chemical approaches.

The two leading desalination technologies are thermal and membrane. A thermal process involves the heating of saline water to produce water vapour that is, in turn, condensed to form fresh water. Thermal desalination is currently the most popular method to desalinate seawater, but in no way cost effective to developing countries. Energy, capital and operating costs are key issues of water desalination [4].

Membrane separation processes have numerous industrial applications and offer the following advantages:

- appreciable energy savings
- They are environmentally benign
- clean technology with operational ease
- high quality products
- greater flexibility in the design of systems.

Membrane processes rely on permeable membranes to separate salts from water. In general, membrane treatment processes use either pressure-driven or electrical-driven technologies. Pressure-driven technologies include reverse osmosis (RO, which is now the most common method of desalination), nanofitration (NF), ultrafiltration (UF) and microfiltration (MF) [5].

Reverse Osmosis is a physical process that uses the osmosis phenomenon, i.e. the osmotic pressure difference between the saltwater solution and the pure water to remove salts from water. In this process an osmotic pressure greater than the osmotic pressure of the saline solution is applied to saltwater (feed water) to reverse the osmotic flow, which results in pure water (freshwater) from the feed water passing through the synthetic membrane pores, hereby separating the fresh water from the saline solution. The concentrated salt solution is retained for disposal. RO has several major drawbacks, these are associated with fouling and scaling problems, and RO has quite high energy demands [3]. A NF membrane operates on a similar principle to reverse osmosis, but NF requires lower pressures because of larger membrane pore size.

Brine contains between 1-2 ppt dissolved solids while seawater has 35 ppt dissolved solids with chloride (55%), sodium (31%), sulphate (8%), magnesium (4%), calcium (1%) and potassium (1%) as the predominant ions.

The overall aim of this study is to investigate the possibility of using composite carbon membranes in the desalination of brine and seawater via electrodialysis.

Electrodialysis is an electro-membrane process in which the ions are transported through the membrane from one solution to another under the influence of an electrical potential. An array of ion-exchange membranes is positioned between a pair of electrodes. They are arranged as alternating anion and cation exchange pairs. Ions become depleted in one compartment and concentrated in the other.

1.2 Ion-exchange membranes

There are various types of ion-exchange membranes, mostly with a homogeneous structure, namely an inert polymer and the polymer which bears the ion-exchanging groups. These membranes are mainly prepared from an active polymer, which is often transformed into the final polymer after the membrane forming step. Thus, inert and active polymers are combined to form the precursor membrane [6].

Electrodialysis (ED) employs cation- and anion-exchange membranes. The cation-selective membrane permits only the cations and anion-selective membranes only the anions to exchange. The most commonly used polymeric membranes used are those based on copolymers of styrene and divinylbenzene with fixed ionic groups, usually SO_3^- for cationic permeable membranes and NR_3^+ for anion permeable membranes. Alternative membranes are based on polymers of tetrafluoroethylene (PTFE). The perflourinated hydrocarbons in these polymers have quite different properties from the ionic groups, leading to hydrophilic and hydrophobic regions in the membrane. Whether the membrane is based on the polystyrene backbone or the perfluoronated hydrocarbon backbone, the membranes all have specific properties such as high selectivity for certain classes of cations and anions, higher rates of transport for these ions across the membrane, and high stability under selected conditions. A combination of these characteristics is normally used in selecting a membrane for a specific application. In practical applications on a large scale, membrane fouling and poisoning, cost and lifetimes of membranes are critical factors [7].

1.3 Why electrochemical membranes?

A recent prototype of an electrochemical cell employing membranes and capable of reducing high salt concentrations in aqueous media is currently under investigation by the CSIR (Tswane). Since the prototype and the membrane used in the prototype are under license to a Canadian company, the technology associated with the prototype is currently

expensive. An approach to make this technology cheaper would be to initiate a process whereby the membrane technology could be "reverse engineered" and locally produced.
This membrane technology is patented, but permission was granted for this patent to be "Reverse engineered" by the CSIR and its associated industrial partner Key Structure Holdings. The mechanism by which this electrochemical cell works is based on membrane technology. This membrane is based on a composite polytetrafluoroethylene (PTFE) carbon membrane either in the heterogeneous or bipolar mode.

1.4 Objectives

The main objectives of the project were to:

- Chemically and structurally characterize the membrane from the desalination unit
- Determine the transport mechanism of the membrane
- Study the surface and bulk conductance properties of the membrane
- Study the reactivity of the membrane in the presence of simple ions
- Electrochemically evaluate the behaviour of simple ions on the membrane and the carbon electrodes used in the electrochemical cell.

The techniques used to determine the elemental composition of the membrane were:

- energy dispersive X-ray analysis (EDX)
- particle induced X-ray emission (PIXE).

The following techniques were also used to characterize the composite membrane:

- scanning electron microscopy (SEM)
- atomic force microscopy (AFM)
- fourier transform infrared (FTIR)
- thermogravimetric analysis (TGA)
- differential scanning calorimeter (DSC)
- liquid chromatography – mass spectroscopy (LC-MS).

The following techniques were used to characterize the membrane as well as the carbon electrodes when applied to a custom made ED half-cell.

- electrochemical measurements
    - linear sweep voltammetry (LSV)

- cyclic voltammetry (CV)

- conductivity measurements
- electrical impedance studies (EIS)

1.5 Project outline

To achieve the objectives of this study several tasks had to be undertaken.

1. US Patent 4,153,661, (1979) which describes the chemical composition of the desalination membrane, had to be reverse engineered. To achieve this objective the composite membrane had to be characterised. This was done using various characterization and electrochemical tools which include SEM, AFM, FTIR, PIXE, TGA, DSC and LC-MS.
2. Secondary reactions, which could take place on the carbon electrode surface, had to be studied. These secondary reactions could add to the overpotential and the new species may have influences on the membrane and the overall conductivity through the membrane. Electrochemical techniques such as cyclic voltammetry and linear sweep voltammetry were utilized for this purpose.
3. The conductive capabilities of the membrane had to be evaluated. Conductivity meters were used to monitor the change in ion concentrations across the membrane.
4. The final task was to create a model for what exactly happens in the ED half-cell. EIS was used for this purpose.

1.6 Layout of thesis

This document comprises of eight chapters:

Chapter 1 gives a general introduction to desalination processes and the role that membranes play.

Chapter 2 deals with the theoretical background of the analytical techniques used and of the cell design for the electrodialysis (ED) half-cell.

Chapter 3 deals with the technical aspects of the experimental methods used in the study.

Chapter 4 discusses the results of the elemental analysis and structural characterization of the composite membrane.

Chapter 5 discusses the results of the electrochemical measurements done on the carbon electrodes by CV and LSV.

Chapter 6 deals with the results of the conductivity studies for the ED half cell.

Chapter 7 deals with the impedance studies on the carbon electrodes and the ion exchange membranes.

Chapter 8 presents the conclusions and recommendations for further studies.

1.7 References

1. Chen, J.; Huang, S. Desalination, **2004,** 169, 161-165
2. Abufayed, A. A. Desalination, **2001**, 139, 297-301
3. Cabassud, C.; Wirth, D. Desalination, **2003**, 157, 307-314
4. Andrianne, J.; Alardin, F. Desalination, **2002**, 153, 305-311
5. Younos, T.; Tulou, K. E. Contemporary Water Research and Education, **2005,** 132, 3-10
6. Kawate, H.; Tsuzura, K; Shimizu, H. *Ion Exchangers*. W. de Gruyter. Berlin, New York, 1991; pp 597-598
7. Davis, T. A.; Genders, J. D.; Pletcher, D. *A First Course in Ion Permeable Membranes*, The Electrochemical Consultancy, Alresford. 1997. Chapter 6

Chapter 2

Theoretical background

2.1 Electrodialysis

Electrodialysis utilizes electromotive force applied to electrodes adjacent to both sides of a membrane to separate dissolved salts in water. The separation of salts occurs in individual membrane units called cell pairs. A cell pair consists of an anion-transfer membrane, a cation-transfer membrane, and two spacers. The complete assembly of cell pairs and electrodes is called the membrane stack. The number of cells within a stack varies depending on the system. The spacer material is important for distributing the water flow evenly across the membrane surface. The ED process is effective for salt removal from feedwater because the cathode attracts the sodium ions and the anode attracts the chloride ions. In general, ED has a high recovery rate and can remove 75% to 98% of total dissolved solids from feedwater. Electrodialysis reversal (EDR) is a similar process, except that the cathode and anode are reversed to routinely alternate current flow. EDR has a higher recovery rate (up to 94%) because of the feedwater circulation within the system and alternating polarity.

ED and EDR can remove or reduce a host of contaminants from feedwater and the process is not as sensitive to the pH or hardness levels of the feedwater. The EDR process is adaptable to various operational parameters, requires little labour, and the maintenance costs are generally low. EDR plants on the west coast of Florida (USA) have had up to 85% water recovery of their municipal waste water [1]. Nitrate-removal EDR plants have been successfully implemented in Delaware (USA), Bermuda and Italy, with NO_3^- reduction of up to 90% and TDS removal of 80%. NO_3^- reduction remained stable for the full lifetime of the membranes and did not decrease over time [2]. Fifty percent of the world's desalination plants are located in the Middle East where the shortage of water is matched by the availability of energy. ED plants have been used since 1959 and found to be a technical and economical success [3]. Figure 2.1 illustrates a schematic diagram for a typical electrodialysis desalination cell.

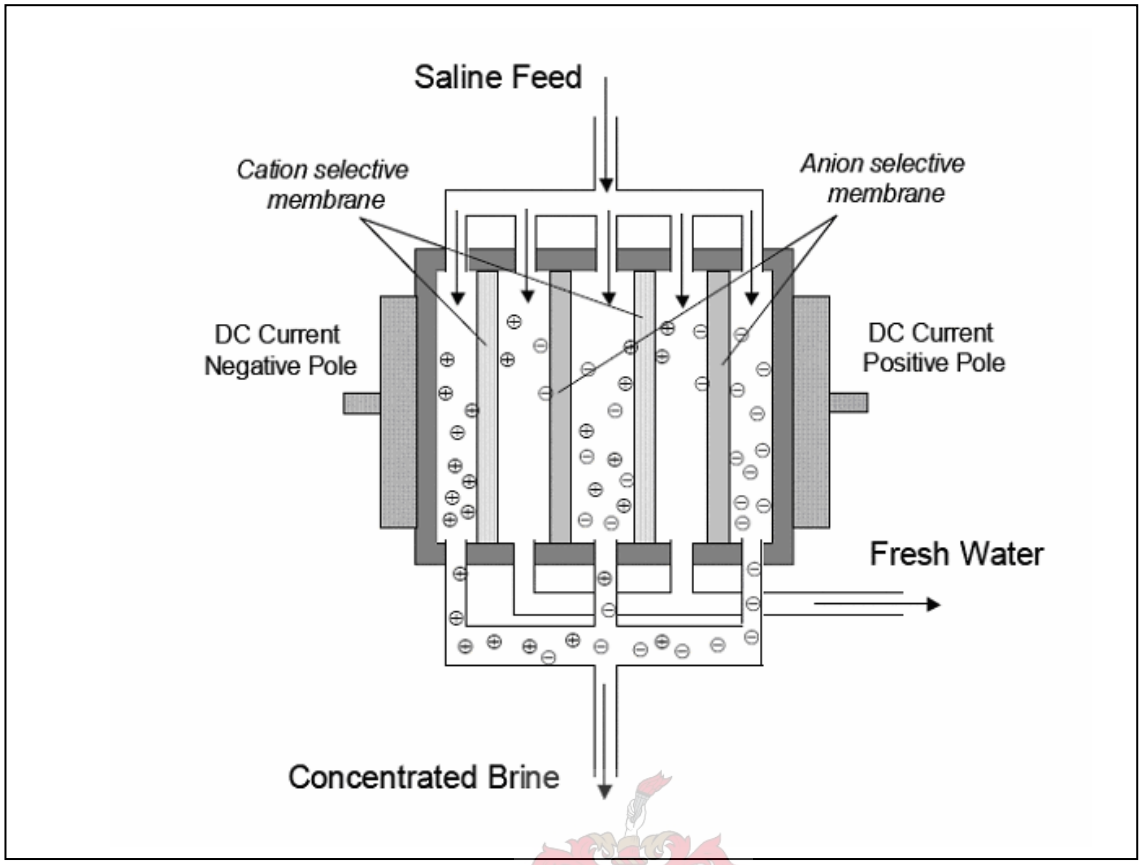

Figure 2.1: Schematic diagram of the electrodialysis desalination process.

A recent prototype of an electrochemical cell employing membranes and capable of reducing high salt concentrations in aqueous media is currently under investigation by the CSIR in Pretoria. This prototype is under license from a Canadian manufacturer, and is run on an operating system known as the ENPAR's DesEl system [4].

2.1.1 The DesEl technique

The DesEl system operates on the principle of capacitive deionization to remove ionic compounds referred to as total dissolved solids (TDS). Capacitive deionization (CDI) is a combination of ion exchange and electrodialysis. The main component of the DesEl system is a novel electrostatic charging system, which behaves as a capacitor and comprises inexpensive carbon electrodes. The capacitor is energized using direct current, creating positive (anode) and negatively (cathode) charged surfaces. Ionic compounds are attracted through the permeable membrane to the surfaces and adsorb onto them. After the pulse is applied the water is then removed and kept in a tank for recirculation. Thereafter the polarity of the cell is reversed (exchanging the cathode and anode), and the ions are then released into a separate cell channel which concentrates waste water [5, 6].

The operation potential of the system is normally 1.2V. Figure 2.2 gives an illustration of the capacitive deionization observed in the DesEl technique.

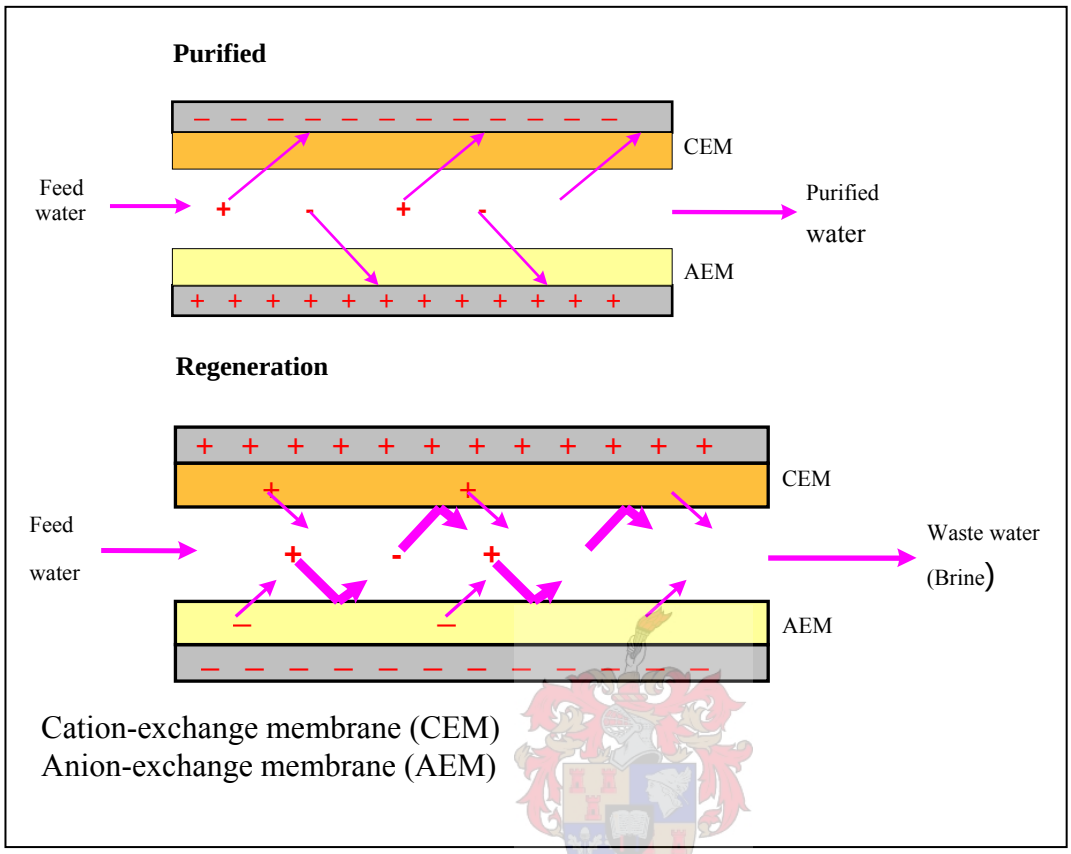

Figure 2.2: Illustration of the DesEl technique, which employs capacitive deionization

2.1.2 *The composite carbon membrane*

The composite membrane used in the ED prototype plant at the CSIR (Tswane) is described in US Patent 4,153,661 [7]. The invention relates to a method of preparing a composite sheet by mixing, in an aqueous medium, particulate material and polytetrafluoroethylene (PTFE) particles, which are subsequently fibrillated therein, to form a unitary matrix of entangled PTFE fibrils containing the particulate material. PTFE has a unique hydrophobic surface character, high temperature stability, and is inert in most strong acids and bases. PTFE is a thermoplastic fluoropolymer, better known as Teflon. It has the lowest coefficient of friction of any known solid material and is very unreactive. Its melting point is 327^0C, but its properties degrade above 260^0C. PTFE also has excellent dielectric properties and high bulk resistivity [8].

The invention provided a novel method of producing a uniformly porous, high void-volume composite sheet with particulate material distributed uniformly throughout a matrix of fibrillated PTFE. The novel sheet has a high tensile strength and is substantially uniformly porous, making it suitable to use as a filtering material for electrolytic cells and gas diffusion membranes. The method did not require organic lubricants or extraction of a removable additive material to produce porosity. The method of making the membrane involved the blending of the particulate material with a PTFE aqueous dispersion and then adding water as lubricant. The resultant putty-like mass was then thoroughly mixed at a temperature between 50^0C and 100^0C. The resultant mass was then biaxially calendered between heated calendaring rolls, maintaining a temperature of between 50^0C and 100^0C, to cause further fibrillation and to produce a composite sheet, which was then dried [7].

In order to reverse engineer the membrane the particulate material needed to be determined. The possibilities for the particulate materials were outlined in Patent 4,153,661 and they where investigated or eliminated through the various techniques outlined in section 2.2.2.

2.1.3 Carbon electrodes

Carbon, with its high surface area and because it is electronically conducting, is an attractive material to use for electrodes, in capacitors as well as in batteries. Glassy carbon is an amorphous form of carbon, whereas pyrolytic graphite has a more ordered structure, with distinct planes, namely the basal plane and the edge plane, with the edge plane considerably more conducting than the basal plane. Glassy carbon is mechanically more durable than pyrolytic graphite [6].

The desirable properties of carbon and graphite for electrochemical applications are the following:

- good electrical conductivity
- acceptable corrosion resistance
- available in high purity
- low cost
- high thermal conductivity
- dimensional and mechanical stability
- light weight and easy to handle
- available in a variety of physical structures

- ease of fabrication into composite structures

Glassy carbon, also called vitreous carbon, is a non-graphitizing carbon which combines glassy and ceramic properties with those of graphite. The most important properties of glassy carbon are high temperature resistance, extreme resistance to chemical attack and impermeability to gases and liquids. It has been demonstrated that the rates of oxidation of certain glassy carbons in oxygen, carbon dioxide or water vapour are lower than those of any other carbon. Thus, while normal graphite is reduced to a powder by a mixture of concentrated sulphuric and nitric acids at room temperature, glassy carbon is unaffected by such treatment, even after several months. Glassy carbon consists entirely of sp^2 bonded atoms, and current research indicates that it may have a fullerene type structure [8].
Glassy carbon is known to have active surface groups of the quinone type [10, 11]. Slow surface oxidation reactions occur, which leads to the formation of an oxide film layer on the surface of the electrode. This film either inhibits or accelerates certain electrode reactions, depending on the mechanism of oxidation or reduction of the particular ion or molecule.

For the purposes of this study, three carbon electrodes will be investigated; a commercial glassy carbon electrode (GCE), a custom glassy carbon electrode and a carbon sheet employed by the CSIR in the prototype plant.
The carbon sheet in the prototype plant is a blend of activated carbon and PTFE. It is obviously desirable to combine the catalytic properties of activated carbon with the advantages of Teflon bonding to obtain active, wet-proofed electrodes [12]. Activated carbon is a carbon material mostly derived from charcoal. This material has an exceptionally high surface area, and includes a large amount of microporosity. These micropores provide superb conditions for adsorption to occur and catalyze surface electrode reactions.

2.2 Elemental analysis and characterisation of the composite carbon membranes

Various analytical tools can be used to structurally and chemically characterise the composite carbon membranes, including SEM, AFM, PIXE, EDX, DSC, TGA, FTIR and LC-MS. SEM and AFM are frequently utilised to investigate the morphology of ion-exchange membranes [13, 14]. Surface studies are done to determine the membrane thickness (for durability), surface roughness, phase distribution, pore sizes and pore distribution. Perfluorosulphonated (Nafion) and perfluorinated membranes are routinely

characterised by TGA, DSC and FT-IR to determine water content, molecular interactions as well as thermal properties [15, 16].

2.2.1 Surface and elemental analysis techniques

a) Scanning electron microscopy (SEM)

SEM creates high-resolution images of the surfaces of solid objects. It creates these images by using electrons instead of light waves. An electron gun emits a beam of high-energy electrons. This beam travels downward through a series of magnetic lenses designed to focus the electrons to a very fine spot. Near the bottom, a set of scanning coils moves the focused beam back and forth across the specimen. As the electron beam hits each spot on the sample, secondary electrons are knocked loose from its surface. A detector counts these electrons and sends the signal to the detector. The final image is built up of the number of electrons emitted from each spot on the sample [17]. SEM is used to study the morphology of membranes in order to obtain data on the homogeneity, the presence of amorphous and crystalline regions and their relative distribution, phase separation and the size, shape and distribution of pores in the membrane [18].

b) Atomic force microscopy (AFM)

AFM is a descendant of Scanning tunneling microscopy (STM) and is used to study solid surfaces. The goal of AFM is to measure very small forces at very small distances in order to obtain images on a molecular level. AFM produces images that mimic the topography of a surface by recording interaction forces between the apex of a probe tip, fastened to a cantilever spring, and atoms at the sample surface as the tip is scanned over the surface of the sample. The displacement of the probe tip, as a result of the surface, is monitored and a three-dimensional picture of the sample surface can then be determined. From the three-dimensional picture the computer can also calculate the following information; average roughness, size of particles or pores as well as distances and angles between objects [19, 20].

c) Proton induced x-ray emission (PIXE)

PIXE is a technique that can be used for non-destructive, simultaneous elemental analysis (Sodium through Uranium) of solid, liquid, thin-film, and aerosol-filter samples. Like other

spectroscopic techniques used for elemental analysis, PIXE is based upon the physics of the atom, not its chemistry. It involves both the excitation of the atoms in the sample to produce characteristic X-rays, and a means of detection, in order for the x-ray intensities to be identified and quantified. When samples are bombarded with the beam, the protons interact with the electrons in the atoms of the sample, creating inner shell vacancies. The energy of the X-rays emitted when the vacancies are refilled is characteristic of the element from which they originate, and the number of X-rays is proportional to the amount of the corresponding element within the sample [21].

d) Energy dispersive X-ray spectroscopy (EDX)

EDX is a method used to determine the energy spectrum of X-ray radiation. An electron beam strikes the surface of a conducting sample. The energy of the X-rays emitted depends on the material under examination. The detector is a semi-conductor which is polarized with a high voltage; when an X-ray photon hits the detector it creates electron-hole pairs that drift due to the high voltage. The electric charge is collected. The increment of voltage of the condensator is proportional to the energy of the photon, and then it becomes possible to determine the energy spectrum of the sample.

2.2.2 Molecular and structural analysis techniques

a) Differential scanning calorimetry (DSC)

DSC measures the temperature and heat flow associated with transitions in materials as a function of time and temperature. It determines transition temperatures, melting and crystallization, and heat capacity. DSC is a thermoanalytical technique in which the difference in the amount of heat required to increase the temperature of a sample and reference are measured as a function of temperature. Both the sample and the reference are maintained at very nearly the same temperature throughout the experiment. When the sample undergoes a physical transformation, such as phase transitions, more (or less) heat will need to flow to it than the reference to maintain both at the same temperature. Therefore the amount of energy absorbed or released during these transitions is measured. With DSC the melting and crystallization temperatures can be determined,in addition to the glass transition temperature (Tg) as well as the heat capacity of the various components in a sample [22, 23].

b) Thermogravimetric analysis (TGA)

TGA is based on the measurement of the weight loss of a material as a function of temperature. The instrument is basically a precisely controlled furnace combined with a microbalance. The balance assembly measures the initial weight at room temperature and then continuously monitors changes in sample weight as heat is applied to the sample. TGA is commonly employed to determine polymer degradation temperatures, residual solvent levels, absorbed moisture content, and the amount of inorganic filler in polymer or composite material compositions [24].

c) Fourier-transform infrared (FTIR)

FTIR measures the adsorption of various infrared light wavelengths by a material. These infrared adsorption bands identify specific molecular components and structures. IR spectroscopy detects the vibration characteristics of chemical functional groups in a sample. When infrared light interacts with matter, chemical bonds will stretch, bend or contract. Therefore a certain functional group will tend to adsorb infrared radiation at a specific wavenumber regardless of the structure of the molecule or the presence of another functional group [25].

2.2.3 Compositional analysis techniques

a) Liquid chromatography - Mass spectroscopy (LC-MS)

LC-MS is a hyphenated technique, combining the separation power of HPLC with the detection power of mass spectroscopy. The interface is a particle beam type, which separates the sample from the solvent, and allows the introduction of the sample in the form of dry particles into the high vacuum region. Gas phase ions are generated which are then transferred to the optics of the mass spectrometer. LC-MS is a powerful technique used for the specific detection and potential identification of chemicals in the presence of other chemicals.

2.3 Electrochemical evaluation of simple reactions occurring at a carbon electrode

As mentioned in Section 2.1.3 carbon electrodes were used at the CSIR. At an applied potential of 1.5V the anions and cations are not only attracted to the respective electrodes,

but may also be oxidized or reduced. To investigate these oxidation and reduction possibilities a study was performed on the most common anions found in brackish water and seawater. These are chloride, sulphate and nitrate. Due to the fact that ED occurs in aqueous solutions, there is the omni-presence of oxygen. ED desalination plants seldom deoxygenate their feedwater, therefore the possible reactions of oxygen were also investigated.

2.3.1 Oxygen reactions

The reactions of oxygen are irreversible in aqueous electrolytes, even at high temperatures with the best of catalysts. This leads to major voltage losses. Yeager [26] proposed the following two pathways (A and B) for the reduction of O_2, which are generally accepted:

A: Direct 4-electron pathway:

Alkaline: $O_2 + H_2O + 4e^- \rightarrow 4OH^-$ (1.1)

Acid: $O_2 + 4H^+ + 4e^- \rightarrow H_2O$ (1.2)

B: Peroxide pathway:

Alkaline: $O_2 + H_2O + 2e^- \rightarrow 4OH_2^- + OH^-$ (1.3)

followed by $4OH_2^- + H_2O + 2e^- \rightarrow 3OH^-$ (1.4)

or $2OH_2^- \rightarrow 2OH^- + O_2$ (1.5)

Acid: $O_2 + 2H^+ + 2e^- \rightarrow H_2O_2$ (1.6)

followed by $H_2O_2 + 2H^+ + 2e^- \rightarrow 2H_2O$ (1.7)

or $2H_2O_2 \rightarrow 2H_2O + O_2$ (1.8)

Yeager's observations were confirmed by Lai and Bergel [27] who suggested that oxygen is reduced to hydrogen peroxide (1.6) at about –0.25V (vs Ag/AgCl) and almost directly afterwards hydrogen peroxide is reduced to water (1.7) at about –0.5V. Hydrogen peroxide is favoured above HO_2^- because H_2O_2 predominates at pH 8:

$$\log ([HO_2^-]/[H_2O_2]) = -11.63 + pH$$

It is widely assumed that oxygen reduction proceeds principally through the peroxide pathway on carbon and graphite [28]. There is no consensus on the mechanism or even the identity of adsorbed intermediates. Most researchers conclude that the adsorption of O_2 or superoxide is involved, but variations in surface conditions and pretreatment cause wide

variations in electrode behavior. Unmodified carbon is of particular interest in alkaline media, in which the first reduction step (to superoxide) occurs in the absence of an added electrocatalyst [29]. The most popular proposed mechanisms for the oxygen reduction reaction (ORR) will now be discussed.

Taylor and Huffray proposed one of the first suggestions for the ORR mechanism at pH>10 [30]:

$$O_2 + e^- \rightarrow O_2^{\cdot -}{}_{\text{(ad, before migration)}} \qquad \text{(the rate determining step)} \qquad (1.9)$$

$$O_2^{\cdot -}{}_{\text{(ad, before migration)}} \leftrightarrow O_2^{\cdot -}{}_{\text{(ad, after migration)}} \qquad (1.10)$$

$$2\, O_2^{\cdot -}{}_{\text{(ad, after migration)}} + H_2O \leftrightarrow O_2H^- + OH^- + O_2 \qquad (1.11)$$

They proved the presence of peroxide as a product in acidic solutions using Ti (IV), and suggested that the rate-determining step was the first electron transfer as in equation (1.9). For a pH>10 they proved that peroxide was the exclusive product. For pH<10 they proposed reduction (1.9), followed by the protonation of $O_2^{\cdot -}$ [31].

Zhang et al [29] proposed the following on glassy carbon electrodes in alkaline media:

$$O_2 \rightarrow O_{2(ads)} \qquad (1.12)$$

$$O_{2(ads)} + e^- \rightarrow [O_{2(ads)}]^{\cdot -} \qquad (1.13)$$

$$[O_{2(ads)}]^{\cdot -} \rightarrow \{ O_{2(ads)}\}^{\cdot -} \qquad (1.14)$$

$$\{O_{2(ads)}\}^{\cdot -} + HOH \rightarrow HO^{\cdot}{}_{2(ads)} + OH^- \quad \text{rate determining step} \qquad (1.15)$$

$$HO^{\cdot}{}_{2(ads)} + e^- \rightarrow HO_{2(ads)}^- \qquad (1.16)$$

$$HO_{2(ads)}^- \rightarrow HO_2^- \qquad (1.17)$$

$[O_{2(ads)}]^-$ and $\{ O_{2(ads)}\}^-$ are two different forms of superoxide on the electrode surface.

Appel and Appleby [32] proposed the following specifically for carbon paste electrodes:

$$O_2 + e^- \rightarrow O_2^-{}_{ad} \qquad (1.18)$$

followed by

$$O_{2ad}^- + H_2O + e^- \rightarrow O_2H^- + OH^- \qquad (1.19)\ 2e^- \text{ mechanism}$$

or

$$O_{2ads}^- + H_2O + e^- \rightarrow O_{ad} + 2OH^- \qquad (1.20)\ 4e^- \text{ mechanism}$$

Alternatively, the first step may be:

$$O_2 + H_2O + e^- \rightarrow O_2H_{ads} + OH^- \qquad (1.18a)$$

followed by:

$$O_2H_{ads} + e^- \rightarrow O_2H^- \qquad (1.18b)$$

or

$$HO_{2ad} \rightarrow \text{products} \qquad (1.18c)$$

Equation (1.18) will be pH dependent.

Morcos and Yeager [33] concluded that:

$$O_2 \rightarrow O_{2(ads)}$$

$$O_{2(ads)} + e^- + H_2O \rightarrow HO_{2(ads)} + OH^- \qquad (1.21)$$

$$2HO_{2(ads)} + OH^- \leftrightarrow HO_2^- + H_2O + O_2 \qquad (1.22)$$

Xu et al [34] concluded that the reduction of O_2 to HO_2^- occurred at about –0.3 V and HO_2^- was reduced to water or OH^- at 1.0V (vs Ag/AgCl) in alkaline medium:

$$O_2 + e^- \rightarrow O_2^-{}_{ad} \qquad (1.23)$$

$$O_2^-{}_{ad} + H_2O \rightarrow O_2H_{ads} + OH^- \quad \text{rate determining step} \qquad (1.24)$$

followed by disproportionation:

$$O_2H + O_2^- \leftrightarrow O_2H^- + O_2 \qquad (1.25)$$

or electrochemical reduction:

$$O_2H_{ads} + e^- \leftrightarrow O_2H^- \qquad (1.26)$$

Reaction (1.24) is accelerated when adsorption occurs. Once HO_2 is formed, it is directly reduced via (1.26). They determined that adsorption is critical in the reduction rate of O_2 by accelerating the protonation of O_2^-.

O_2 reduction on carbon involves a strong interaction of O_2 with the functional groups on the surface. Garten and Weiss [35] proposed that surface quinone groups are involved in the reduction of O_2 to peroxide. The catalytical reduction on the surface of the glassy carbon electrode is attributed to o-quinone-like structures [29, 33, 39, 40]. Pyrolytic graphite's behaviour strongly indicates the presence of functional groups that influence the electrochemical properties.

Although there is general agreement that superoxide is an intermediate in the oxygen reduction reaction (ORR) on carbon, its adsorption and eventual fate is unclear. The O_2/O_2^- couple is chemically reversible on carbon in non-aqueous solvents, but superoxide rapidly decays in water, and a peak for electrogenerated O_2^- is rarely observed. Superoxide is unstable in acidic and neutral media. Reactions of superoxide in acidic and neutral media have been studied in detail by Bielski and Allen [36]:

$$O_2 + e^- \leftrightarrow O_2^{\cdot -} \qquad (1.27)$$

$$O_2^{\cdot -} + H_2O \leftrightarrow O_2H^{\cdot} + OH^- \quad (1.28)$$

$$O_2H^{\cdot} + O_2^{\cdot -} \leftrightarrow O_2H^- + O_2 \quad (1.29)$$

Reactions (1.28) and (1.29) are combined into the following disproportionation

$$2O_2^{\cdot -} + H_2O \leftrightarrow O_2H^- + O_2 + OH^- \quad (1.30)$$

Superoxide adsorption sites depend strongly on surface pretreatment.

According to Humffray and Taylor [30, 31] as well as Yang and McCreery [37], O_2 reduction is unusually pH dependant. The more positive reduction peak (ca –0.3 V vs Ag/AgCl) decreases in height with decreasing pH (till about pH10), and a peak develops at ca –0.55 V. which shifts very slightly with decreasing pH. Two peaks thus occur at pH 9. These imply an overall $2e^-$ reduction, as expected, as many reports stated that H_2O_2 or HO_2^- are the reduction products. The reduction peaks themselves imply that the reduction of oxygen to H_2O_2 or HO_2^- is pH independent. In conclusion, Yang and McCreery [37] proposed that at a pH lower than 10, the electrogenerated $O_2^{\cdot -}$ and $O_2H^{\cdot}$ disproportionate to O_2 and H_2O_2 by established homogeneous routes.

Humffray and Taylor [38] summarised the ORR at various pH values. In acidic media the yield of peroxide is very low. At pH 6 peroxide and water are both produced, with water dominating over the entire potential range. At pH<9 the same rate-determining steps are operating regardless of surface state and reaction products. Formation of both peroxide and water from oxygen requires protons to be supplied for the reaction to proceed to completion, and the pH of the solution near the electrode may increase. If the rate of the reaction depends on the pH, then changes in the voltammetric characteristics may be expected.

2.3.2 Chloride reactions

During the electrolysis of sodium chloride in aqueous solution in an electrochemical cell one does not only consider the sodium and chloride ions as possible reactants but also the water. Sodium will not be produced in aqueous solution because it will spontaneously react with water to produce Na^+. At the cathode of the sodium chloride cell the reduction of water dominates:

$$2H_2O + 2e^- \rightarrow H_2 + 2OH^- \qquad E^0_{red} = -0.83 \text{ V (vs SCE)}$$

rather than the reduction of sodium

$$Na^+ + e^- \rightarrow Na \qquad E^0_{red} = -2.71 \text{ V}$$

At the anode of the cell, Cl^- and H_2O are both candidates for oxidation. The two possible half reactions are:

$2H_2O \rightarrow O_2 + 4H^+ + 4e^-$ $\qquad E^0_{ox} = -E^0_{red} = -1.23$ V

$2Cl^- \rightarrow Cl_2 + 2e^-$ $\qquad E^0_{ox} = -E^0_{red} = -1.36$ V

Because the water has a more positive potential than the chlorine reaction, it should be oxidized more readily. But the water oxidation requires a considerable over-voltage to make the reaction rate appreciable. Since the latter reaction is quite rapid in comparison to the water oxidation, it will dominate at slightly elevated voltages.

Since the hydrogen is produced by the breaking up of water molecules the solution becomes basic around the cathode and a solution of sodium hydroxide is produced. If the electrolysis is carried out in an undivided cell and the chlorine gas and the caustic are allowed to mix and react with each other, sodium hypochlorite (bleach) is produced if the cell operates close to room temperature, and sodium chlorate is produced if the cell is operated near the boiling point of water.

The overall cell reaction is:

$2NaCl + 2H_2O \rightarrow Cl_2 + H_2 + 2NaOH$

Chlorine gas and sodium hydroxide react to form sodium hypochlorite and sodium chloride:

$Cl_2 + 2NaOH \rightarrow NaOCl + NaCl + H_2O$

Sodium hypochlorite will react further at high temperature to form sodium chlorate and sodium chloride:

$3NaOCl \rightarrow NaClO_3 + 2NaCl$

(although, sodium chlorate can also form by direct electrochemical oxidation).

The general chlorine reduction mechanisms on various electrodes are listed below [41]

(A) $Cl_{2(aq)} \leftrightarrow 2Cl_{ads}$ (Tafel) (1.31)

$Cl_{ads} + e^- \leftrightarrow Cl^-_{(aq)}$ (Volmer) (1.32)

(B) $Cl_{2(aq)} + e^- \leftrightarrow Cl_{ads} + Cl^-_{aq}$ (Heyrovsky) (1.33)

$Cl_{ads} + e^- \leftrightarrow Cl^-_{(aq)}$ (Volmer) (1.34)

(C) $Cl_{2(aq)} \leftrightarrow Cl_{2ads}$

$Cl_{2(aq)} + e^- \leftrightarrow Cl_{ads} + Cl^-_{aq}$ (Heyrovsky) (1.35)

$Cl_{ads} + e^- \leftrightarrow Cl^-_{(aq)}$ (Volmer) (1.36)

(D) $Cl_{2(aq)} \leftrightarrow Cl_{(aq)}^{-} + Cl_{ads}^{+}$ (Krishtalik) (1.37)

$Cl_{(ads)}^{+} + e^{-} \leftrightarrow Cl_{ads}$ (Heyrovsky) (1.38)

$Cl_{(ads)} + e^{-} \leftrightarrow Cl^{-}_{(aq)}$ (Volmer) (1.39)

2.3.2.1 Anode materials

a) Platinum

The obvious disadvantage of platinum is its high price. However, platinum anodes corrode only at a very slow rate and are suitable for perchlorate production. They therefore provide an almost ideal anode material. High efficiency can be reached with platinum and processing of the electrolyte is greatly simplified.

Chloride is oxidized to chlorine gas at 1.4 V (vs SCE) on Pt electrodes. ClO^{-} is reduced to chlorine at 1.3V and chlorine itself is reduced at 1.11 V. The reduction of oxygen is observed at 0.16 V on Pt, therefore it does not interfere with the chloride reactions. The chloride reactions are independent of pH between 5 and 11 [42].

The reduction of hypochloride on Pt is as follows [43]:

$ClO^{-} + H_2O + 2e^{-} \rightarrow Cl^{-} + 2OH^{-}$ 0.26 V (vs Hg/HgO)

This is an overall 2e process that proceeds with a slow step (which is slightly retarded by the formation of an oxide film on the surface of the electrode,) followed by faster desorption step:

$ClO^{-} + H_2O + e^{-} \rightarrow Cl_{ad} + 2OH^{-}$ slow

$Cl_{ad} + e^{-} \rightarrow Cl^{-}$ fast

The film on the Pt electrode surface forms simultaneously with the reduction of OCl^{-}. Oxides, hydroxides and chemisorbed oxygen form on the Pt surface during the chlorine electrode reaction (ClER) in aqueous solutions. These inhibit the evolution and reduction of chlorine. Dickinson et al [44] found a decrease in the rate of chlorine reduction with an increase in the surface oxide layer on Pt electrodes.

Thomassen et al [41] suggested a mechanism for the reduction of chlorine on Pt surfaces to take into account the surface oxide, namely adsorption of chlorine molecules and then a rate determining Heyovsky discharge step. This is in agreement with mechanism (C).

b) Oxide electrodes

The reaction mechanism for the oxidation of chloride can be determined by the d-configuration in the oxide, i.e. the reaction proceeds by the Volmer-Heyrovsky mechanism on the electrode containing the transition metal cation with partially filled t_{2g} orbitals and empty e_g orbitals. For RuO_2 electrodes the chlorine reaction was thought to proceed by the following reaction mechanism, with a reaction order of 2:

$$Cl^- \leftrightarrow Cl_{ad} + e$$

$$Cl^- + Cl_{ad} \leftrightarrow Cl_2 + e$$

The same was found for graphite, IrO_2 and $Eu_{0.1}WO_3$.

Pt, Pt-Ir alloy, TiO_2, Pt/MnO_2, Ti/PtO_2 follow the Volmer-Tafel mechanism on the electrode containing the transition metal cation with just half filled t_{2g} orbitals and partially filled e_g orbitals. The active site on the oxide electrode is generally the metallic cation site. The coverage of the electrode surface depends not only on the concentration of Cl^-, but also on the pH of the solution. The mechanism is determined by the interaction of the electrode surface and the adsorbed Cl atom [45]and is illustrated by (1.40) to (1.42).

The Volmer step: $S + Cl^- \rightarrow S\text{-}Cl^{\cdot} + e$ (S is the site for the reaction) (1.40)

The Tafel step: $2S\text{-}Cl^{\cdot} \rightarrow 2S + Cl_2$ (1.41)

The Heyrovsky step: $S\text{-}Cl^{\cdot} + Cl^- \rightarrow S + Cl_2 + e$ (1.42)

The Volmer-Heyrovsky mechanism was proposed by Tomcsányi et al [46] for the electrooxidation of chloride on the RuO_2/TiO_2 working electrode. They observed the oxidation of chloride to chlorine via an adsorbed $S\text{-}Cl^-$ intermediate at 1.1 V (vs SCE) and a desorption peak at 0.8 V, which they propose is due to the reduction of HOCl produced by Cl_2 hydrolysis.

$$Cl_2 + H_2O \leftrightarrow OCl^- + Cl^- + 2H^+$$

$$OCl^- + 2H^+ + 2e^- \leftrightarrow Cl^- + H_2O$$

In the case of RuO_2/TiO_2 coated electrodes, the oxygen evolution process occurs around the same potential as for the Cl^- oxidation process (but the oxygen reaction in most of these circumstances is less than 5%).

c) Carbon electrodes

***i)* Graphite**

Graphite is inexpensive and easy to obtain. It is an attractive material from which to manufacture electrodes, because it is inexpensive compared with platinum or gold yet relatively chemically inert in most electrolyte solutions, while retaining high surface activity [47]. It does however corrode at a comparatively fast rate. This makes it necessary to replace the anodes every so often and to filter the electrolyte before further processing, which can be difficult and laborious due to the small size of the carbon particles. Cells operating with graphite anodes must also be maintained at a relative low temperature to limit anode erosion, which translates to a lower cell capacity. Basal plane pyrolytic graphite electrodes show chlorine evolution at 1.275V (vs SCE) and 1.240V for edge plane electrodes.

The Volmer-Heyrovsky mechanism by Janssen and Hoogland [48, 49] was proposed for pyrolytic graphite:

Volmer: $Cl^- \leftrightarrow Cl_{ad} + e$

Heyrovsky: $Cl^- + Cl_{ad} \leftrightarrow Cl_2 + e$ rate determining step for used graphite

Like H_2 evolution reactions, chlorine reaction kinetics are sensitive to the electrocatalytic and adsorptive properties of the anode material (both for Cl^- and $Cl^{\cdot}$). Because chloride oxidation is an anode reaction, it normally proceeds in aqueous solutions at the electrode surfaces that are, in some way, covered or partially covered with an electrolytically generated oxide film. In the case of carbon anodes corresponding states of surface oxidation of carbon structures arise, e.g. the formation of quinonic, ketonic, and carboxylic functions at the anodic interface. In earlier process development carbon anodes were commonly employed but their lifetime and anode overvoltage characteristics are less than favourable; consumption of the carbon anode material occurs through oxidation to CO and CO_2, and erosion. The gradual oxidation of graphite to CO_2 results in widening of the anode-cathode gap and hence increased power consumption for the production of chlorine. This also leads to a higher CO_2 content in gas streams and high maintenance costs.

In concentrated Cl^- solutions formation of these quinonic, ketonic, and carboxylic species are restricted and some irreversible exchange between surface oxygen and surface Cl^- species occurs. The formation and reduction of oxygen species on glassy carbon (GC) is

less reversible than on pyrolytic graphite. The potential range for oxidation processes on pyrolytic graphite is large (1.9 V vs SCE) but smaller (to 1.0 V) at GC. Hine at al [50] suggested that the carbon oxide layer should influence the Cl_2 evolution reaction. Their work indicated two states of oxidation of the graphite surface:

- Lower oxide which begins to form at 0.78 V E_h
- Higher oxide which ranges from 1.26 – 1.56 V E_h

Under normal conditions graphite electrodes are initially covered with the lower oxide, which is easily removed from the surface as CO, O_2 and CO_2. High oxide it difficult to remove and occurs only at 2.24 V. Hine et al [50] also found that specific adsorption of Cl^- ions takes place on graphite surfaces only when the electrode surface is free from either type of oxide [51].

Janssen et al [49] also found that chlorine evolution is temperature dependant. A significant reduction in the overpotential is observed on the edge-plane pyrolytic-graphite electrode (EPPGE) in contrast with the other carbon based electrode substrates [47].

A study done by Lowe et al [52], revealed that a key feature of the successful carbon working electrode for reduction of chlorine is the presence of edge plane sites. For the oxidation of chloride to chlorine on EPPGE the potential is over 1.5 V. Reduction of chlorine to chloride is observed at 0.52 V (SCE) for EPPGE, 0.38 V for GCE and 0.45 V for boron doped diamond electrodes. These studies were done in acid media (0.1 M HNO_3). In the case of EPPGE the reduction peak moved to higher potentials and decreased current response with decreasing pH. GCE showed increased reactivity, which is linked to surface oxidation, because the scan commenced at high electrochemical potentials, where quinone-type functional groups are introduced. Al these reduction values are considerably lower than the standard electrode potential (1.39 V vs NHE), indicating the considerable irreversibility of the chloride/chlorine couple. EPPGE and GCE therefore have lower reduction potentials for chlorine and are used in gas sensors for chlorine detection [52].

ii) Diamond doped electrodes

The main feature of diamond doped electrodes (DDEs) is a wide potential window of about 3 V without significant water decomposition (the window becomes much narrower with increasing sp^2 carbon content). The electrochemical history of the electrode influences its electrochemical activity. Reversibility of a redox system on DDEs is affected by the details of film preparation, and only reactions with simple electron transfer maintain a certain degree of reversibility. Voltammetric measurements show the formation of a redox couple prior to the onset of oxygen evolution, which agrees with the formation of oxygen-containing functional groups (diamond oxide) at the diamond surface. Argoitia et al. [53] have observed the redox couple and ascribed it to the oxidation of sp^2 carbon sites in the grain boundaries. The formation of oxidized forms of carbon makes the diamonds surface more hydrophilic and the direct consequence is a larger activity, also for the chlorine evolution.

On DDEs the onset of chlorine evolution shifts to less positive potentials as the chloride concentration increases; in the solution with the highest NaCl concentration chlorine evolution starts at just below 1 V. The reduction of produced chlorine is only observed at a chloride concentration higher than 1 M, and the reduction peaks are localised at about 0.67 V (vs SCE) and a second peak at about 0.29 V. At acidic concentrations only one chlorine reduction peak is observed. The distance between the two peaks increases with increasing pH. This suggests that two dissolved and electroactive species of chlorine can be present, depending on the pH: the chlorine itself and probably the hypochlorous acid, formed by the direct electro-oxidation of Cl^-. The reaction order for DDEs for the oxidation of chlorine is first order (as for graphite). This agrees with the Volmer/Heyrovsky mechanism in which the discharge of the chloride ion is the rate-determining step.

$$Cl^- \rightarrow Cl^{\cdot} + e$$

$$2Cl^{\cdot} \leftrightarrow Cl_2$$

On DDEs chlorine evolution is stimulated by higher acidity, unlike oxide anodes where acidity has a general depressing effect on the reaction rate. The high overpotential for oxygen evolution and possibly for chlorine evolution (compared to graphite and commonly used dimensionally stable anodes (DSA)) can allow the electrochemical formation of chlorine as well as hypochlorous acid, with the redox potential of the couple $HClO/Cl_2$ being pH dependant. The chlorine overpotential at DDEs is 0.4 to 0.5 V higher compared

with graphite or ruthenium oxides. A DDE is highly selective for chlorine evolution reactions and is very stable under high polarization conditions [54], but the electrode requires frequent cleaning and polishing [52].

iii) Glassy carbon electrode

Reduction of chlorine to chloride is observed at 0.38V (vs NHE) for a GCE [52]. This reduction value is an indication of the considerable irreversibility of the chloride/chlorine couple. GCE shows increased reactivity, which is linked to surface oxidation, because the scan is started at high electrochemical potentials, where quinone-type functional groups are introduced. The amount of oxide put on the electrode in the anodic sweep is not completely removed in the cathodic sweep unless the potential is held at the negative potential. The added amount of oxide layer hinders the hydrogen evolution and consequently the hydrogen evolution keeps shifting to more cathodic potentials (NaOH solution with rotating disk electrode). The mechanism is similar to the reduction observed on Pt. The reaction is irreversible and has a 1 e^- slow step in a 2e^- overall reaction (Tafel-Heyrovsky mechanism) [51].

$$Cl_2 + H_2O \leftrightarrow OCl^- + Cl^- + 2H^+ \quad (1.43)$$

$$ClO^- + H_2O + e^- \rightarrow Cl_{ad} + 2OH^- \quad \text{slow} \quad (1.44)$$

$$Cl_{ad} + e^- \rightarrow Cl^- \quad \text{fast} \quad (1.45)$$

The oxide film forms on Pt as well, also parallel with the reduction of OCl^-. In the case of Pt the oxide initially strongly inhibits the reduction, whereafter there is a relaxation in the oxide structure and then the inhibition disappears [43].

Novak et al [51] proposed the states of surface oxidation and reduction on GCE from their experimental results with cyclic voltammetry: the desorption (reduction peak) of oxygen gas on the carbon surface at 0 V (vs H), the desorption of water oxygen (reduction) at -0.5V and hydrogen adsorption at -1.5 V. The (oxidation) desorption peak of hydrogen is also at 0V and the adsorption (oxidation) peak of oxygen onto the carbon surface is at 0.4 V.

Kodera [55] based his studies on the following reduction reactions:

$$ClO^- + H_2O + 2e \rightarrow Cl^- + 2OH^- \quad pH > 8.5 \quad (1.46)$$

$$HOCl + 2e \rightarrow Cl^- + OH^- \quad pH < 5.5 \quad (1.47)$$

HOCl is dominant in the acidic region, whereas the rest of the free chlorine is in ClO^- for all higher pHs. At neutral pH ClO_3^- is formed by self oxidation:

$$2HOCl + ClO^- \rightarrow ClO_3^- + 2Cl^- + 2H^+ \quad (1.48)$$

2.3.3 Nitrate reactions

Nitrate poses as a health risk due to the reduction of nitrate to nitrite in the gut, which causes methemoglobinaemia in people with a deficiency in glucose phosphate dehydrogenase. Nitrite ions interact with amines to form carcinogenic nitrosamines [56]. An excess of nitrate in our drinking water is due to unclarified wastewater, leaking sewers and excessive application of artificial fertilizers and manure on agricultural fields. The World Health Organization recommends 44 mg NO_3^-/L, whereas the EU guideline is 25mg NO_3^-/ L.

Biological denitrification is the process most widely used for the removal of nitrogen oxides from water, but at a very low rate. Biological processes (autotropic and heterotropic biological denitrification) cause the direct degradation of nitrate to molecular nitrogen, with biomass as the only byproduct. Biological treatment of nitrate has several disadvantages, e.g. it is slow, difficult to control, produces organic residues and requires intensive maintenance and a constant supply of organic substrate [57 - 59].

Nitrate can also be chemically reduced, but several byproducts are formed and much energy goes into the regeneration of the chemicals and catalysts [60].

$NO_3^- \rightarrow NH_4^+ + N_2$ with metallic ion

$NO_2^- \rightarrow NH_4^+ + N_2$ with metallic ion under weak acid or neutral conditions

Except for the removal of nitrate from our drinking water, electroreduction of nitrate also produces useful chemicals:

- N_2O, used in anaesthetic medical applications
- NH_3, nitrogen source in fertilizers
- NH_2OH, hydroxylamine, used to manufacture caprolactam.

All of these have high energies of activation [61 - 64].

The direct reduction of nitrate is not generally possible or highly irreversible at the most commonly used electrodes, such as glassy carbon, platinum, gold and mercury electrodes. However adding a copper coating catalyzes the reduction on glassy carbon. Adding Cl^- and F^- increases the nitrate current peak and suppress the hydrogen evolution peak [64].

The reduction mechanism for nitrate and the nature of the products depends on the following [65, 66]:

- nature of the electrodes
- electrolyte pH
- electrode potential
- presence of molecular/ ionic additives in the solution.

Assigning the peaks for reaction in nitrate solutions is quite difficult because the electrode processes take place at potentials that are quite close to the decomposition potentials for water. Thus pH changes are possible in the vicinity of the electrode as H_2 or O_2 is evolved or as H^+ is consumed or produced during electrolysis [67].

a) Reduction of nitrate on metals

The reduction of nitrate on platinum and palladium electrodes is inhibited at potentials that impose high hydrogen coverage. Nitrate has a low adsorption enthalpy on platinum and palladium. The reduction process is very slow and no gas products are formed, only NH_3 and NH_2OH. Electroreduction of nitric acid on Pt is thought to occur via the adsorption of HNO_3 which reacts with adsorbed hydrogen to form nitrous acid [67]. Hydrogen adsorption in the E = 0 V inhibits the formation of volatiles like N_2O and N_2 [65]. The effective reduction of nitrate on transition metals is listed as follows [65, 69, 70]:

Rh > Ru > IR > Pd and Pt.

On coinage metal electrodes the best results are found on copper electrodes where nitrate is reduced to NH_3 [69, 71]. Although copper has the highest activity towards nitrate reduction the electrode is dissolved during the reaction. Nitrate is reduced to nitrite on gold electrodes [66]. The proposed mechanism for the reduction of nitrate on metal electrodes is as follows:

$NO_3^-(sol) \leftrightarrow NO_3^-(ads)$ (a)

$NO_3^-(ads) + 2H^+ + e^- \rightarrow NO_2^- + H_2O$ rate determining step (b)

$NO_2^-(ads) + 2H^+ + e^- \rightarrow NO(ads) + H_2O$ (c)

$NO(ads) \rightarrow NO(sol)$ (d)

and further reduction: $NO(ads) \rightarrow NH_3$ or NH_2OH .

No appreciable desorption of NO(ads) or $NO_2^-(ads)$ occurs except on copper [70]. Adsorbed NO can only be reduced to NH_2OH or NH_3. NO in solution can produce N_2O and N_2. This

is related to the formation of a weakly adsorbed NO-dimer, which serves as a precursor to N_2O and which can only form when NO is in solution [72].

b) Reduction of nitrate on carbon electrodes

The chemical and electrochemical reductions of nitrate are complex reactions and the products depend strongly on the conditions. Nitrite, nitrogen and ammonia, involving $2e^-$, $5e^-$ and $8e^-$, respectively, are the most common products [71]. According to Solak et al [64] the direct reduction of nitrate is not generally possible or highly irreversible on GCEs. Newbery and Lopez de Haddad [73] and Kaminskaya et al [74] agree, but both groups observed a strong oxidation peak at 0.9 V (vs Ag/AgCl reference electrode), which they believe to be the oxidation of nitrite to nitrate. This was again confirmed by Jiang et al [75] who assigned the following electrode reaction for the oxidation of nitrite:

$$NO_2^- + 2H_2O \rightarrow NO_3^- + 2H^+ + 2e^- \quad \text{(e)}$$

Nitrite itself has very little reduction activity, and Xiaorong etal [76] described the reduction of nitrite to NO on glassy carbon at -0.36 V. They also concluded that the redox of nitrogen oxide (NO_x) is pH dependent. Chebotareva and Nyakong [66] observed a higher negative reduction potential for nitrite on unmodified GCE. They also observed a very small increase in current with an increase in concentration for the reduction of nitrite or nitrate on GCE. Constant potential electrolysis on GCE for NO_3^- at -1.6 V leads mainly to NH_3 formation. Reduction of both nitrite and nitrate in acid media occur at more positive potentials and hence are more favourable, than reductions in basic media [77]. However overall, glassy carbon is not suited for the reduction of nitrate or nitrite.

According to Carpenter and Pletcher [71] the reduction wave for nitrate at vitreous carbon occurs just positive to the potential for H_2 evolution and it is difficult to obtain a reproducible current – potential curve. Diamond electrodes have also been used to reduce nitrate to ammonia. Glassy carbon electrodes exhibit larger current densities than diamond electrodes under the same bias, but boron-doped electrodes are remarkably more stable against electrochemical and photoelectrochemical corrosion [78].

The following electrode reactions describe the possible reduction of nitrate and nitrite on carbon electrodes [66]:

	vs Ag/AgCl
$NO_3^- + H_2O + 2e^- \rightarrow NO_2^- + 2OH^-$	-0.19V
$NO_3^- + 3H_2O + 5e^- \rightarrow 1/2N_2 + 6OH^-$	0.06V
$NO_3^- + 6H_2O + 8e^- \rightarrow NH_3 + 9OH^-$	-0.32V
$NO_2^- + 2H_2O + 3e^- \rightarrow 1/2N_2 + 4OH^-$	0.23V
$NO_2^- + 5H_2O + 6e^- \rightarrow NH_3 + 7OH^-$	-0.36V
$NO_2^- + 4H_2O + 4e^- \rightarrow NH_2OH + 5OH^-$	-0.65V

2.3.4 Sulphate reactions

Unfortunately there is not much literature available on the reduction of sulphate, especially on glassy carbon electrodes. In industry sulphate is reduced in the following ways:

- Chemical – reduction with Fe^{2+} in acidic solutions
- Biomimetric reduction [79]
- Thermal reduction of H_2SO_4 at 1000^0C.

Electrolysis of H_2SO_4 with a platinum cathode electrode leads to the formation of H_2S, S and H_2. This reduction is however not due to the direct electrochemical reduction of H_2SO_4, but to reduction by means of hydrogen in the atomic state liberated from water splitting [80, 81].

The proposed reduction process of sulphate is as follows:

$2H_2SO_4 + 8H^+ + 8e^- \leftrightarrow H_2S_2O_6 + 2H_2O$	-0.22 V	(i)
$H_2S_2O_6 + 2H^+ + 2e^- \leftrightarrow 2H_2SO_3$	0.564 V	(ii)
$H_2SO_3 + 4H^+ + e^- \leftrightarrow S + 3H_2O$	0.449 V	(iii)
$S + 2H^+ + 2e^- \leftrightarrow H_2S$ (aq)	0.143 V	(iv)

or the one step reduction to H_2SO_3

$H_2SO_4 + 2H^+ + 2e^- \leftrightarrow H_2SO_3 + H_2O$	0.172 V	(v)

As can be seen the reduction is favoured by acidic conditions. The electrochemical reduction of sulphate in aqueous solutions is thermodynamically possible. Sulphate reduction is however kinetically inhibited and needs high overvoltage to take place [82]. The largest component of the overvoltage is due to the inhibited charge transfer from the

electrode surface to the sulfate in the solution, depending on the electrode material, the temperature, the current density and the physical and chemical conditions of the sulfate, particularly the degree of association between H^+ and SO_4^{2-} which influences the electron distribution along the S-O bond.

Bilal and Tributch [82] found no reduction of sulphate in sulphate salt solutions, even at elevated temperatures (145^0C). Ag and Cu have relatively high hydrogen coverage and reacted with concentrated H_2SO_4 to form SO_2, which is easily reduced to H_2S, forming Ag_2S as well as CuS. With Pt, formation of H_2S is observed only after water splitting (H_2 evolution) took place.

Graphite is a material that remains relatively corrosion resistant in conditions of aqueous sulfate solutions at elevated temperatures compared to other metal electrodes. The layer structure of this material shows hexagonal C-rings with conjugated π-bonds and therefore has a conduction band with delocalized electrons. It offers the interesting possibility that H_2SO_4 forms an intermediate compound $C_mxH_2SO_4$ in which the S-O of the sulphate may be conjugated with the double π-bond system of the hexagonal C-rings in the layer. This compound may have lower activation energy of reduction due to easier charge transfer from the conduction level in graphite to sulphate. Although graphite is a more suitable cathode for the reduction of sulphate it still requires elevated temperatures and relatively high concentrations. Reduction with graphite has H_2S as the main reaction product [82].

2.4 Impedance studies on membranes

Electrochemical impedance spectroscopy (EIS) is a powerful tool for examining processes occurring at the electrode and membrane surfaces. When a circuit is supplied with steady direct current, the impedance equals the total resistance of the circuit. The resistance depends upon the number of electrons that are free to become part of the current and upon the difficulty that the electrons have in moving through the circuit.

A small amplitude alternating current (ac) excitation signal (potential or current), covering a wide range of frequencies, is applied to the system under investigation and the response (current or voltage or another signal of interest) is measured. If the input signal (potential) is sinusoidal, the response would be an ac current signal containing the excitation frequency and its harmonics [83]. Due to the small amplitude of the excitation signal the measurement can be carried out without significantly disturbing the properties being measured.

Comparison is usually made between the electrochemical cell and the equivalent electrical circuit that contains combinations of resistances and capacitances.

Due to the wide range of frequencies used, the complex sequence of coupled processes such as, electron transfer, mass transport, chemical reaction, etc. can often be separated and investigated with a single measurement. EIS is routinely used in electrode kinetics and mechanism investigations, and in the characterization of batteries, fuel cells and corrosion phenomena [84, 85].

a) Principles of AC circuits

For the application of a sinusoidal voltage (excitation signal) at time t:

$$V(t) = V_o \sin \omega t \qquad (A)$$

V_o = the maximum amplitude

ω = the frequency (rad s^{-1}) of an electrical circuit that contains a combination of resistances and capacitances which will adequately represent the electrochemical cell

$\omega = 2\pi f$

f = frequency in Hz

The response is given by:

$$I = I_o \sin (\omega t + \varphi) \qquad (B)$$

φ = the phase angle between the perturbation and the response.

Therefore

$$Z = \frac{V(t)}{I(t)} = \frac{V_0 \cos(\omega t)}{I_0 \cos(\omega t - \varphi)} = \frac{Z_0 \cos(\omega t)}{\cos(\omega t - \varphi)} \qquad (C)$$

with Z_o = the amplitude of the impedance

$\frac{\cos(\omega t)}{\cos(\omega t - \varphi)}$ = the phase shift

The proportionality factor between V and I is the impedance, Z. Impedances consist of resistances, reactances (derived from capacitive elements) and inductances (but only at very high frequencies) [84 - 87].

b) Resistance

In the case of pure resistance < R, Ohm's law V = IR, leads to:

$$I = \frac{V_0 \sin(\omega t)}{R} \qquad (D)$$

and $\varphi = 0$.

There is no phase difference between the potential and current.

c) Capacitance

For the pure capacitor

$$I = C \frac{dV}{Dt} \qquad (E)$$

Substituting dV/dt into (A) leads to

$$I = \omega C V_o \sin(\omega t + \pi/2) \qquad (F)$$

$$= \frac{V_0 \sin(\omega t + \pi/2)}{X_C} \qquad (G)$$

$X_C = (\omega C)^{-1}$ = the reactance (measured in ohms).

The diagram below is a representation in the complex plane of impedance containing resistive and capacitive components.

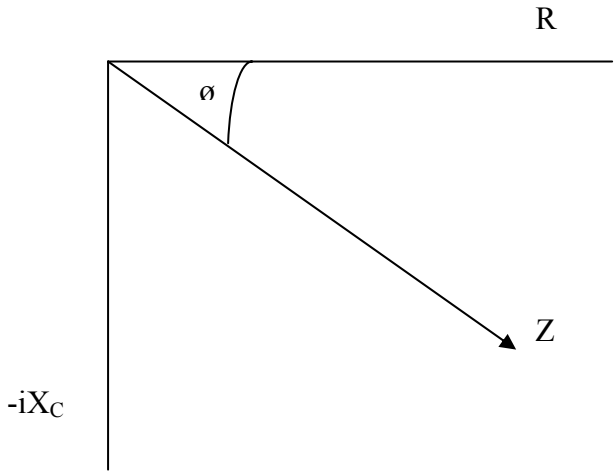

On the x-axis the phase angle is zero; rotating anticlockwise about the origin the phase angle increases; pure reactances are represented on the y-axis. The distance from the origin corresponds to the amplitude. Therefore the real axis is for resistances and the imaginary axis is for reactances. By convention the current is always on the real axis. Thus it becomes necessary to multiply the reactance by –i (√ - 1) [85, 87, 88].

2.5 Conductivity across ion exchange membranes

2.5.1 Conductivity of ions in solution

Electrical conductivity is a measure of a material's ability to conduct an electric current. The conductivity σ is defined as the ratio of the current density J to the electric field strength E:

$$J = \sigma E \qquad \text{(eq 1)}$$

Conductivity is measured in the SI unit siemens per meter ($S.m^{-1}$). Electrical conductivity is the most accurate way to determine the TDS (total dissolved solids) in solutions. TDS is the total amount of organic and inorganic dissolved substances in a particular liquid. The value of TDS is also related to the salinity of the water. Electrical conductivity of water is directly related to the concentration of dissolved ionised solids in water. Ions from the dissolved solids create the ability for the water containing the TDS to conduct electric current, which can be measured using a conventional conductivity meter. The more salt in the water, the more easily it conducts electricity [8].

$$TDS\ (mg/L) = 640 \times EC\ (dS.m^{-1})$$

Seawater has a conductivity of 5 $S.m^{-1}$ at 20^0C.

The fundamental measurement used to study the motion of ions is that of electrical resistance, R, of the solution. Conductance, C, is the inverse of resistance:

$$R = 1/C \qquad \text{(eq 2)}$$

Therefore one siemens is equivalent to Ω^{-1}.

$$C = \frac{\sigma A}{l} \qquad \text{(eq 3)}$$

A = Area of motion

l = length of the cell used

The conductivity of a solution depends on the number of ions present and the molar conductivity, Λ_m (S m^2mol^{-1}).

$$\Lambda_m = \frac{\sigma}{C} \quad \text{(eq 4)}$$

C = molar concentration

Ions interact with each other and therefore the conductivity may not be exactly proportional to the concentration of ions in the solution.

The molar conductivity of strong electrolytes decreases only slightly as the concentration is increased. Strong electrolytes fully ionise in solution.

$$\Lambda_m = \Lambda_m^0 - K\, c^{1/2} \quad \text{(eq 5)}$$

Λ_m^0 = limiting molar conductivity

K = Kohlausch's constant

Λ_m^0 is the molar conductivity in the limit of zero concentration (when the ions are so far apart they do not interact).

In ionic solutions

$$\Lambda_m^0 = \upsilon_+ \lambda_+ + \upsilon_- \lambda_- \quad \text{(eq 6)}$$

υ = the number of ions in a formula

λ = the molar conductivity of the ions

Table 2.1 tabulates the molar conductivities, λ, of the ions that will be investigated in this study (S m^2mol^{-1}) [89]:

Table 2.1: The molar conductivities, λ, of the ions under investigation

Ion in solution	molar conductivities, λ (S m^2mol^{-1})	Ion in solution	molar conductivities, λ (S m^2mol^{-1})
H^+	34.96	OH^-	19.91
Cl^-	7.63	Na^+	5.01
SO_4^{2-}	16.00	Mg^{2+}	10.60
NO_3^-	7.15	K^+	7.35

2.5.2 Mobility of ions in solutions

Although the motion of ions remains largely random, the presence of an electric field influences their motion, and ions undergo net immigration through the solution. A cation

responds to the application of a electric field by accelerating towards the negative electrode and an anion responds by accelerating towards the positive electrode. The acceleration is however short-lived and they experience frictional forces that bring them to their drift speed. This drift speed governs the rate at which charge is transported; the conductivity can be expected to decrease with increasing solution viscosity and ion size. This holds true for larger molecules, but a paradox occurs with smaller alkali metals, where the hydrodynamic radius must also be taken into account. Smaller ions can be extensively solvated; therefore an ion of smaller ionic radius may have a large hydrodynamic radius, and drag many solvent molecules through the solution as it migrates. The mobilities of the ions under investigation are listed in Table 2.2 [89].

Table 2.2: The mobilities, μ, of the ions under investigation ($10^{-8}m^2s^{-1}v^{-1}$)

Ion under investigation	mobility of ion, μ ($10^{-8}m^2s^{-1}v^{-1}$)	Ion under investigation	mobility of ion, μ ($10^{-8}m^2s^{-1}v^{-1}$)
H^+	36.23	OH^-	20.64
Cl^-	7.91	Na^+	5.19
SO_4^{2-}	8.29	Mg^{2+}	
NO_3^-	7.40	K^+	7.62

Ionic mobilities provide a link between measurable and theoretical quantities.

$\lambda = z \mu F$

F = Faraday constant (= $N_A e$)

Therefore the limiting current Λ_m^0 for ions in solution is

$$\Lambda_m^0 = z (\mu_+ + \mu_-) F$$

2.6 References

1. GE Infrastructure Water and Process technologies, Ionics case study 5400, www.ionics.com, accessed July 2006
2. Reahl, E. R. Ionics Incorporated technical paper. Half a century of desalination with electrodialysis. Delaware (USA), 2004
3. Clayton, R. Desalination for water supply. Review of current knowledge. Foundation for Water Research. Florida (USA) 2006

4. Shelp, G.; Seed, L. P.; De Beer, M.; Maree, J.; Strobos, G. The DesEl system – Capacitive deionization for the removal of ionic contaminants from water. Technical Report 2004. ENVIRONMENTREK, CSIR, Pretoria, South Africa
5. Younos, T.; Tulou, K. E. Journal of Contemporary Water Research and education, **2005**, 132, 3-10
6. Wang, S.; Jin, M. Desalination, **2000**, 132, 349-352
7. Bee, B. R.; Errede, L. A.; Jefson, G. B.; Langager, B. A. United States Patent 4,153,661 (1979)
8. Wikipedia, the free encyclopedia. http://en.Wikipedia.org/wiki/carbon_element, updated 2005
9. Wikipedia, the free encyclopedia. http://en.Wikipedia.org/wiki/waterdesalination, updated March 2006
10. Kinoshita, K. Carbon: Electrochemical and Physiciochemical Properties, Wiley, New York (1988), Chapter 2
11. Barbero, C.; Silber, J. J.; Sereno, L. J. Electroanal. Chem., 1988, 248, 321-328
12. Cifrian, M.; Kordesch, K. Handbook of Fuel Cells – Fundamentals, Technology and Applications. John Wiley & Sons, Chichester, 2003. Volume 1 (4) 267-280
13. Schiraldi, D. A. Pol. Rev. **2006**, 46 (3), 315-327
14. Kim, J. Y; Lee, H.K.; Kim, S. C. J. Mem. Sci. **1999,** 163 (2), 159-166
15. Laporta, M.; Pegoraro, M.; Zanderighi, L. Phys. chem. chem. phys. 1999, 19 (1), 4619-4628
16. Li, S.; Liu, M. Electrochim. Acta **2003,** 48, 4271–4276
17. Walls, J. M.; Smith, R. Surface science techniques. Loughborough University of Technology, Loughborough, Leicestershire (1992) pp 1-4
18. Tanaka, K.; Nishimori, K.; Maeda, K; Matsuda, J.; Hotta, M. Journal of Tribology, **1992**, 114 (2), 274 - 279
19. Yalamanchili, M. R.; Veeamasuneni, S.; Azevedo, M. A. D.; Miller, J.D. Colloids and Surfaces. A: Physiochemical and Engineering Aspects, **1998**, 133, 77-88
20. Goh, M. C; Markiewicz, P. Chemistry and Industry (London) **1992**, 18, 687-691

21. Earwaker, L. G. Rutherford Backscattering and Nuclear Reaction Analysis. School of Physics and Space Research, University of Birmingham, Edgbaston, Birmingham. 135 – 155
22. Dean, J. A. The Analytical Chemistry Handbook. New York. McGraw Hill, Inc. 1995. Section 15.1 -15.5
23. Pungor, E.A. A Practical Guide to Instrumental Analysis. Boca Raton, Florida. 1995. pp 181 – 191
24. http://en.Wikipedia.org/wiki/thermogravimetric_analysis updated July 2006
25. Smith, B.C. Fundamentals of Fourier Transform Infrared spectroscopy. CRC Press, Boca Raton. 1996
26. Yeager, E. J. Mol. Cat. **1986**, 38, 5-25
27. Lai, M.E.; Bergel, A. J. Electroanal. Chem. **2000**, 494, 30-40
28. Yeager, E. Electrochim. Acta, 1984, 29 (11), 1527-1537
29. Zhang, Z.W.; Tryk, D.; E.Yeager. Electrode kinetics of the O_2/HO_2^- couple on glassy carbon in alkaline solution, loc. Cit. Extended abstracts, Vol. 83 –2, Abst. 394.
30. Taylor, R.J.; Humffray, A.A. J. Electroanal. Chem. **1975**, 64, 63-83
31. Taylor, R.J.; Humffray, A.A. J. Electroanal. Chem. **1975**, 64, 85-94
32. Appel, M.; Appleby, A. J. Electrochim. Acta, **1978,** 23, 1243-1246
33. Morcos, I.; Yeager, E. Electrochim. Acta, **1979**, 25, 195-203
34. Xu, J.W.; Huang, R.; McCreery, L. J. Electroanal. Chem. 1996, 410, 235-242
35. Garten, V. A.; Weiss, P.E Austral. J. Chem. **1955**, 8, 81-84
36. Bielski, B. H. J.; Allen, A. O. J. Phys. Chem. **1977** 81, 1048-1054
37. Yang, H.; McCreery, R. L. J. Electrochem. Soc. **2000,** 147 (9), 3420-3428
38. Taylor, R.J.; Humffray, A.A. J. Electroanal. Chem. **1975**, 64, 95-105
39. Tammeveski, K.; Kontturi, K.; Nichols, R. J.; Potter, R. J.; Schiffrin, D.J. J. Electroanal. Chem. **2001,** 515, 101-112
40. Hossain, M.S.; Tryk, D.;Yeager, E. Electrochim. Acta, 1989, 34 (12), 1733-1737
41. Thomassen, M.; Børresen, B.; Hagen, G.; Tunold. R. Electrochim. Acta, **2005**, 50 1157-1163
42. Czarnetzki, L.; Janssen. L.J. J. Electrochim. Acta, **1988**, 33 (4), 561 – 566
43. Harrison, J.A.; Khan, Z. A. J. Electroanal. Chem. **1971,** 30, 87 –92
44. Dickinson, T.; Greef, R.; Wynne-Jones, L. Electrochim. Acta, **1969**, 14,467
45. Arikado, T.; Iwakura, C.; Tamura, H. Electrochim. Acta. **1978**, 23, 9 – 15

46. Tomcsanyi, L.; De Battisti, A.; Hirschberg, G.; Varga, K.Electrochim. Acta, **1999**, 44, 2463 – 2472
47. Moore, R. R.; Banks, C. E.; Compton, R. G. Analyst, **2004,** 129, 755-761
48. Janssen, L. J. J. Electrochim. Acta, **1974,** 19, 257 – 265
49. Janssen, L. J. J.; Hoogland, J. G. Electrochim. Acta, **1970**, 15, 941 – 951
50. Hine, F.; Yasuda, M.; Iwata, M. J. Electrochem. Soc. **1974**, 749-757
51. Novak, D. M.; Tilak, B. E.; Conway, B.E. Modern Aspects of Electrochemistry No 14. Plenum Press, NY (1982) 195-318
52. Lowe, E.R.; Banks, C.E.; Compton, R.G. Anal Bioanal Chem. **2005**, 382, 1169 – 1174
53. Agoitia, A.; Martin, H. B.; Angus, J.C.; Landau, U. Diamond Materials V, Davidson, J. L.; Brown, W. D.; Gicquel, A.; Spitsyn, B. V.; J. C. Angus, Editors, The Electrochemical Society Proceedings Series, Pennington, NJ (1997) PV 92 – 32, p364
54. Ferro, S.; De Battisti, A.; Duo, I.; Comninellis, C.; Haenni, W.; Perret, A. J. Electrochem. Soc. **2000**, 147(7), 2614 – 2619
55. Kodera, F.; Umeda, M.; Yamada, A. Anal. Chim. Acta, **2005** ,537, 293-298
56. Murphy, A.P. Nature. **1991**, 350**,** 223 –225
57. Mateju, V.; Cizinska, S.; Krejci, J.; Tomas, J. Enzyme. Microb. Tech. **1996**, 14, 170
58. Hell, F.; Lahnsteiner, J.; Frischhertz, H.; Baumgartner, G. Desalination, **1998**, 117, 173 –180
59. Hu, H-Y.; Goto, N.; Futjie, K. Wat. Res. **2001**, 35 (11), 2798 – 2793
60. Heckner, H.N. J. Electroanal. Chem. **1973**, 44. 9-21
61. Blokhiva, A.P.; Izinov, S.O. Electrokhimiya **1972**, 8, 29-36
62. Van der Plas, J.F.; Barendrecht, E.; Electrochim. Acta, **1979**, 25, 1463-1468
63. Horanyi, G.; Rizmayer, E.M. J. Electroanal. Chem. **1985**, 188, 265
64. Solak, A.O.; Gülser, P.; Gökmeçe, E.; Gökmeçe, F. Microchim. Acta. **2000**, 134, 77-82
65. Nishimura, K.; Mashida, K.; Enyo, M. Electrochim. Acta, **1991**, 36 (516) 877
66. Chebotareva, N.; Nyokong, T. J. Appl. Electrochem. **1997**, 27, 975 –981
67. W.M Latimer. The oxidation state of the elements and their potentials in aqueous solutions. Chapter 7. New York Prentice Hall, Inc. 1938
68. Ureta-Zañartu, S.; Yañez, C. Electrochimica Acta, **1997**, 42 (11), 1725-1731

69. Pletcher, D.; Poorabedi, Z. Electrochim. Acta. **1979**, 24, 1253
70. Dima, G.E.; De Vooys, A. C. A.; Koper, M. T. M. J. Electroanal. Chem. **2003**, 554-555, 15-23
71. Carpenter, N.G.; Pletcher, D. Anal. Chim. Acta, **1995**, 317, 287 –293
72. De Vooys, A. C. A.; Beltrama, G. L.; Van Riet, B.; Van Veen, J.A.R.; Koper, M.T.M. Electrochim. Acta, **2004**, 79, 1307 –1314
73. Newbery, J. E.; Lopez de Haddad, M. P. Analyst, **1985**, 110, 81 –82
74. Kaminskaya, O.V.; Zakhaova, E. A.; Slepchenko, G. B. J. Anal. Chem. **2004**, 59 (11), 1091 – 1096
75. Jiang, L.; Wang, R.; Li, X.; Jiang, L.; Lu, G. Electrochem. Comm. **2005**, 7, 597-601
76. Xiaorong, T.; Cheng, F.; Bing Y.; Wuming, Z. Microchem. Jnl. **1999**, 62, 377 – 385
77. Sun, W.; Zhang, S.; Liu, H.; Jin, L.; Kong, J. Anal. Chim. Acta, **1999**, 388 (1-2) 103-110
78. Tenne, R.; Patel, K.; Hashimoto, K.; Fujishima, A. J. Electoanal. Chem. **1993**, 347, 409-415
79. Shigeru, O. A. E.; Togo, H. Bull. Chem. Soc. Jpn. **1983**, 56, 3828
80. Schluederberg, C. G. J. Phys. Chem**. 1908**, 12, 574
81. Brandcroft, W. D.; Magoffin, J.E. J. Am. Soc. **1935**, **57,** 2561
82. Bilal, B.A.; Tributsch, H. J. Appl. Electrochem. 1998, 28, 1073 -1081
83. Application notes from Gamry instruments (http://www.gamry.com) accessed May 2006
84. Priscilla G.L. Baker. PhD Thesis (2004). Sol-Gel Preparation, characterization and electrochemistry of mixed metal tin oxide electrodes. Chapter six. University of Stellenbosch. 76 – 113
85. Macdonald, D. D.; Urquidi-Macdonald, M. J. Electrochem. Soc. **1985**, 132, 2316
86. Textbook of electrochemistry. G. Kortüm, JO' M Bockris, volume 1951
87. Lancaster, G., Dc and Ac circuits, Oxford Physics Series, Oxford University Press, 1973
88. Brett, C. M. A; Brett, A. M. O. Electrochemistry. Priciples, methods and applications. (1996) Oxford Univerity Press. Chapter 11, 224 – 251
89. Atkins, P. W. Physical chemistry. Sixth edition 1998. Oxford University Press. Chapter 24

Chapter 3

Experimental

3.1 Introduction

The elemental composition of the composite carbon membrane was determined by XRD and confirmed by PIXE. Thereafter it was characterized using TGA, DSC, FTIR and LC-MS. The surface morphology of the membrane was investigated using SEM and AFM. CV and LSV were used for electrochemical evaluation of the carbon electrodes in the custom ED cell. EIS was used to acquire an equivalent electrical circuit, which could model the cell in terms of capacitors and resistors. This could be used to explain the results of the conductivity studies and determine the various interface reactions (between the electrolyte and membrane, electrode and membrane, etc.).

3.2 Elemental analysis of the carbon composite membrane

3.2.1 EDX and PIXE analysis of the carbon composite membrane

Compositional analysis of the composite carbon membrane was obtained by PIXE and EDX. for PIXE, a Van der Graaf accelerator was used to bombard a sample of membrane with protons and the energy of the beam was kept at 3 eV. A selected section of the membrane surface (5 μm × 5 μm), taken to be representative of the total surface composition (5 mm × 5 mm), was bombarded. The backscattered energy was recorded using an X-ray detector. Semi quantitative on-line imaging was made possible by the use of a GEO-PIXE suite of programs. The composition (ppm of element) was based on matrix determination.

An EDX (X-ray analyzer) is a link system fitted to the Leo 1430 scanning electron microscope, using AN1000 software. For X-ray analysis the working distance was 13 mm and the accelerated voltage was 25 kV.

3.3 Characterization of the carbon composite membrane

3.3.1 TGA and DSC analysis of the carbon composite membrane

A Perkin Elmer, Thermal Gravimetrical Analyzer 7, was used to carry out the TGA analysis. The sample was heated from an initial temperature of 45^0C to 750^0C, at a constant rate of 10^0C/min and 2^0C/min, and the sample weight loss was monitored.

DSC analysis was done on a DSC-Q100, manufactured by TA instruments. The sample was heated from 20^0C to 440^0C, where the sample was completely degraded. The sample was again heated at a constant rate of 10^0C/min.

3.3.2 SEM and AFM surface analysis of the membrane

SEM and AFM were employed to determine the characteristics of the surface topography of the membrane. A Leo 1430VP scanning electron microscope was fitted with a Backscatter detector and the images were obtained at 20000 × and 10000 × magnification. The working distance was 12 mm and an accelerated voltage of 7.5 kV was applied. The samples were coated with a 15 nm layer of gold.

AFM measures the topography with a force probe. The micrographs were taken with a Multimode AFM from Veeco (USA). Images were acquired in non-contact mode with a low resonance frequency cantilever (160 kHz).

3.3.3 FTIR analysis

FTIR was used to identify the various functional groups of the various compounds inside the composite membrane. Mid-range FTIR (700 cm^{-1} to 4000 cm^{-1}) spectra were recorded of the composite membrane with a Thermo-Nicolet Avator 330 FT-IR. The samples were compressed with a Nicolet Smart Performer between ZnSe plates.

3.3.4 LC-MS analysis

For LC-MS a Waters API Q-TOF Ultima instrument was employed with a Waters Acquity UPLC BEH column, 2.1x50mm. The LC was run at a constant rate of 3.5 mL/min with a mobile phase of 40% (m/v) acetonitrile. An ESI source, with a capillary voltage of 3.5 kV, was used to ionize the molecules.

3.4 The custom-made ED cell for comparative studies

For a comparative study, a custom cell was build to investigate the conductivity across the membrane and for electrochemical evaluation with EIS. A image of this ED cell is given in Figure 3.1.

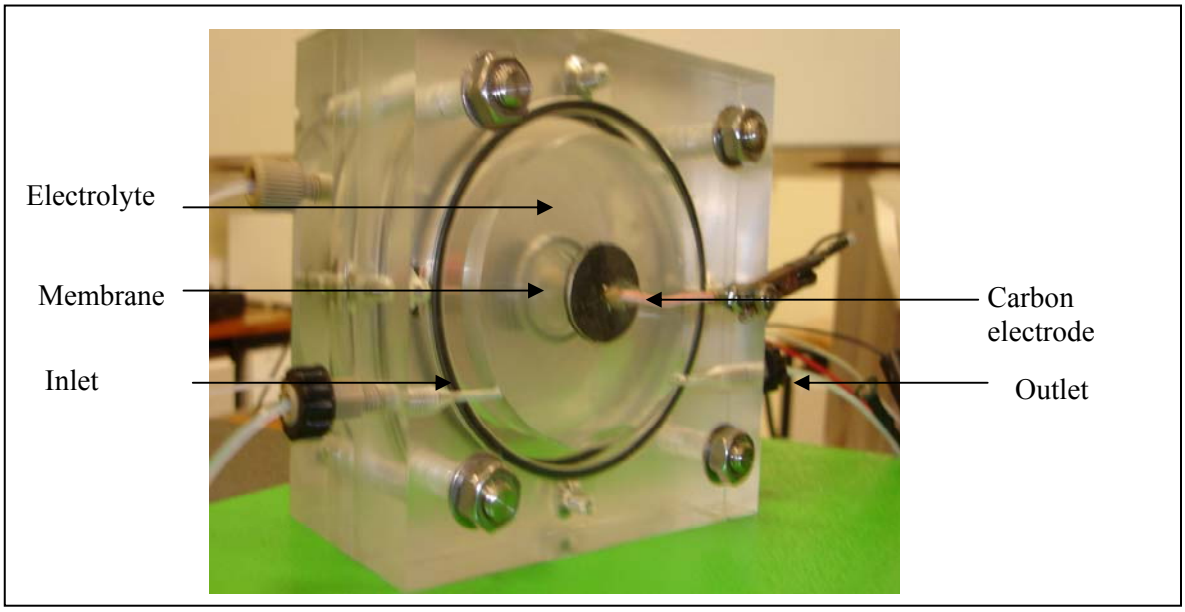

Figure 3.1: The custom-made electrodialysis cell used to investigate the conductivity through the membrane and for EIS studies.

The cell was constructed from Perspex. It was fitted with two glassy carbon electrodes with a surface area of 2.54 cm^2. The two compartments both had an inlet and an outlet. The inlet was connected to a Watson Marlow digital pump and the outlet was connected to anexternal reservoir. The electrolyte in each compartment was continuously circulated through the pump to an external reservoir containing a 4330 Jenway conductivity/pH meter. Each compartment had a volume of 17.24 cm^3. The electrode was situated 0.7 cm from the membrane. The total surface area of the membrane on either side was equal to that of the electrode (2.54 cm^2). Figure 3.4 gives a schematic representation of the experimental setup used for the conductivity studies.

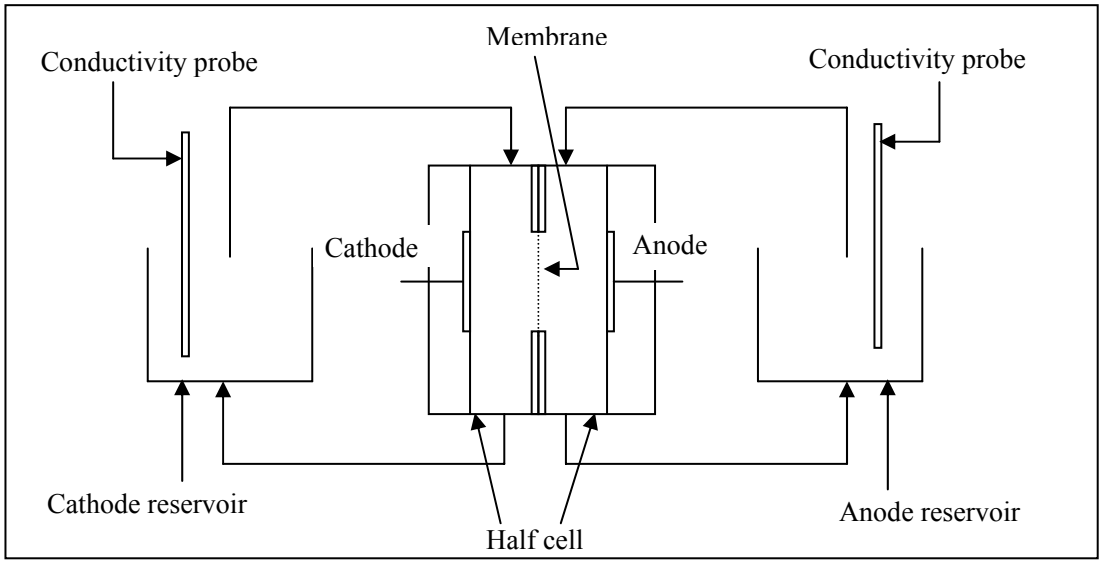

Figure 3.2: Schematic representation of the experimental setup used for conductivity studies.

3.5 Electrochemical studies of simple anions

The oxidation and reduction reactions of various anions were studied on the commercial glassy carbon electrode (GCE), the carbon sheet employed as an electrode in the desalination pilot plant, and the glassy carbon inside the prototype ED-cell made for this project. These various reactions were studied and compared using cyclic voltammetry (CV) and linear sweep voltammetry (LSV).

These voltammetric experiments were carried out with an electrochemical analyser, Epsilon EC. A three-electrode system was employed. A Ag/AgCl reference electrode was used for all three carbon electrodes, but for the commercial glassy carbon electrode a Pt wire was used for a counter electrode, whereas a platinum mesh was used for the carbon sheet and the ED-cell carbon electrode. The working electrodes were the GCE, the carbon sheet and the custom glassy carbon electrode (in the ED-cell).

These experiments were carried out at 20^0C within a potential window of -1500 mV and 1500 mV. The measurements were recorded at different scan rates: 20 mV/s, 50 mV/s and 100 mV/s for CV and 1mV/s, 5mV/s, 10 mV/s, 20 mV/s and 100mV/s for LSV. The concentrations of the electrolyte solutions were varied from 0.001M to 0.05M and solutions were deaerated by bubbling with nitrogen gas for 5 to 10 minutes. The pH of the electrolyte was also varied (pH 2, pH 6 and pH 9). pH was measured with a 4330 Jenway

conductivity/pH meter. The electrolyte solutions were NaCl, HCl, $MgSO_4$, H_2SO_4, KNO_3 and HNO_3, of varying concentrations.

3.6 Conductivity studies across the composite carbon membrane

The cell described in Section 3.4 was used to determine the conductivity/mobility of the ions through the composite membrane. The cell was filled with different electrolyte solutions on either side of the membrane and the difference in conductivity was measured with a 4330 Jenway conductivity/pH meter. Measurements were done for up to 400 minutes. These various electrolytes were also investigated at various concentrations and various pHs (pH 2, 7 and 9).

3.7 Impedance studies

EIS was used to determine the electrical parameters of the composite carbon electrode in the custom-made ED cell as well as the electrical parameters associated with the interface of the 0.05M electrolyte solutions within this composite membrane. The electrolyte solutions employed here were NaCl, $MgSO_4$ and KNO_3.

EIS measurements were carried out over a frequency range of 10 kHz to 100 mHz, with an AC voltage amplitude of 5mV. The response of a sample was measured over a wide frequency range and then analysed in the complex plane. The frequency response analyzer was an Autolab, Model PGSTAT 30, and the potentiostat (Solartron 1286) was used for electrochemical control. Data manipulation was done with Z-plot (version 2). The cell used for the EIS was the same cell as described in Section 3.4. The cell setup was as follows:

Electrode	Electrolyte	Membrane	Electrolyte	Electrode

Chapter 4

Elemental analysis and characterisation of the composite carbon membrane

4.1. Summary

The composite carbon membrane was subjected to EDS and PIXE for elemental analysis. To determine the functional groups of the various materials that make up the membrane, FTIR and LC-MS were carried out. The thermal properties of the membrane were investigated by DSC and TGA. Surface studies where done with SEM and AFM.

4.2. Introduction

Two composite carbon membranes were used in all investigations, i.e. a darker and a lighter membrane. The darker membrane will be referred to as M1 and the lighter membrane will be referred to as M2. These membranes were manufactured according to US Patent 4,153,166 [1]. To determine the composition of the composite carbon membranes a process of elimination will be followed. The first step was to eliminate possibilities from the content of this patent by means of elemental analysis, thereafter on the grounds of functional groups, and then thermal properties.

The compounds that comprise the membrane under investigation listed in Patent 4,153,661 are briefly summarised below:

1. *Additives*: Polyethylene, polypropylene, hexafluoropropylene tetrafluoroethylene copolymer (PEP), ionomer (Surlyn), polychlorotrifluoroethylene (PCTFE), styrene butadiene block copolymer (Kraton 1107), ethylene vinylacetate copolymer (Elvax 260), cellulose acetate, polyurethane, polyamide
2. *Particulate material*: Koalin ($H_2Al_2O_8Si_2.H_2O$), carbon, talc ($MgO.4SiO_2.H_2O$), titanium dioxide (TiO_2), silica, lead, copper, zinc, aluminum, iron, steel (Fe_3C), copper oxide (CuO), ferrous oxide (FeO), barium ferrite ($BaFe_{12}O_{19}$), mica (SiO_2, Al_2O_3, K_2O, Fe_2O_3, MgO), molybdenum sulphide (MoS_2), silicon carbide (SiC), vermiculite ($(Mg,Fe,Al)_3(Al,Si)_4O_{10}(OH)_2{\cdot}4H_2O$), calcium carbonate ($CaCO_3$), casein ($C_{47}H_{48}N_3NaO_7S_2$), zein, alumina ($Al_2O_3$), garnet ((Mg, Fe, Ca or Mn) with

$Al_2Si_3O_{12}$), phthalocyanine pigment, glass, polyethylene, polypropylene, polyurethane ($C_{22}H_{36}N_2O_8$)

3. *Wetting agents*: Zinc stearate $(CH_3(CH_2)_{16}COO)_2Zn$, ammonium perfluorooctoate
4. *Added thermoplastic*: Casein, zein, cross-linked hide glue and polyamide (with glycerin)
5. *Abrasive particles*: Silica, garnet, alumina, silicon carbide
6. *Dispersing agents:* Polyoxyethylene oxide (Carbowax 750) ($C_{14}H_{30}O_2$), polyoxyethylene distearate $(C_{17}H_{35})_2CO_2CO(CH_2CH_2O)_n$ (Emerest 2642) polyethylene glycol (MW: 727.149 | MF: $C_{44}H_{86}O_7$), lecithin ($C_{37}H_{71}PO_8N$)

4.3. Experimental

The experimental procedures used for characterisation of the carbon composite membrane have been discussed in Section 3.2.

4.4. Results and discussion

4.4.1. Surface and elemental analysis

The abundances of each element in the membrane are given in Table 4.1 as weight percentage, normalised to 100 wt% due to unpolished surfaces. Only elements heavier than boron can be detected and oxygen is calculated as a stoichiometric component. From the results of EDS it was found that there were no metals in either of the two sample membranes tested. The gold listed in Table 4.1 is the gold layer deposited on the membrane for the SEM analysis.

Table 4. 1: Elemental analysis of M1 and M2 as determined by EDS analysis

Element	C %	F %	S %	Cl %	Au %	O %	Total %
M1	21.8	5.6	0.6	9.9	2.5	59.4	100
M2	21.7	6.7		10	3.3	58.2	100
M1 retry (used)	49	25.2		8		17.8	100

Due to the nature of PIXE analysis only elements sodium through uranium could be analysed. Table 4.2 tabulates the results of the PIXE analysis. The only elements to appear

on the PIXE spectra were sulphur and chloride. This also confirmed that no metals were present in any of the membranes. It therefore excludes a large number of compounds listed in the patent, for example, the particulate materials, added thermal plastics, wetting agents and abrasive materials.

Table 4.2: Elemental analysis of M1 and M2 as determined by PIXE analysis

Element	S %	Cl %
M1	0.45	86.32
M2	2.3	68.22

Compounds containing any other elements than those listed in Tables 4.1 and 4.2 were eliminated as possible compounds in the membranes, M1 and M2. The following compounds remained as possible components: polyethylene, polypropylene, cellulose acetate, hexafluoropropylene tetrafluoroethylene copolymer, polychlorotrifluoroethylene, styrene butadiene block copolymer, ethylene vinylacetate copolymer, polyoxyethylene oxide, polyoxyethylene distearate, polyethylene glycol
These compounds are all polymers and most contain carbon, oxygen, hydrogen, fluoride and chloride as principal elements.

The surface of the membrane was investigated with SEM and AFM. The AFM image of M2 in Figure 4.1, illustrated an entangled fibrillated matrix with a particulate material. Upon closer investigation one can see the phase separation in the composite carbon membrane. M2 has a very high surface roughness of 117.7 nm on a 5 μm × 5 μm scan range and 77.7nm on 2μm x 2 μm. The three-dimensional image of M2 confirms the high surface roughness as well as the lack of pores at this enlargement.

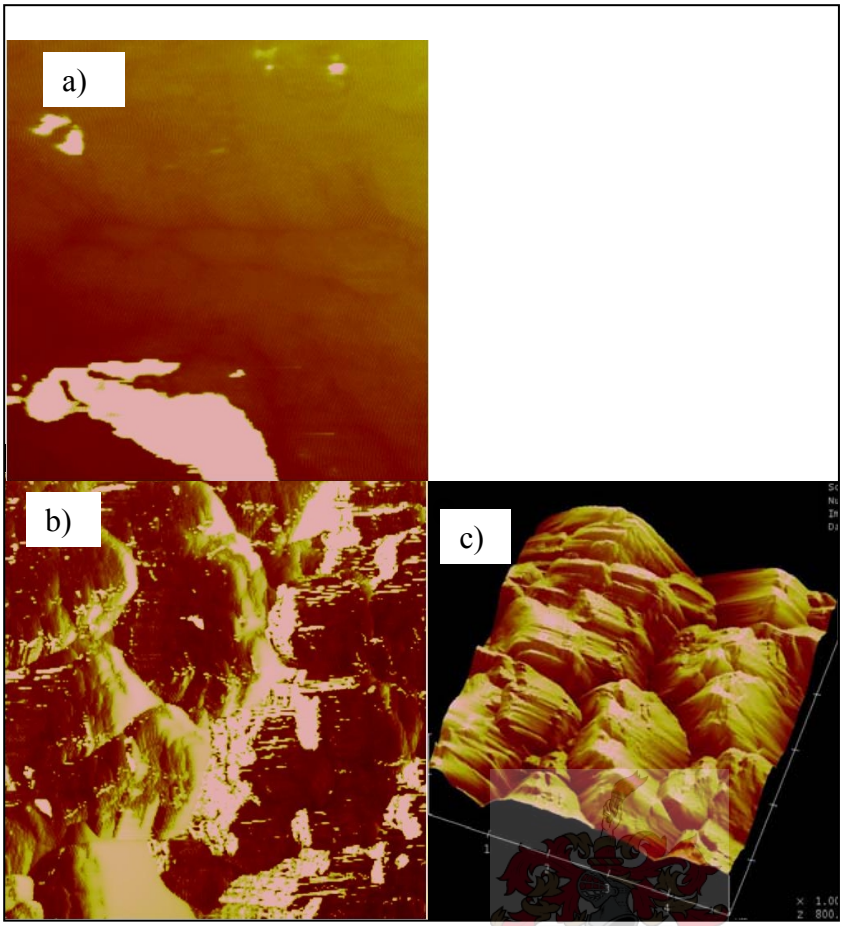

Figure 4.1: AFM images on M2 at a) 5 µm × 5 µm scan range b) at 350 nm × 350 nm scan range and c) in three-dimensional mode

The phase separation of M1 seen in figure 4.2 was not as clear as M2, but the PTFE matrix was more defined. Upon closer inspection the granular particulate material was also observed in between the entangled PTFE. The surface roughness of M1 was also significantly less than M2: 8.2 nm in the 500 nm × 500 nm scan range and 7.1 nm in 350 × 350 nm scan range. No pores were observed on either of the membranes. It is therefore concluded that both membranes contain two phases, but here M1 was more evenly blended than M2.

.

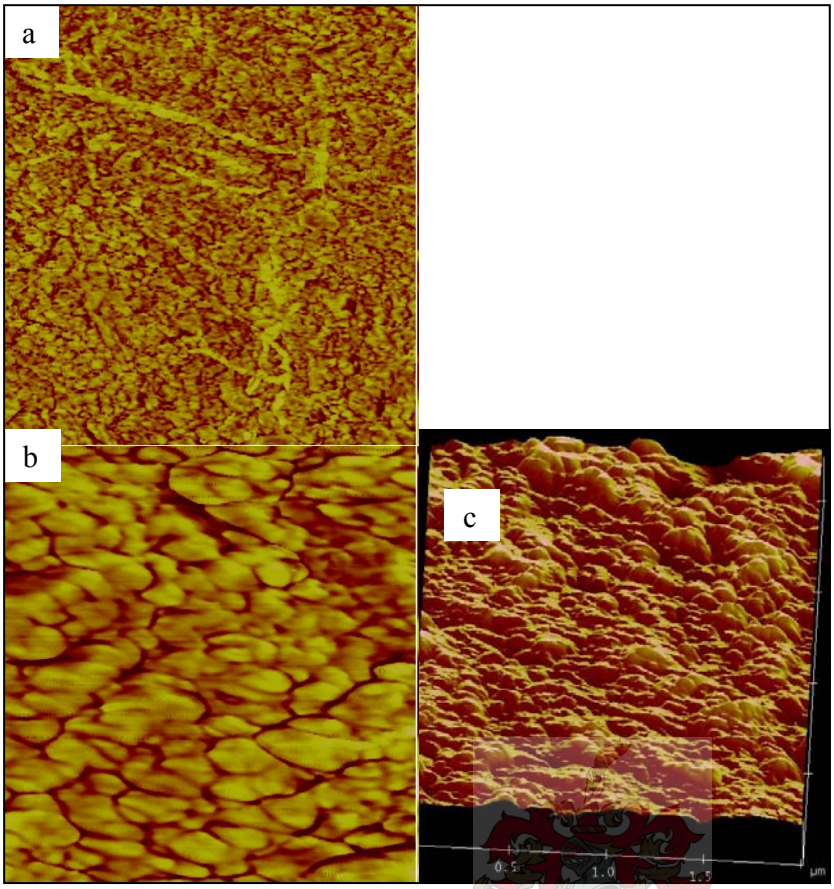

Figure 4.2: AFM images of M1at a) 2 µm × 2 µm, b) 500 nm × 500 nm scan range and c) in three-dimensional mode

Figure 4.3 compares the SEM images of the two membrane surfaces. A more evenly blended surface was observed for M1, whereas M2 had a high degree of surface impurities, which added to the surface roughness observed in the AFM images. Phase separation could not be observed on either of the membranes. SEM also confirmed that there were no visible pores in either of the membranes.

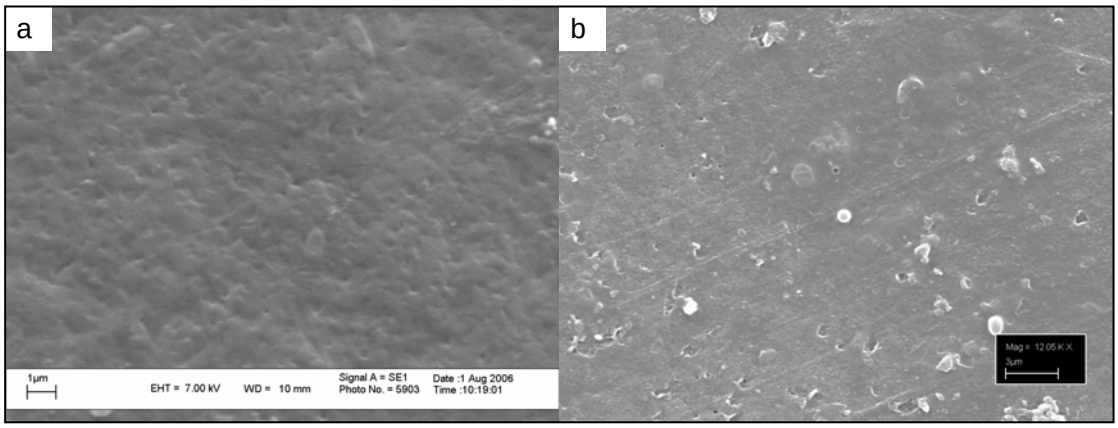

Figure 4.3: SEM images of a) M1 and b) M2 surfaces.

4.4.2 Compositional analysis

a) LC-MS

The membrane samples did not dissolve in any of the common organic solvents. They were only soluble in concentrated sulphuric acid, at elevated temperatures. The author concluded that the membrane consisted of PTFE cross-linked with a particulate material, or that the particulate material was a cross-linked polymer. The higher the degree of cross-linking in a membrane, the higher its mechanical strength will be. Unfortunately, because the membrane was insoluble in anything other than concentrated sulphuric acid characterization by standard analytical methods was very difficult.

After dissolving the membrane in concentrated sulphuric acid, the solution was diluted with deionised water and a LC-MS chromatogram was acquired. Figure 4.4 is a chromatogram of the solution of M2. All the peaks after 5 min are from the water, acid and acetonitrile mobile phase. Two clusters of peaks were observed between 2 and 4 minutes.

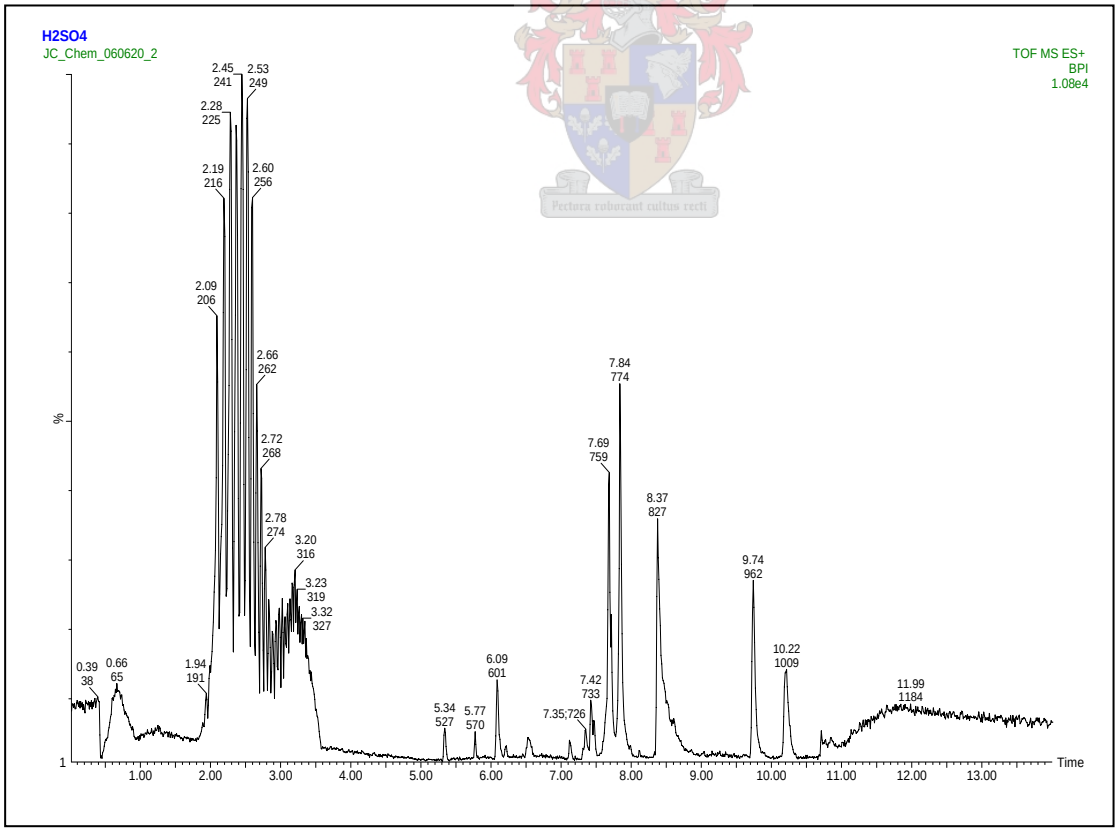

Figure 4.4: LC-MS chromatogram of M2

These two clusters of peaks represent two different polymers. The MS spectra measured for two consecutive peaks in both clusters and are compared in Figure 4.5. All the peaks in both clusters have a molecular ion above 400 m/e. The first set of peaks have molecular ions separated by of m/e = 44 and the second set have a molecular ion difference m/e = 22. These differences represent the approximate molecular weight of a repeating unit in the polymer chains. The overlapping in the two clusters also indicates that the two polymers have similar functional groups.

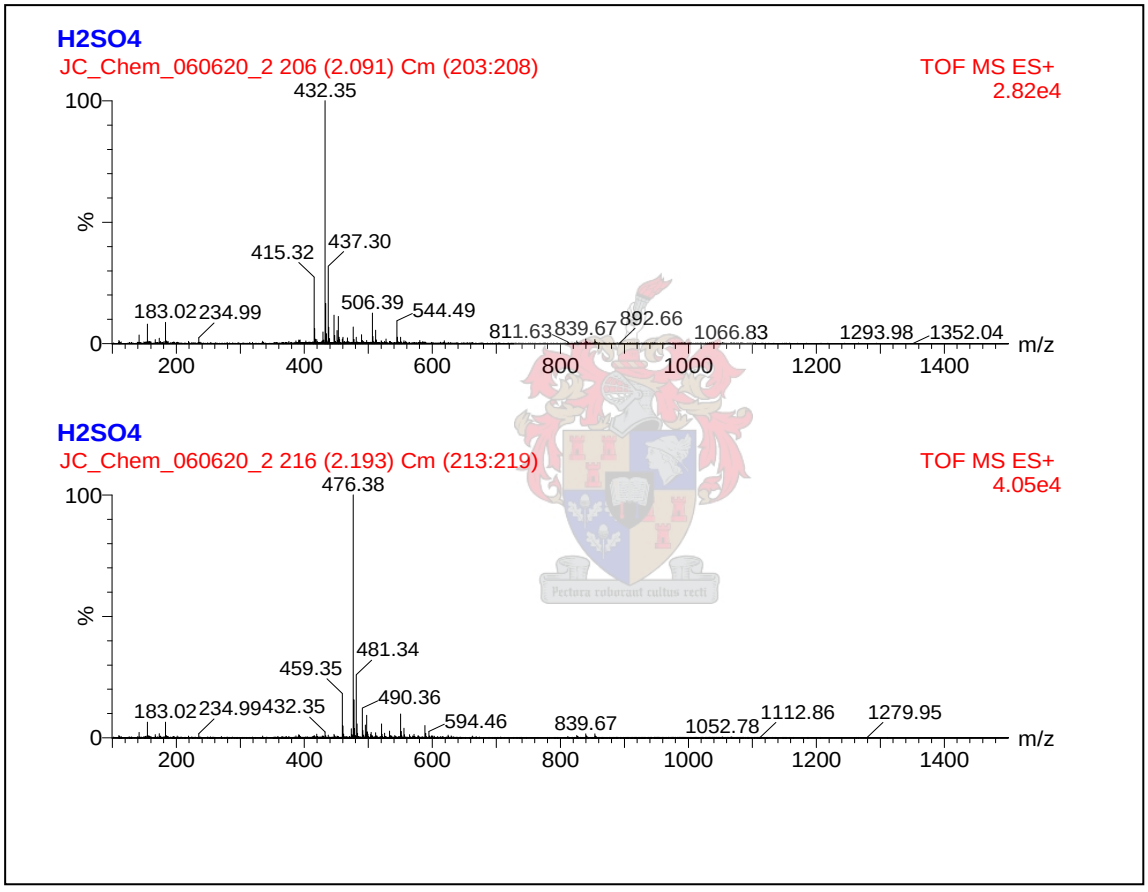

Figure 4.5: MS spectrum of consecutive peaks in the first cluster in the chromatogram in Figure 4.4

b) FT-IR

Figure 4.6 shows the FTIR spectrum of M2. The frequencies (wavenumbers) at which various vibrations are transmitted are tabulated in Table 4.3.

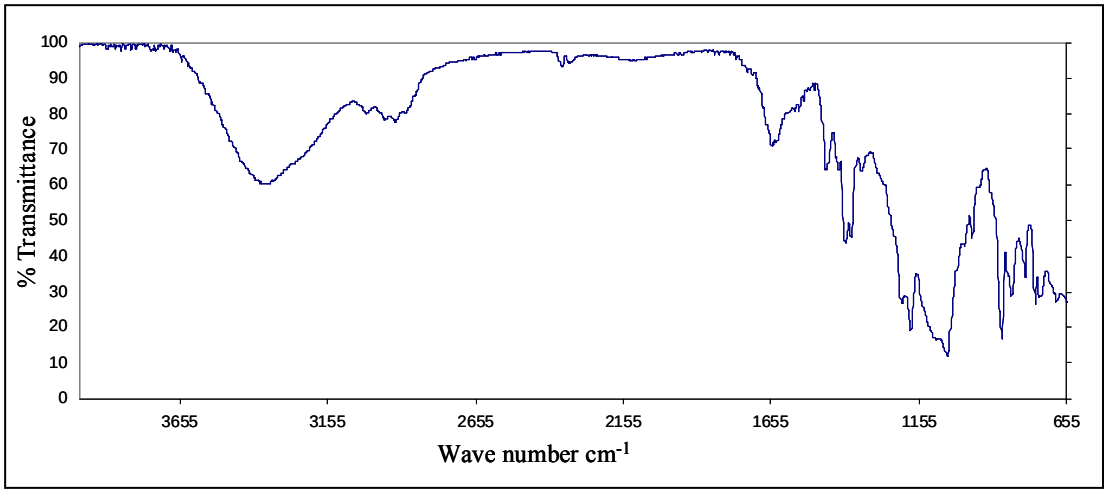

Figure 4.6: FTIR spectrum of M2.

Table 4.3: Assignment of the various vibrations of M2 as observed in Figure 4.6

Wavenumber (cm^{-1})	Assignment
3376	O-H stretch, H-bonded
2969	C-H stretch (alkane)
1650	C=C stretch
1471	-CH_2- bending
1405	C-O-H bending
1214	C-F stretch
1186	C-F stretch
1106	C-F stretch
1062	C-O stretch
875	
842	
798	

Assignments were made according to Pavia [3]. A C-Cl stretch could not be observed in figure 4.6, because the stretch is located outside of the particular window.

The absense of a carbonyl group as well as no evidence of aromatic character reduced the number of possibilities from US patent 4,153.166 to the following:
hexafluoropropylene tetrafluoroethylene copolymer, polychlorotrifluoroethylene, polyoxyethylene oxide, polyethylene glycol

4.4.3 Thermal analysis

Thermal analysis of M1 and M2 was carried out with DSC and TGA. Figure 4.7 contains the thermograms of the TGA analysis of the composite carbon membranes. The samples were measured during a constant heat-rate of 10 ^{o}C/min. At an onset temperature of 276 ^{o}C a mass loss of 23 % had already occurred. At 356 ^{o}C, 39.8 % weight loss occurred. At 702 ^{o}C another 20.2 % weight was lost.

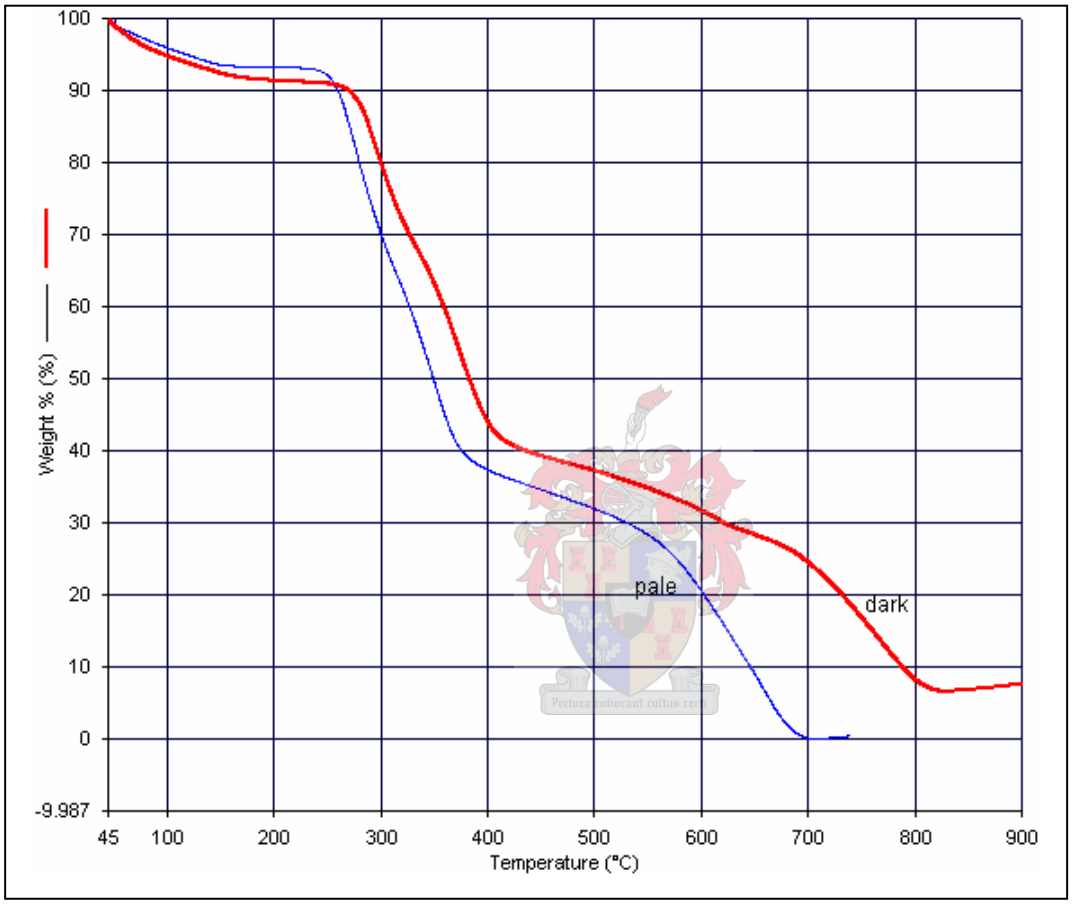

Figure 4.7: TGA thermogram for M1 (dark) and M2 (pale).

After about 450 ^{o}C degradation of the polymer occurs and no meaningful information about the compounds in the membrane can be determined. The two primary weight loss processes is an indication that the composite membranes consist of two primary compounds. From the TGA thermogram it is also clear that the same compounds are present in both membranes. Further thermal investigation included DSC analysis. DSC provides information on the thermal properties of a polymer such as the glass transition temperature (Tg), melting temperature (Tm) and the crystallization temperature (Tc). Above Tg, the secondary, non-covalent bonds between the polymer chains become weaker in comparison to thermal

motion, and the polymer becomes rubbery and capable of plastic or elastic deformation. This behaviour is not observed in cross-linked thermosetting plastics. Once set, they will shatter rather than deform, never becoming plastic again when heated, nor melting.

If the polymers in the compound are known, then the respective enthalpies of transition can also be determined.

DSC analysis of M2 was carried out at a constant heating rate of 2 ^{o}C / min and 10 ^{o}C /min. The results for M2 are illustrated in Figure 4.8. The positive peak represent crystallization, whereas the negative peaks represent melting processes. The Tg appears as simply a step in the baseline. A melting peak was observed at 138 ^{o}C for both heating rates.

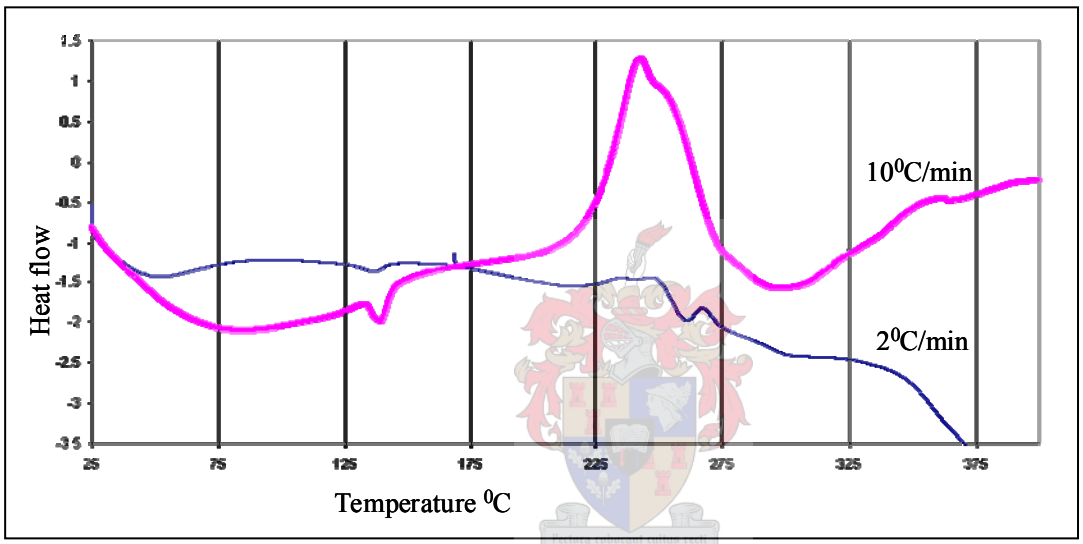

Figure 4.8: DSC thermogram for M2 recorded at heating rates of 2 ^{o}C/min and 10 ^{o}C/min.

For the quicker heat-rate, a crystallization peak was observed at 256 ^{o}C and another melting peak appeared at 300 ^{o}C. For the slower heat rate the enthalpies of transition (area beneath the peak) were much less, and the membrane seemed to be degrading throughout the scan. Additional melting temperatures were observed at 52 ^{o}C and 261 ^{o}C. The crystallization peak observed for the quicker heat-rate was split into two peaks during the slower scan (238 ^{o}C and 248 ^{o}C). After 275 ^{o}C the membrane degrades and no further useful information can be extracted from the thermogram. PTFE has a crystalline melting temperature of 327 ^{o}C and the Tg is in the area of 125 ^{o}C, but neither of these was observed on the DSC thermogram.

4.4. Conclusions

Elemental analysis shows that only five elements are present in the membrane, i.e. chloride, fluoride, oxygen, carbon and possibly hydrogen. The sulphur observed in the elemental analysis is thought to be due to impurities from instrumentation, due to the fact that it is not included in the patent possibilities.

Determination of functional groups by IR analysis determined that no carbonyls or aromatic compounds are present in the membrane. Strong alcohol absorption is however observed. This is an indication that the membrane is alkaline and possibly used as an anion-exchange membrane. Because the membrane can only be dissolved under extreme conditions, it is now concluded that at least one of the compounds is a cross-linked polymer. LC-MS indicated only two clusters of peaks, which may indeed be of the same family.

After functional and elemental analysis the following possibilities remained: hexafluoropropylene tetrafluoroethylene copolymer, polychlorotrifluoroethylene (PCTFE), polyoxyethylene oxide (PEO) and polyethylene glycol (PEG).

The molecular ion peaks in the first cluster of peaks in the LC-MS chromatogram are separated by 44 m/e. PEO and PEG both have a molecular mass of 44n + 18 g/mol. The melting peak of PEG is 55 ^{o}C and PEO is 62 ^{o}C. In the thermograms a characteristic melting peak is observed at 52 ^{o}C. Due to the fact that this may be part of a cross-linked polymer this melting peak may be either PEG or PEO, or a blend of both. PEO is often used as a separator or electrolyte solvent in lithium polymer cells [4]. PEO is also cross-linked with chlorinated polymers to make membranes used for treatment of acid waste water (PC membranes) [5, 6]. These membranes are reinforced with polyester and are strongly alkaline.

The observed mass loss at a temperature of 276 ^{o}C is in agreement with the crystalline melting temperature of fluorinated ethylene propylene (hexafluoropropylene tetrafluoroethylene copolymer). After this melting peak, in the slower DSC heat-scan, the polymer decomposes. In neither of the thermal scans was the Tg or the characteristic Tm of PTFE observed.

The chloride found in the elemental analysis results could not be found in the IR window. The melting temperature of PCTFE varies, but the Tm for Kel-F is set at 155 ^{o}C. This is also in range of the melting peak at 138 ^{o}C observed in the thermograms.

M1 and M2 used in this investigation were made from the same compounds, due to the fact that they had approximately the same elemental analysis, the same IR spectra and the same thermogram results. The presence of PTFE is questioned, but it was confirmed that one of the compounds is indeed a cross-linked polymer.

4.5. References

1. Bee, B. R.; Errede, L. A.; Jefson, G. B.; Langager, B. A. United States Patent 4,153,661 (1979)
2. Wikipedia, the free encyclopedia, http://en.wikipedia.org/wiki/cross-linked updated July 2006
3. Pavia, D. L.; Lampman, G. M.; Kritz, G. S. Introduction to Spectroscopy. Third edition. (2001). Harcourt College Publishers. Chapter 2
4. Castriota, M.; Teeters, D. Ionics. **2006,** 11 (3-4), 220-225
5. Cheng, H. ACS Symp. Ser. **1992**, 496, 157 -169
6. http://www.pca-gmbh.com/membrane/datasht3.htm, accessed August 2006

Chapter 5

Electrochemical evaluation of carbon electrodes

5.1 Summary

During the desalination process the current is carried through the cell via carbon electrodes. cyclic voltammetry and linear sweep voltammetry were carried out using various carbon electrodes to investigate the following characteristics:

i) possible electrode reactions in electrolyte solutions containing Cl^-, SO_4^{2-}, or NO_3^-, and

ii) the formation of the diffusion double layer, which determines the capacitive characteristics of the electrode-electrolyte interface, and the possible adsorption of various species in the electrolyte solutions.

The three carbon electrodes investigated were the commercial glassy carbon electrode from BAS Bio-analytical Systems, a custom-made glassy carbon electrode fitted inside the flow through cell, and a carbon sheet used in the prototype desalination plant.

5.2 Introduction

For a simple electron transfer reaction the following applies:

$$O + e^- \leftrightarrow R$$

The forward reaction is known as the reduction reaction and the reverse is the oxidation reaction. In LSV the potential is swept at a constant scan rate over a selected potential region. In CV the same ramp is applied, but the scan is reversed back to the initial potential. These are illustrated in Figure 5.1.

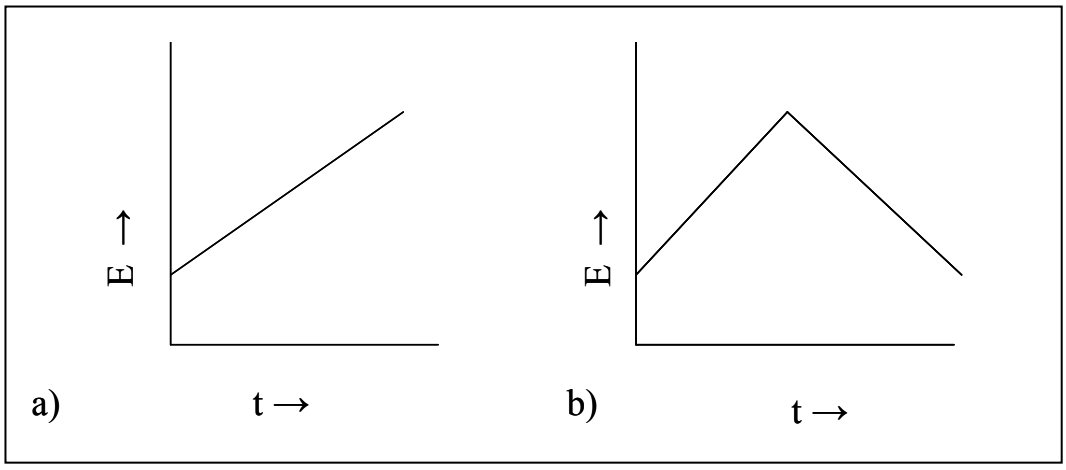

Figure 5.1: Potential sweep scans for a) linear sweep voltammetry and b) cyclic voltammetry.

The formation of a voltammogram as observed in Figure 5.2 can be explained with concentration profiles of species at the electrode surface. If one considers the reduction of O to R in a quiescent solution, the slope of the concentration gradient is given by

$$\frac{C_O(b, t) - C_O(0, t)}{\delta}$$

$C_O(b, t)$ = the bulk concentration of O

$C_O(0, t)$ = the surface concentration of O

δ = distance from the electrode

The changes in the slope and hence the resulting current, is due to changes in both $C_O(0, t)$ and δ. When the potential is scanned negatively, and the standard potential, E_0, for the certain half reaction is approached, the surface concentration of O rapidly decreases. At the potential equal to E_0, the concentration ratio ($C_O(0, t)/ C_R(0, t)$ is equal to 1. For a potential 59 mV more negative than E_0, $C_R(0, t)$ is present at around a 10-fold excess. The decrease in $C_O(0, t)$ is coupled with an increase in the diffusion layer thickness, which dominates the change in the slope after $C_O(0, t)$ approaches zero [1].

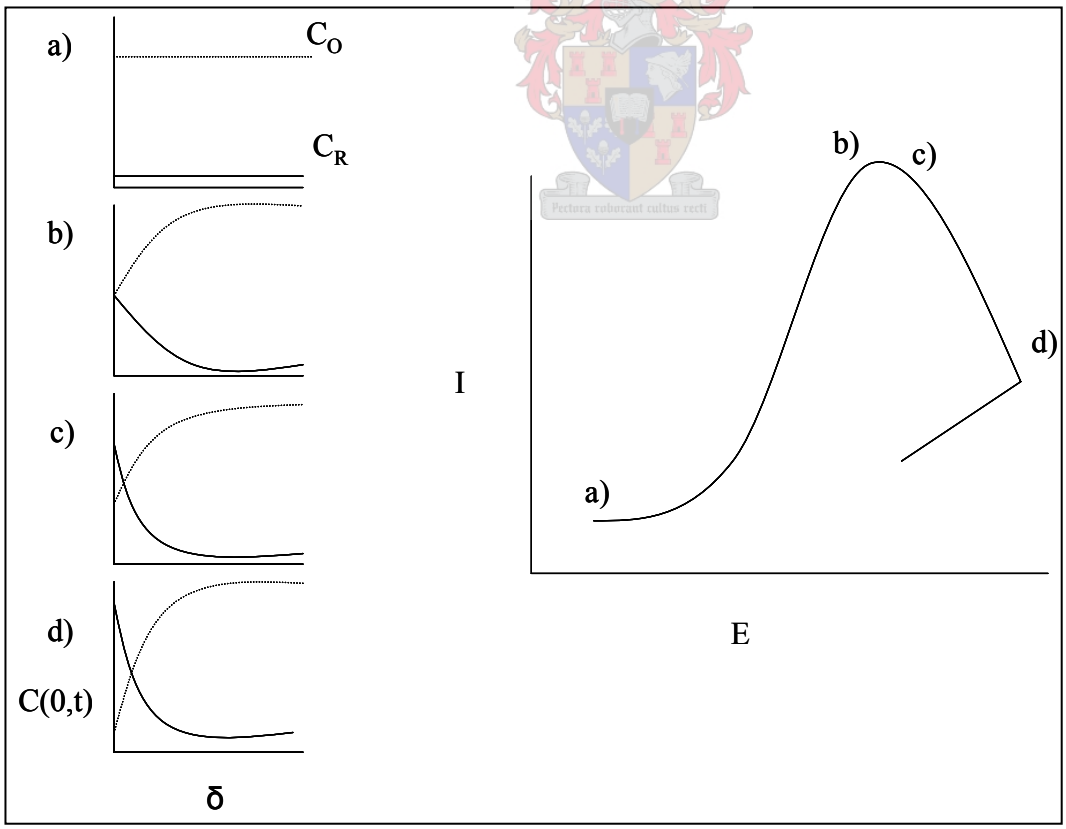

Figure 5.2: The current-potential curves and the corresponding concentration-distance profiles for the reaction $O + e^- \leftrightarrow R$.

Figure 5.3 illustrates a cyclic voltammogram for a reversible redox reaction. E_{pa} and E_{pc} are the anodic and cathodic peak potentials and I_{pc} and I_{pa} are the respective cathodic and anodic peak currents. For reversible redox reactions the peak potential separation ΔE_p (= E_{pc} - E_{pa}) = 58/n mV at all scan rates at 25 ^oC, the peak current ratio = i_{pa}/i_{pc} = 1 at all scan rates, and the peak current function $i_p/\upsilon^{1/2}$ (υ = scan rate) is independent of the potential.

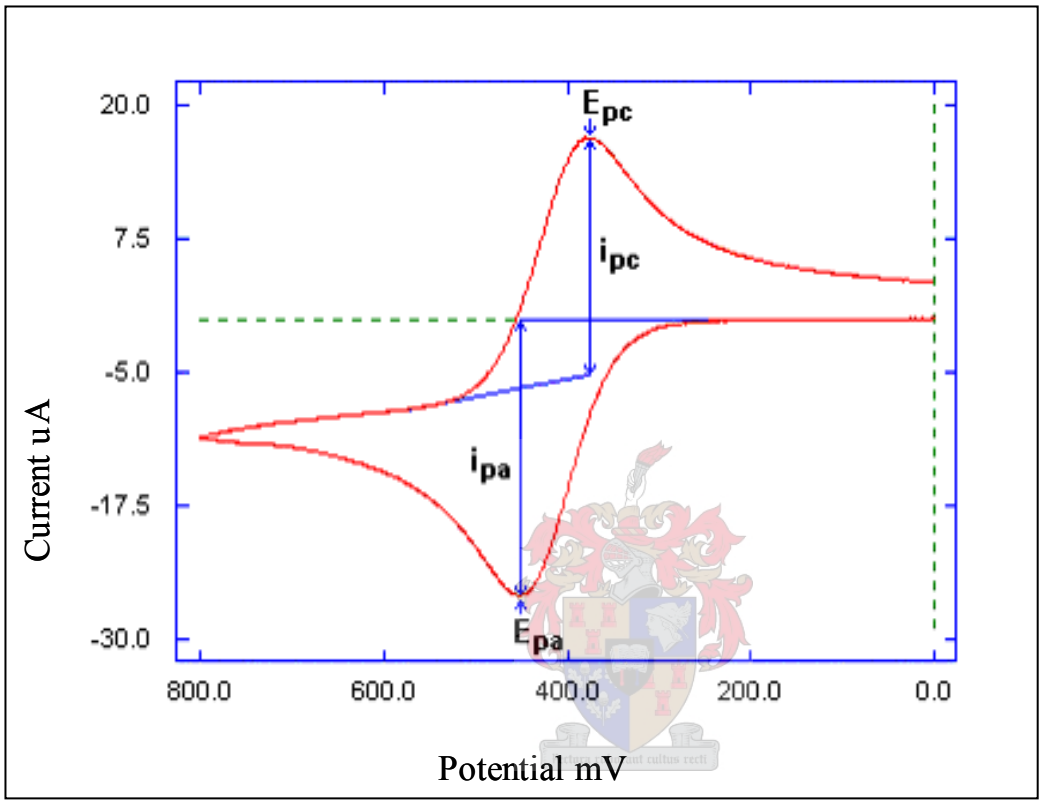

Figure 5.3: A standard cyclic voltammogram for a reversible redox reaction [2].

5.2.1 Redox reactions

The concentration gradient at the surface of the electrode changes as a result of applied potential. A current, proportional to this gradient, flows in the external circuit. As the sweep rate is increased in the CV experiment, the time scale of the experiment is shortened and the concentration gradient has less time to relax. Therefore, at fast sweep rates, high concentration gradients with resulting large currents will develop. The relationship between the peak current and the scan rate (sweep rate) is given by the Randles-Sevcik equation [1]:

$$i_p = 0.4463\ (F^3/RT)^{1/2}\ n^{3/2}\ AC_0\ (D\upsilon)^{1/2} \qquad \text{(eq 5.1)}$$

i_P = peak current (A)

D = diffusion coefficient ($cm^2\ s^{-1}$)

υ = scan rate (V s^{-1})

C_0 = concentration of the electroactive species (mol cm^{-3})

A = area of the electrode (cm^2)

n = number of electrons

The proportional relationship between the peak current and the square root of the scan rate should give a straight line. If the peak is part of a reversible reaction then the straight line will go through the origin [1, 7]. The proportionality of the peak current towards $\upsilon^{1/2}$ indicates the diffusion control at the electrode interface. The linear relationship will be an indication that the electron transfer is dependant on mass transfer towards the electrode surface.

5.2.2 Capacitance

The behaviour of the electrode-solution interface is analogous to that of a capacitor. This behaviour is governed by the equation

$$q = CE \qquad \text{(eq 5.2)}$$

where q is the charge stored on the capacitor (in coulombs), and E is the potential across the capacitor. When E is applied across a capacitor, charge will accumulate until q satisfies equation 2. During the charging process, a current (the charging current) will flow. At a given potential, there will exist a charge on the electrode, q^M, and a charge in the solution, q^S. At all times, during the applied potential, $q^M = -q^S$. The charge on the electrode represents an excess or deficiency of electrons and resides in a very thin layer on the electrode surface. The charge of the solution is made up of an excess of either cations or anions in the vicinity of the electrode surface. The whole array of charged species and orientated dipoles existing at the metal-solution interface is called the electrical double layer [2].C_d, the capacitance representing the double layer, is generally a function of potential.

Consider a cell consisting of a working electrode and a reference electrode in an electrolyte solution. This cell will be represented by the following electrical circuit:

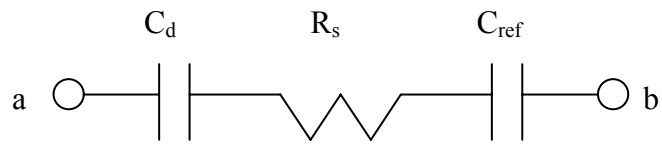

a = the working electrode

b = the reference electrode

C_d = the double layer

R_s = the solution resistance

C_{ref} = the double layer of the reference electrode

Figure 5.4: The electrical circuit representation of the two-electrode cell setup.

The sum of the voltages across the capacitor (E_C) and the resistor (E_R) must be equal to the voltage applied.

$$E = E_R + E_C = iR_S + q/C_d \qquad \text{(eq 5.3)}$$

i = the charging current

During a potential sweep

$$E = \upsilon t \qquad \upsilon = \text{scan rate mV/s} \qquad \text{(eq 5.4)}$$

Therefore

$$\upsilon t = R_s(dq/dt) + q/C_d \qquad \text{(eq 5.5)}$$

If q = 0 at t =0,

$$i = \upsilon C_d [1 - \exp(-t/R_S C_d)] \qquad \text{(eq 5.6)}$$

During a potential sweep experiment the current increases from zero as the scan starts and attains a steady state value of υC_d. This steady state value can then be used to estimate C_d. If the time constant, $R_S C_d$, is small compared to υ, the instantaneous current can be used to measure C_d as a function of E. Figure 5.5 illustrates how the value of C_d can be estimated on a voltammogram.

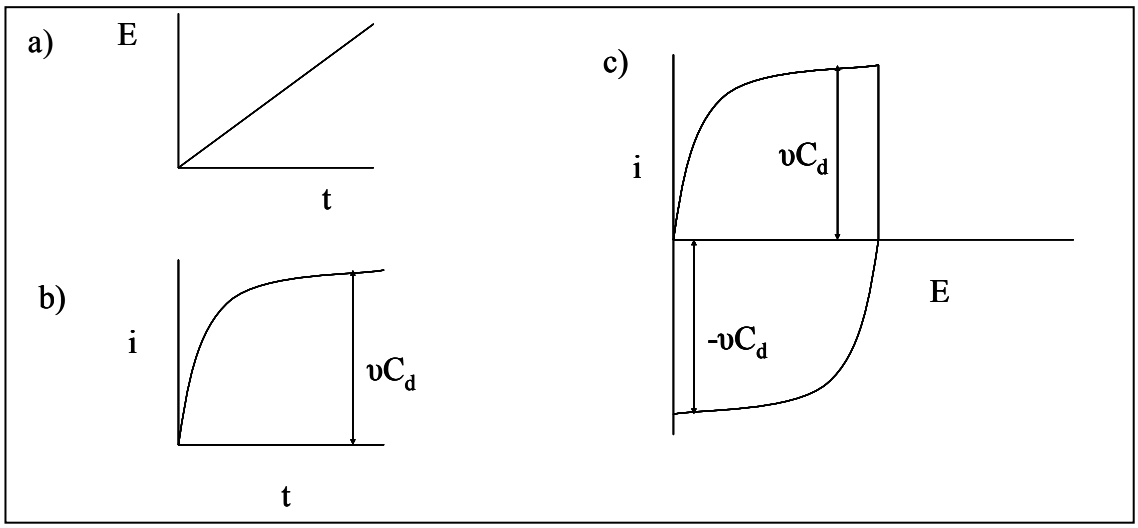

Figure 5.5: a) The linear potential sweep with b) the current-time behaviour resulting from a linear sweep applied to an RC circuit and c) the current-potential plot for a cyclic voltammogram.

The charging of the double layer is responsible for the background (residual) current known as the charging current. This charging process is non-faradiac because electrons are not transferred across the electrode-solution interface. Figure 5.6 illustrates how the charging double layer forms the background current from which the peak current must be measured [3].

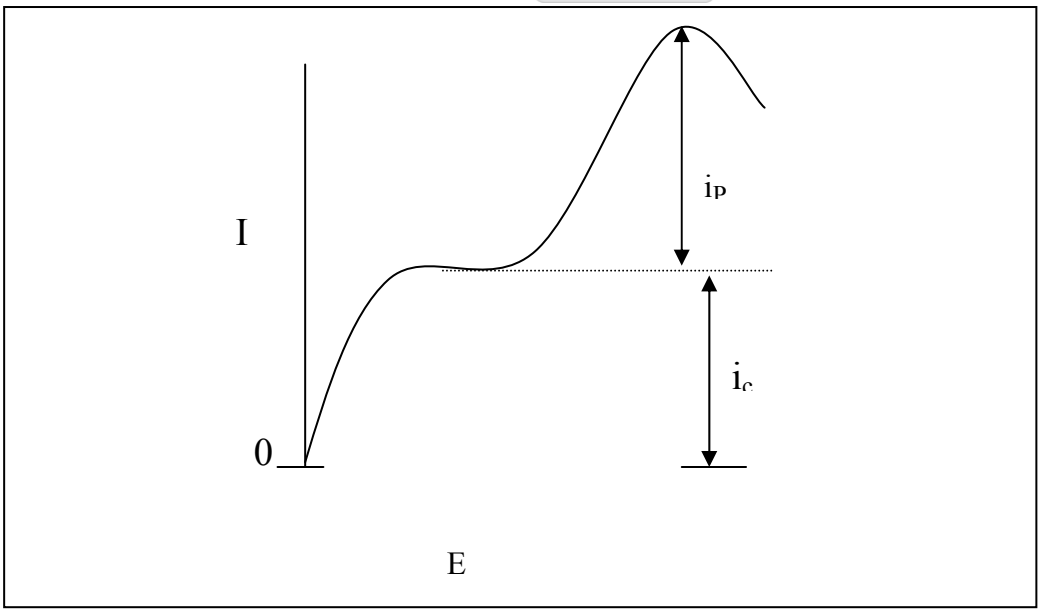

Figure 5.6: The effect of the double layer charging during a potential sweep. The magnitude of the charging current (i_C), and the faradiac peak current (i_P) are shown.

5.3 Experimental

The experimental procedures and cell design are discussed in Section 3.5.

5.4 Results and discussion of the electrochemical evaluation of the carbon sheet electrode

Figure 5.7 illustrates a cyclic voltammogram of various simple anions on a composite carbon sheet. It is clear that the carbon sheet behaves more like a capacitor than an electron-transfer electrode. The shape of the voltammogram illustrates the formation of the double layer, i.e. accumulation of ions of opposite charge next to the surface of the electrode. The voltammograms in Figure 5.7 were taken at a relatively fast scan rate of 100 mV/s.

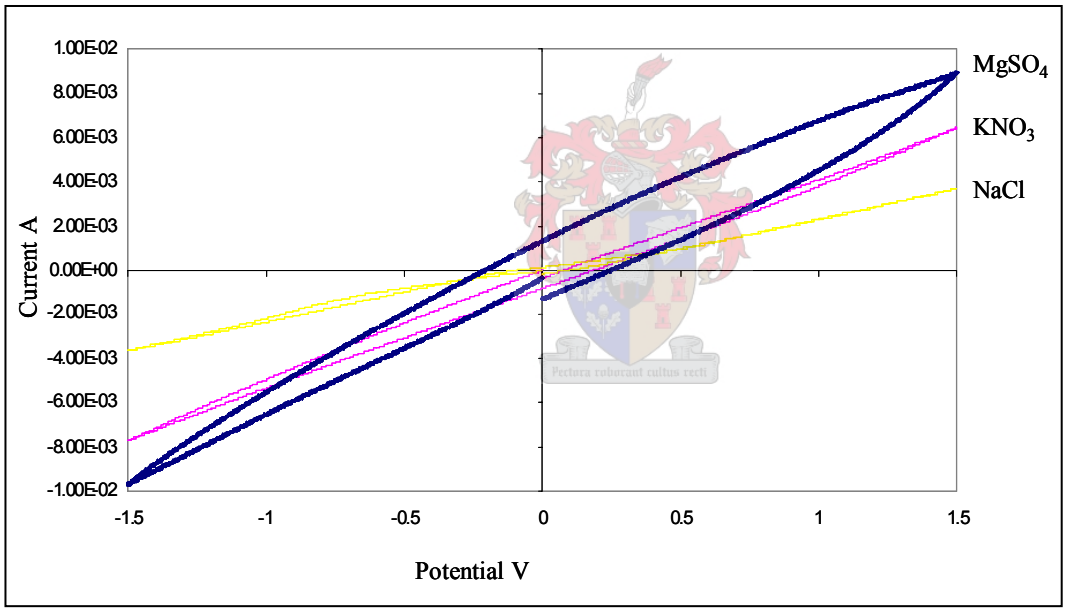

Figure 5.7: Cyclic voltammograms for the carbon sheet in 0.05 M NaCl, $MgSO_4$ and KNO_3.

The nature of the current-potential curve can be explained if one takes into account the morphology of the carbon sheet electrode. The edge of the basal plane of carbon atoms in a graphite structure, where bonding in the plane is terminated, contains unsaturated carbon atoms. These sites are associated with high concentrations of unpaired electrons and therefore play a significant role in chemisorption. Activated carbon has a significant disordered structure and more edge area than graphite and amorphous carbon, which results in a larger propensity for oxygen chemisorption. Moreover, since activated carbons are highly porous, they have a large surface area and hence a high active surface area for

chemisorption on the surface [3]. Due to the high surface area and good electrical conductivity properties, activated carbon is very efficient in electric double-layer capacitors (EDLCs).

It was reported that the capacitance increased with the amount of surface oxygen functional groups on the carbon electrode [4]. Analyses of these functional groups on activated carbon have shown that the oxidized carbons contain a significant amount of carbonyl and quinone-like groups (C=O) on the surface. Protons can then be adsorbed by these carbonyl groups.

$$>C_xO + H^+ + e^- \rightarrow >C_xO//H^+ \qquad (5.1)$$

It is thus suggested that the increase of capacitance during oxidation arises partially from the enhanced dipole affinity towards protons in solutions. Kim and Pyun [4] concluded that these surface oxygen groups impede ions penetrating the pores during the charging of the double layer, therefore discouraging electron transfer between the electrolyte solution and the activated carbon electrode. From the results represented in Figure 5.7, the capacitance of the activated carbon sheet increases with increasing potential. The capacitance effect for the various anions in the electrolyte solutions increases in the following order:

$$Cl^- < NO_3^- < SO_4^{2-}$$

Farmer et al [6] stated that the difference in double layers (charging current) for these ions is based on size, charge, and complexation in water. Sulphate has a higher charge, it is the larger molecule (of the three) and also has the highest degree of complexation in water, therefore, it has a larger charging current.

From the electrochemical studies of the activated carbon sheet it is concluded that the sheet in the prototype plant is charged to form a capacitor. After polarisation and applying a constant potential of 1.2 V, the non-reducible and non-oxidizable ions are removed from the electrolyte by the imposed electrical field and held in electrical double layers formed near the surface of the carbon electrode. Therefore the ions are removed from the bulk solution through capacitive deionisation, rather than electrodialysis [6].

Figure 5.8 illustrates the function of scan rate on the current voltage curves of NO_3^- on a carbon sheet. The charging current decreases with decreasing scan rate.

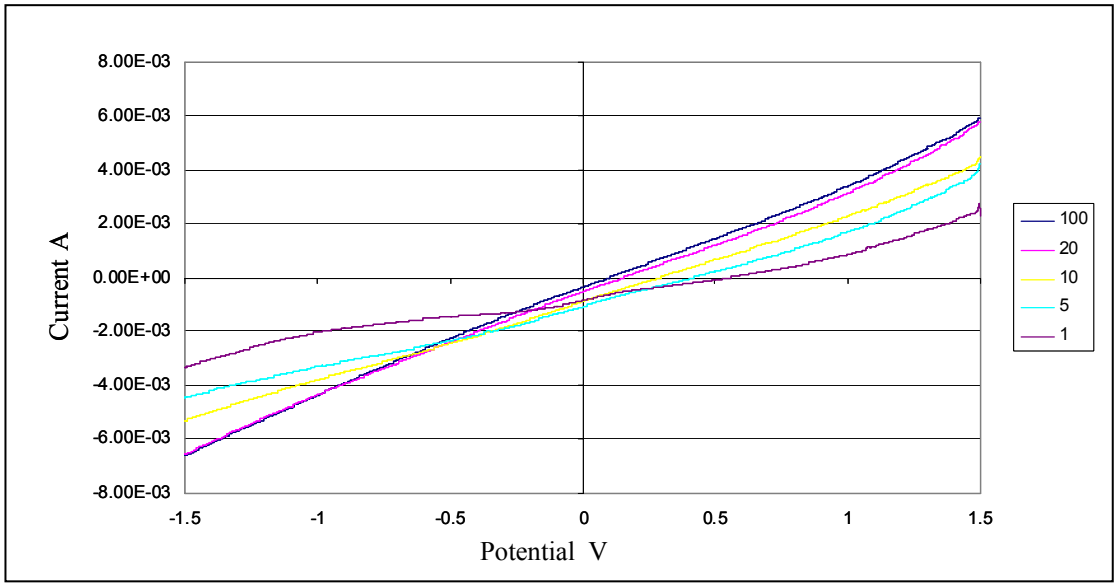

Figure 5.8: Current voltage curves for the reduction run on the carbon sheet in 0.05M KNO_3 at various scan rates (mV/s).

From Figure 5.9 the slopes of the three plots of charging current versus the scan rate are used to determine C_dA (the capacitance for the charging double layer multiplied by the area of the electrode surface) for each electrolyte solution. The plots in figure 5.9 are not straight lines due to polarisation of water molecules that can also add to the diffuse layer, therefore an average trend line is used to describe the slopes for figure 5.9. The charging current for Figure 5.8 was measured at an applied potential of 0.6 V. At scan rates higher than 100 mV/s surface effects (like formation of the oxide layer) start to dominate, and the charging current is no longer directly proportional to the scan rate. At lower scan rates however the extensive oxidation of the carbon sheet to CO and CO_2 is observed on the voltammograms, as seen in figure 5.8 and figure 5.10. The solution is slightly discoloured, and after approximately 10 minutes a dark suspension is observed at the bottom of the reaction flask which gives reason to believe that the carbon sheet is degrading.

Therefore the charging current was measured at a potential where surface oxidation would be at a minimum and at a scan rate from 1 – 100 mV/s. The capacitance (C_dA) was measured as follows for the various electrolyte solutions: $MgSO_4$ = 0.118 F, KNO_3 = 0.0948 F and NaCl = 0.0889 F. To compare these values to those of the glassy carbon electrodes, the values were divided by the active surface area of the electrode. The area for the carbon sheet working electrode used in these measurements was 1.8 cm^2. To compare the capacitance of each electrode, the capacitance must be divided by the area of the working electrode. This comparison will be as described in Section 5.7.

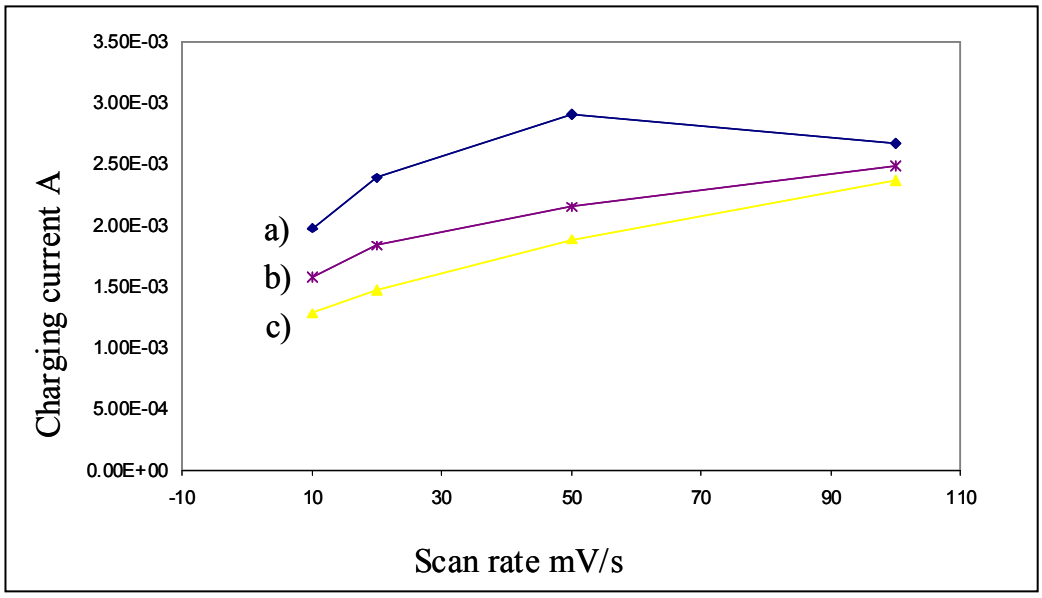

Figure 5.9: The charging current measured at an applied potential of 0.6 V for various scan rates in 0.05M a) NaCl, b) KNO_3 and c) $MgSO_4$.

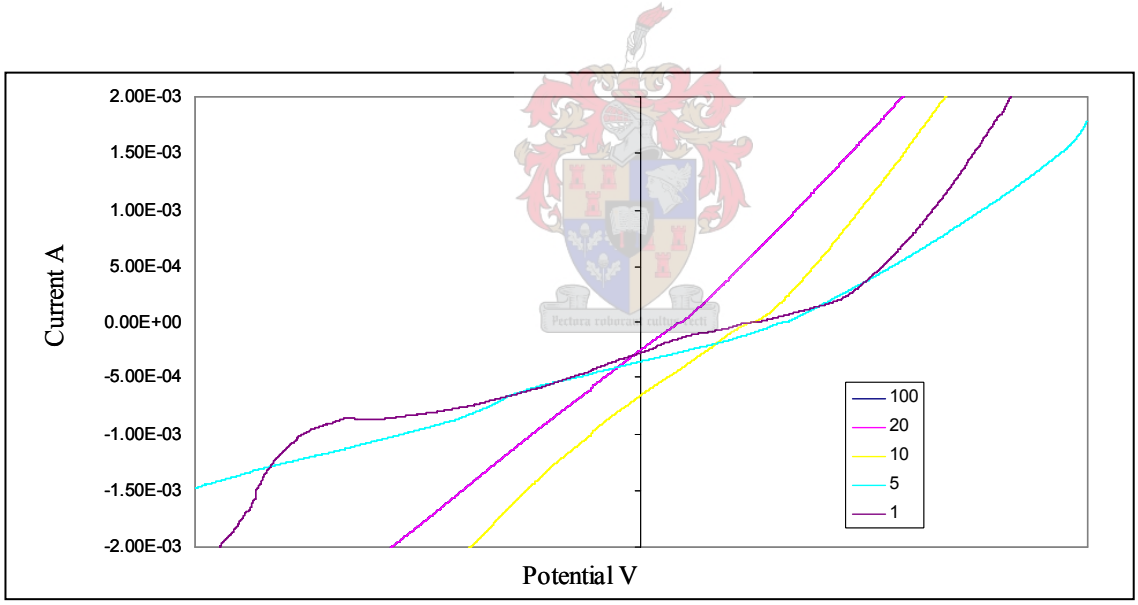

Figure 5.10: The current response measures at various scan rates in 0.05M NaCl.

5.5 Capacitance on glassy carbon electrodes

5.5.1 Capacitance on the custom glassy carbon electrode

To determine the capacitance effect on the custom carbon electrode, the current response was measured at an applied potential of 0.6 V, during various scan rates. The slope of each plot in Figure 5.11 will again give the value C_dA. The active surface area of the working custom electrode used in these measurements, was 2.84 cm^2. The slope of each plot was

determined to be the following:

sulphate = 0.0648 F

chloride = 0.0780 F

nitrate = 0.0818 F

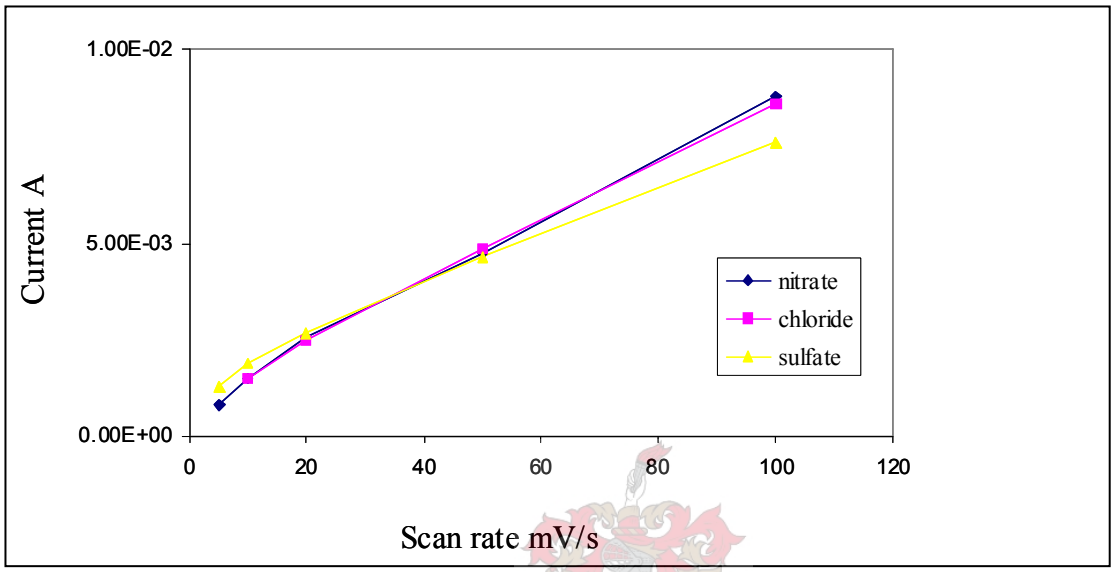

Figure 5.11: The current response to the applied potential sweep measured at a potential of 0.6 V on the custom carbon sheet in 0.05 M NaCl, $MgSO_4$ and KNO_3.

5.5.2 The commercial glassy carbon electrode (GCE)

The capacitance and the electrode reactions were investigated on both a used and a new (polished) glassy carbon electrode, to investigate the effect of surface oxidation and deterioration of the electrode,and the capacitance. These studies were done to estimate which of the commercial electrodes will have a similar behavior to that of the custom carbon electrode.

5.5.2.1 Capacitance on the polished GCE

The charging current was measured for various scan rates, in 0.05 M electrolyte solutions. The current was measured at an applied potential of 0.4 V before reduction of oxygen could occur. According to eq 5.6 and the discussion in Section 5.2.2, the slope of the proportionality of the scan rate and the charging current can be used to determine the capacitance at the surface of the electrode. From Figure 5.12 the capacitances (C_dA) for the

various 0.05 M electrolyte solutions at 0.4 V are: $MgSO_4$ = 0.869 µF, NaCl = 3.8 µF and KNO_3 = 2.15 µF.

Until now, sulphate had indicated a larger capacitance effect, but due to the oxidation reaction:

$$2SO_4^{2-} \leftrightarrow S_2O_8^{2-} + 2e^- \qquad 0.85\ V \qquad (5.2)$$

which occurs just prior to the potential where the capacitance was measured, the sulphate in the vicinity of the electrode interface is depleted and the larger peroxydisulphate moves away from the electrode. This oxidation reaction will be discussed further is Section 5.6.

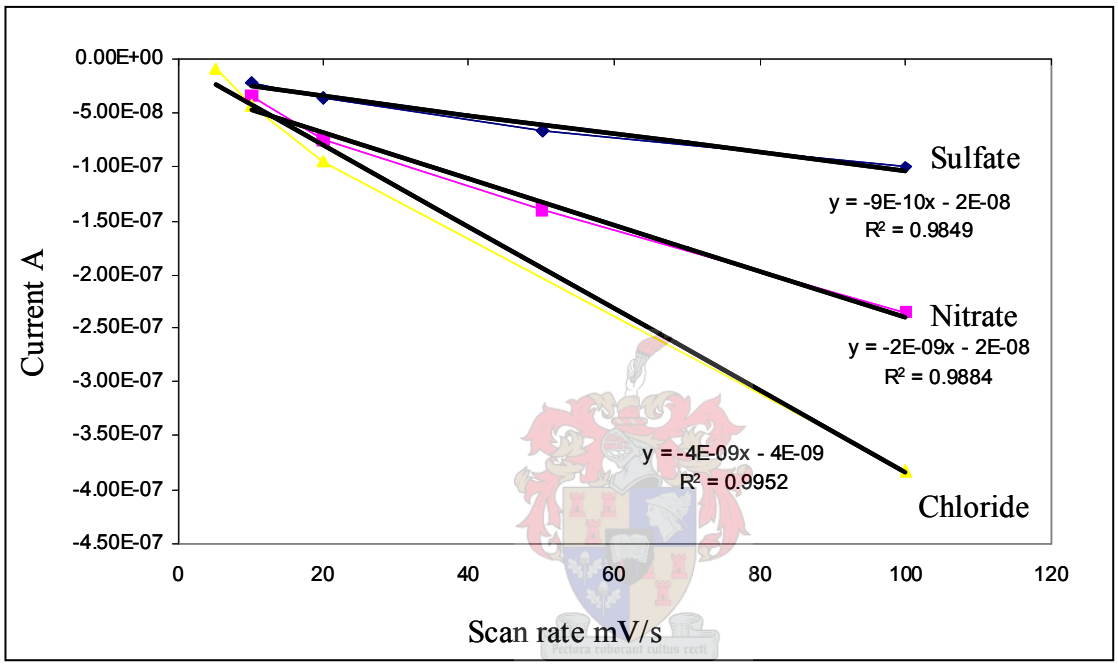

Figure 5.12: The current measured at various scan rates in 0.05M $MgSO_4$, KNO_3 and NaCl on the polished GCE.

5.5.2.2 Capacitance on the used GCE

The charging current was also measured for the used GCE. The capacitance for the KNO_3 and $MgSO_4$ solutions were measured at 0.4 V and for NaCl at 1 V. The reduction of chlorine gas in this same region in the 0.05 M NaCl electrolyte causes a large faradiac current and after the reduction of chlorine gas the electrode is "discharged", therefore an accurate value of the capacitance is difficult to determine. At higher applied potentials the reduction of water and oxygen in the water invoke a broad continuous faradiac current in all electrolyte solutions, which complicates measurement of the charging current. The capacitance (C_dA) is determined from the trend line for each of the 0.05 M electrolyte

solutions in Figure 5.13, and the results were as follows: $MgSO_4$ = 28.1 µF, NaCl = 22.8 µF and KNO_3 = 1.45 µF.

The larger capacitance for chloride electrolyte solutions is mainly due to their affinity for and interaction with the surface functional groups on the carbon electrode. A used GCE has been oxidised extensively and the deterioration due to the formation of CO and CO_2 causes a surface roughness and increases the surface activity. The active surface area for both commercial glassy carbon electrodes was 0.283 cm^2.

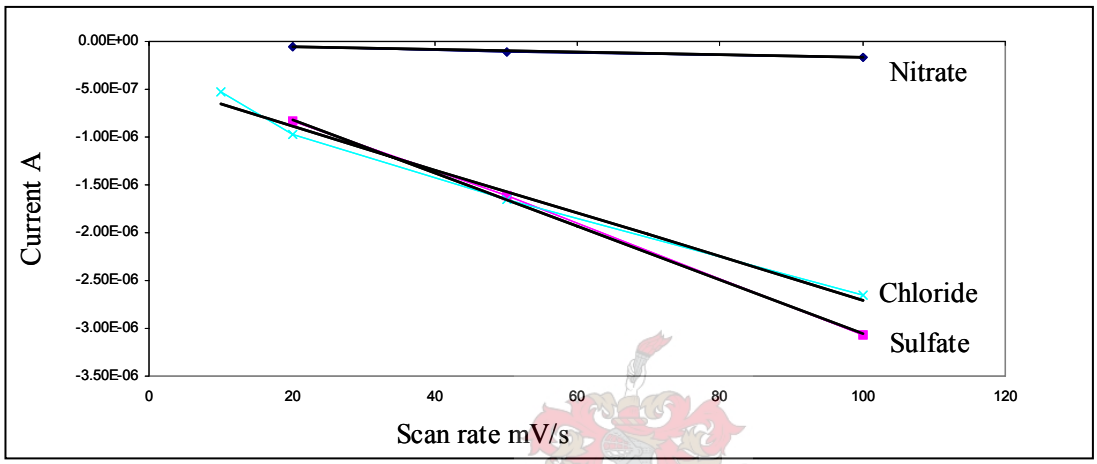

Figure 5.13: The charging current response to the applied potential 0.4 V in 0.05 M $MgSO_4$ and KNO_3, and 1 V for 0.05 M NaCl.

5.6 Electrode reactions occurring at the glassy carbon electrodes

5.6.1 Surface redox reactions on the glassy carbon electrodes

The redox peaks observed in the cyclic voltammograms of Figure 5.14 at -0.185 V and -0.225 V are found in both the 0.05 M $MgSO_4$ and KNO_3 solutions on the polished GCE. These peaks are diffusion (mass-transport) controlled (illustrated in Figure 5.15) and the peaks are separated by 60 mV. Therefore these peaks represent a quasi-reversible (the trendline does not intercept at 0) reaction involving 1 e^-. The reduction of oxygen is excluded for it is highly irreversible on the GCE. Other authors have also observed these redox peaks [9-14]. These have been ascribed as the redox reactions of surface functional groups and, more specifically,

as o- and p-quinone structures [8, 15].

$$>C=O + H^+ + e^- \leftrightarrow >COH \qquad (5.3)$$

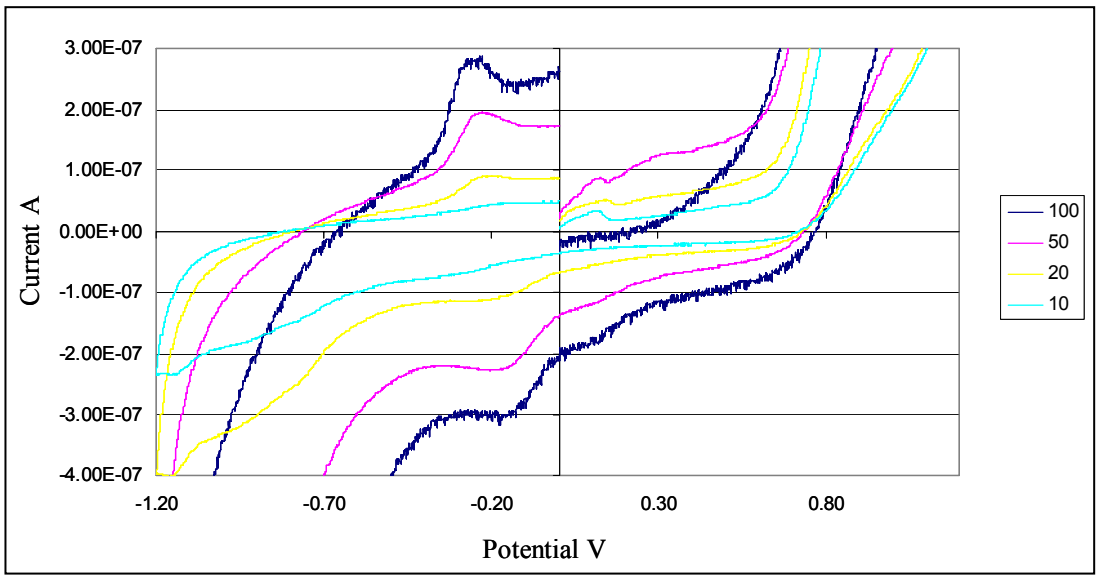

Figure 5.14: The current response for the potential sweep at various scan rates in 0.05 M $MgSO_4$. The reversible oxidation and reduction of the surface functional groups are illustrated.

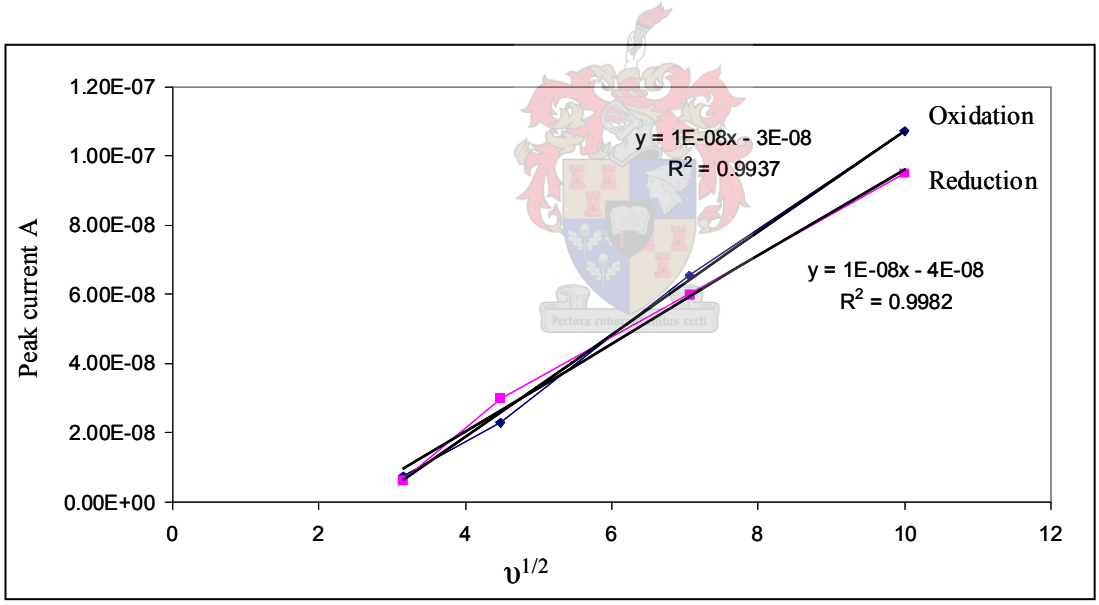

Figure 5.15: Oxidation and reduction of the surface functional groups on the surface of the polished GCE.

The surface redox reactions were however much more difficult to observe in the voltammograms for the used and custom GCEs, as illustrated in Figures 5.16 and 5.17.

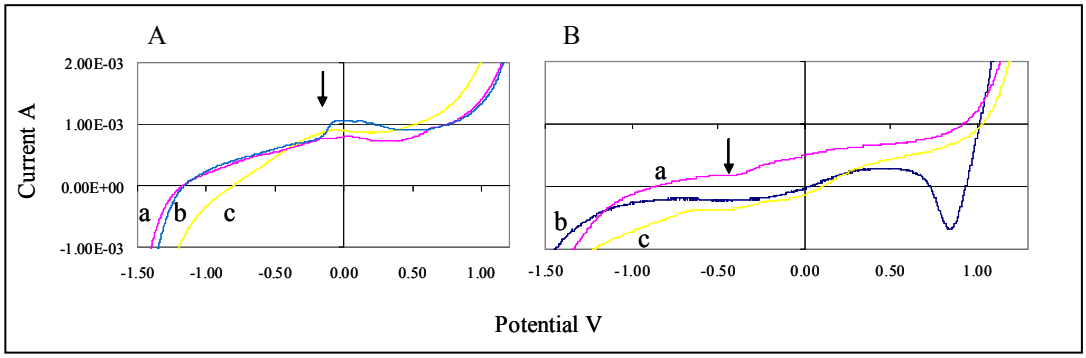

Figure 5.16: The surface oxidation (A) and reduction (B) on the custom carbon electrode in a) 0.05 M KNO_3, b) 0.05 M NaCl and c) 0.05 M $MgSO_4$.

The peaks marked in Figure 5.16 are the surface redox reactions that occur on the surface of the custom carbon electrode and are observed at lower scan rates (10mV/s). For higher concentrations (0.05 M), the oxidation of nitrate occurs in the same region as the surface oxidation. The reduction of hypochloride on the used GCE also occurs in the same region as for surface reduction.

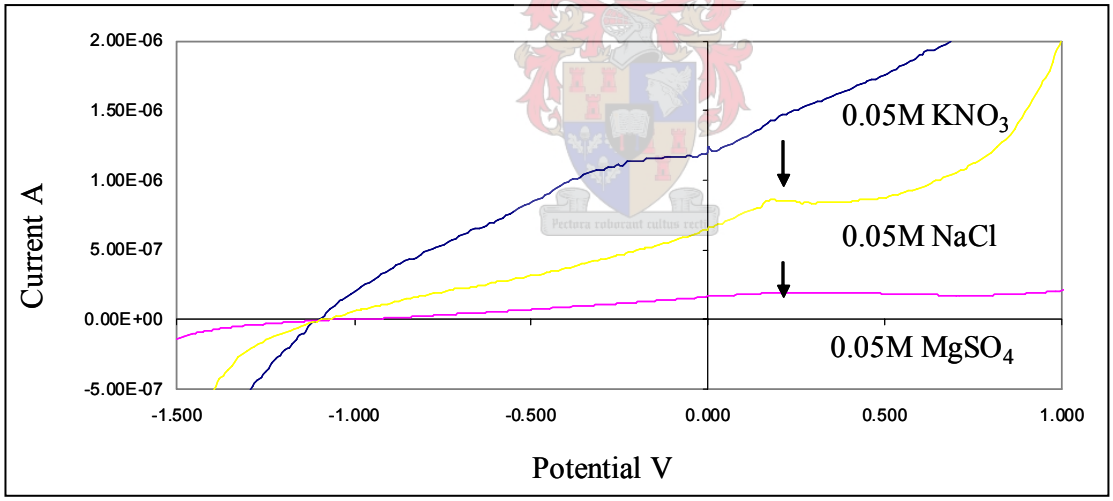

Figure 5.17: The surface oxidation on the used glassy carbon electrode.

5.6.2 Reduction of chloride on the polished, used and custom GCE

Figure 5.18 illustrates the potential shift for the reduction of chlorine, when the polished GCE is exchange for the used GCE.

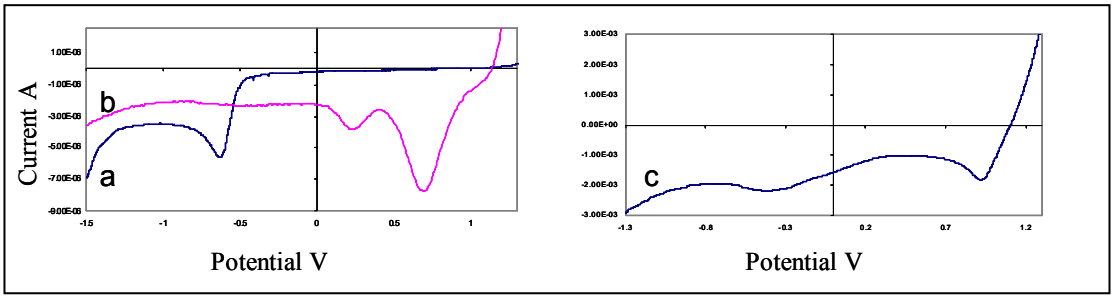

Figure 5.18: LSV voltammograms for reduction of chlorine gas on a) polished, b) used and c) the custom GCE in 0.05 M NaCl solutions for a scan rate of 20 mV/s.

At an initial applied potential of 1.5 V the chloride on the electrode surface is oxidized to chlorine gas. This gas is reduced on the used electrode at 0.5 V and only after a potential of -0.65 V is chlorine reduced on the new polished GCE.

Therefore if we consider the Tafel-Heyrovsky mechanism [18]

$$Cl_2 + H_2O \leftrightarrow OCl^- + Cl^- + 2H^+ \quad (5.4)$$

$$ClO^- + H_2O + e^- \rightarrow Cl_{ad} + 2OH^- \text{ slow} \quad (5.5)$$

$$Cl_{ad} + e^- \rightarrow Cl^- \text{ fast} \quad (5.6)$$

This mechanism does indeed hold for the results observed for the polished GCE of this study. The large shift in reduction potential for the used GCE implies that the reduction occurs via another mechanism.

According to Lowe et al [17] the successful working of a carbon electrode in the reduction of chlorine is determined by the number of edge plane sites. Hine et al [16] suggested that the carbon oxide layer should influence the Cl_2 evolution and reduction reaction. Cl_2 kinetics are sensitive to the electrocatalytic and adsorptive properties of the anode material. Therefore, because all the previous experiments were carried out with the used GCE in aqueous solutions, the used GCE is covered or partially covered with an electrolytically generated oxide film. The oxide film layer and the increase in surface roughness (due to consumption of the carbon anode material occuring through oxidation to CO and CO_2, and erosion) [18], suggested that the mechanism used to describe the reduction of chlorine on graphite [19, 20] was far more accurate for the used GCE. The reduction of chlorine on the used GCE is mechanism B as given in Section 2.3.2;

$$Cl_{2(aq)} + e^- \leftrightarrow Cl_{ads} + Cl_{aq}^- \quad \text{(Heyrovsky) rate determining step} \quad (5.7)$$

$$Cl_{ads} + e^- \rightarrow Cl^-_{(aq)} \quad \text{(Volmer)} \quad (5.8)$$

The same reversible mechanism is suggested by Urushibata et al [21] for chlorine evolution and reduction on glassy carbon in molten salts.

The second reduction peak in the used GCE voltammogram is considered to be the direct reduction of hypochlorite:

$$ClO^- + H_2O + 2e \rightarrow Cl^- + 2OH^- \qquad 0.4\ V \qquad (5.9)$$

For slower sweep rates on the used GCE, the reduction peak of chlorine no longer appears on the LSV voltammograms. This is due to the fact that the chlorine gas has time to move away from the electrode surface and therefore cannot be reduced.

The reduction potential for chlorine gas on the custom carbon electrode moved to an even higher potential of 1 V. The reduction mechanism seems to be very similar to the one proposed for the used GCE. Due to an even higher degree of surface impurities and the surface oxide layer on a larger electrode surface, the reduction is accelerated on the custom electrode surface, and surface effects (including the adsorption of hydrogen to form hydrogen gas) inhibit the reduction of hypochlorite. In Figure 5.19 the square root of the scan rate is plotted against the peak current for the reduction of chlorine on the polished and the custom electrode. The responses in both accounts are linear, which indicates that they are diffusion controlled reactions, dependent on the mass transfer from the solution to the electrode.

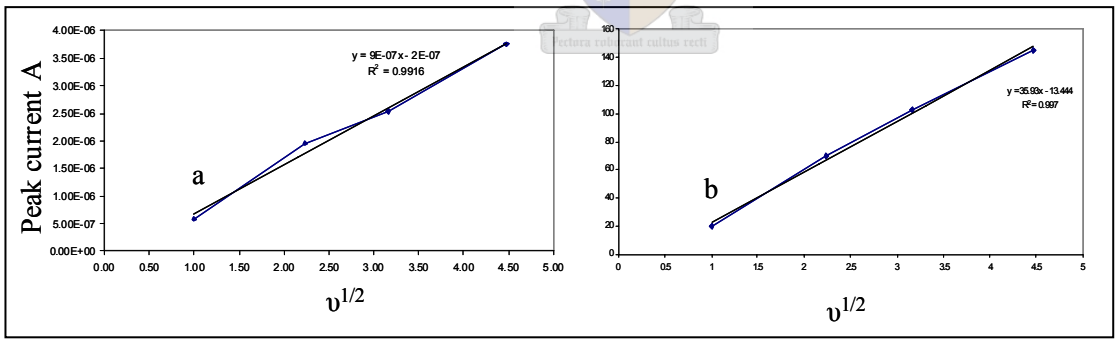

Figure 5.19: The current response versus the square root of the scan rate for the reduction of chlorine gas on a) a polished GCE and b) the custom carbon electrode.

5.6.3 Reactions of $MgSO_4$ on polished and used GCE

The oxidation of sulphate to thiosulphate was observed on the new polished GCE, whereas the reduction of sulphate to form H_2SO_3 was observed for both GCEs at the same potential (-0.6 V). Figure 5.20 illustrates the cyclic voltammograms for 0.05M $MgSO_4$ on the used and polished GCEs.

$$SO_4^{2-} + 4H^+ + 4e^- \leftrightarrow H_2SO_3 + H_2O \quad (5.10)$$

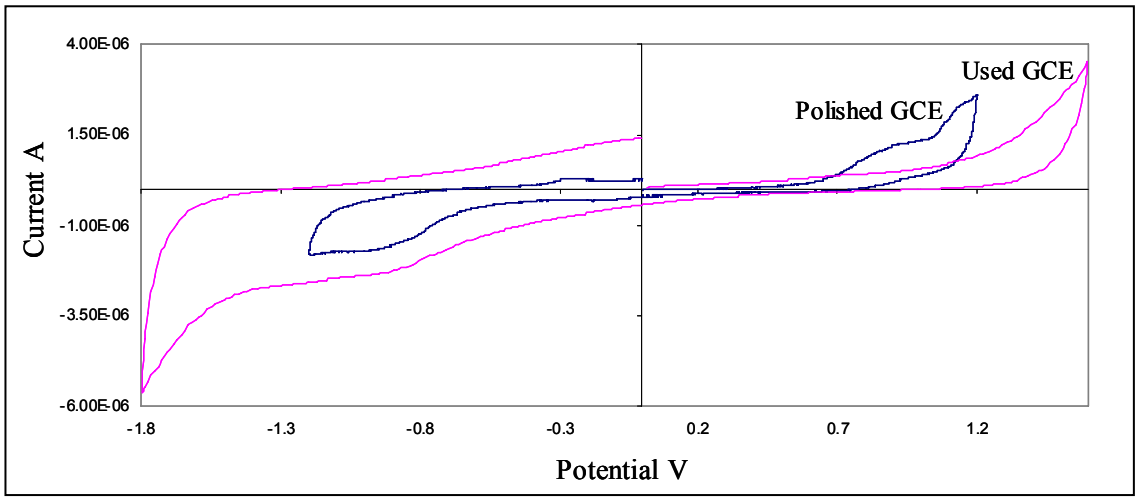

Figure 5.20: CV voltammograms comparing the reaction peaks observed on the used and polished GCE in 0.05 M $MgSO_4$.

The oxidation of sulphate to peroxydisulphate at 0.85 V is a mass-controlled electron transfer reaction. This is determined by the linear relationship of $\upsilon^{1/2}$ and the peak current (as described in Section 5.2.3). The result is illustrated in Figure 5.21.

$$2SO_4^{2-} \rightarrow S_2O_8^{2-} + 2e^- \qquad E = 0.85\ V \quad (5.2)$$

The broad cathodic peak observed on the polished as well as the GCE arises from the reduction of dithionate.

$$2SO_4^{2-} + 2e^- + 4H^+ \rightarrow S_2O_6^{2-} + 2H_2O \qquad E = -0.85\ V \quad (5.11)$$

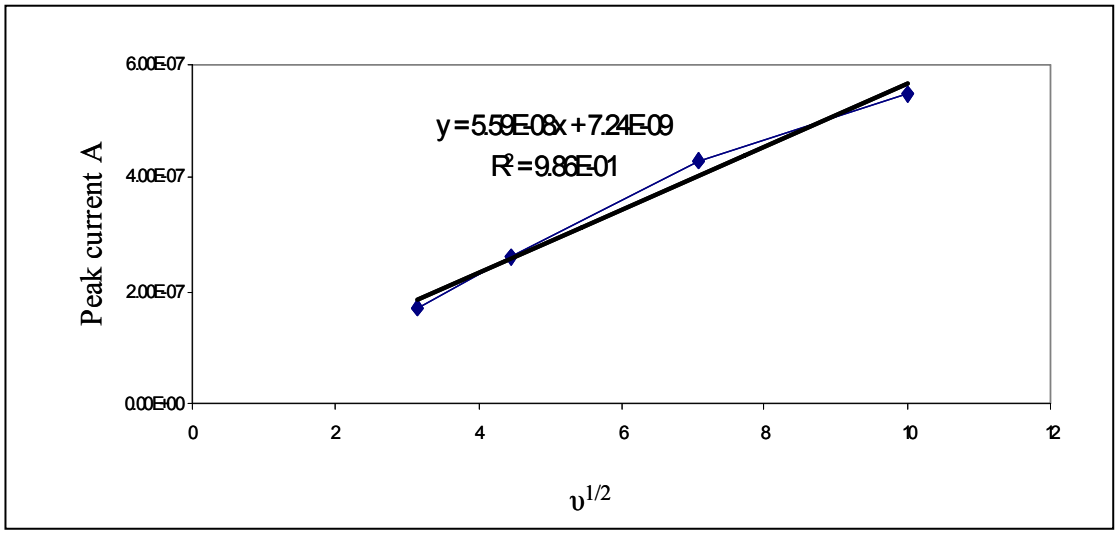

Figure 5.21: The linear proportion of the square root of the scan rate and the peak current at a potential of 0.85 V for a 0.05 M $MgSO_4$ solution.

No redox reactions could be observed on the custom carbon electrode in the 0.05 M $MgSO_4$ electrolyte solutions.

5.6.4 Reactions of KNO_3 on used, polished GCE and the custom electrode

In Figure 5.22 the cyclic voltammograms for KNO_3 on polished GCE, used GCE and the custom electrodes are compared. The scan rate was 100 mV/s and the electrodes were submerged in 0.05 M KNO_3.

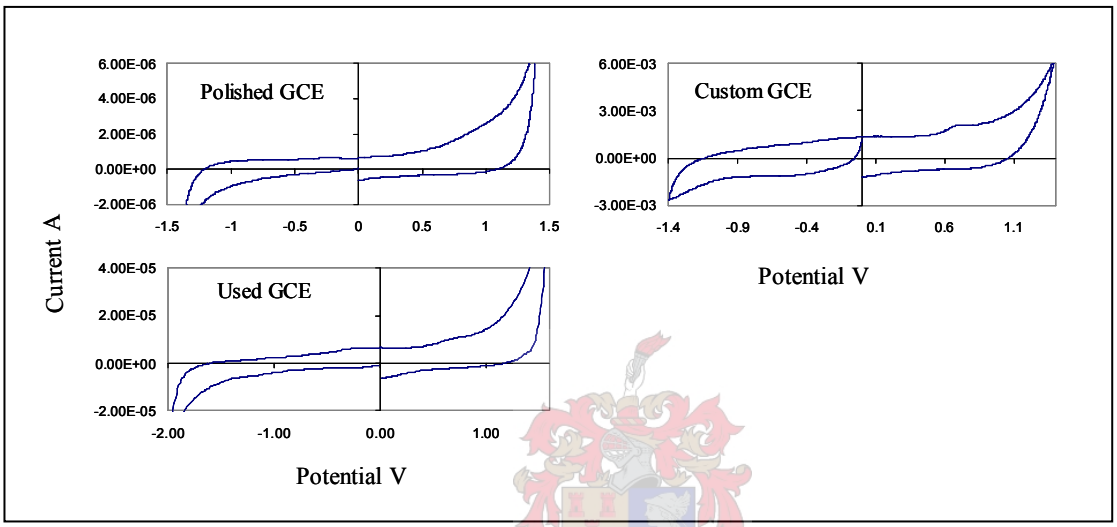

Figure 5.22: Cyclic voltammograms for polished GCE, the used GCE and the custom electrode in the cell, in 0.05 M KNO_3.

In Section 3.2 it was discussed that the reduction of nitrate on glassy carbon is very unlikely and highly irreversible, but the oxidation of nitrite can be observed at a potential of 0.9 V [22- 24].

$$NO_2^- + 2H_2O \rightarrow NO_3^- + 2H^+ + 2e^- \qquad (5.12)$$

The oxidation of nitrite to nitrate was observed on all three carbon electrodes. The peak intensity was considerably higher for the used and custom electrode, which indicates that the reduction is also dependent on the surface of the carbon electrode. As found by Chebotareva and Nyokong [25], the quality of the potential-current curves is highly dependent on the electrode surface. Bare GCE do not indicate a high degree of electrocatalytic surface area for the oxidation of nitrite. Therefore it is concluded that the oxidation observed on the used and custom GCEs are attributed to the change in surface properties due to impurities on the surface and the formation of an oxide layer. The oxidation is observed on all three GCEs at 0.7 V.

5.7 Effect of pH

5.7.1 Effect of pH on the capacitance of the electrolyte solutions

The effect of pH on the capacitance of the electrodes in the electrolyte solutions was studied on the used glassy carbon electrode. The pH was investigated at pH 2 and pH 9 and compared to capacitance values already obtained at pH 6.5. For the acidic solutions, 0.05 M HCl, H_2SO_4 and HNO_3 were used as electrolyte solutions. The capacitance for these electrolyte solutions was measured at an applied potential of 0.6 V, to avoid the effects of hydrogen adsorption. The charging currents measured for the various scan rates are plotted in Figure 5.23 and from the slope of the trend line the following results were acquired:

HCl = 27.7 µF

H_2SO_4 = 312 µF

HNO_3 = 144 µF

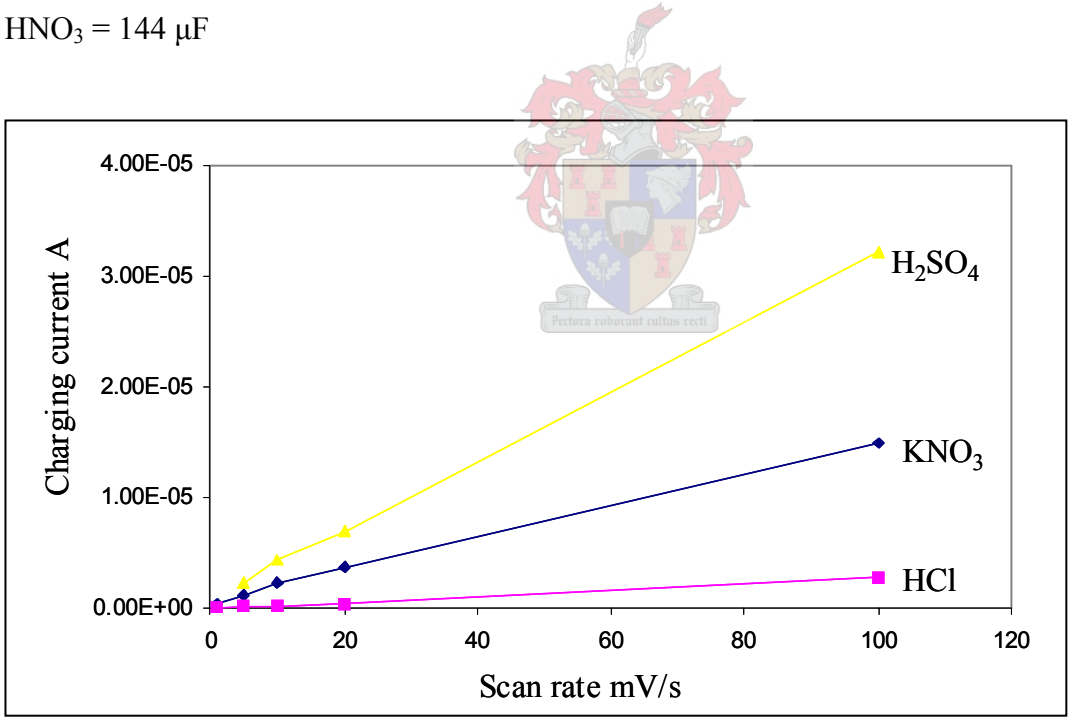

Figure 5.23: The charging current measured for various scan rates in 0.05 M electrolyte solutions at pH 2.

To compare these capacitance values to those determined at pH 6.5 in Section 5.4, the capacitance was divided by the active surface area, 0.283 cm^2. The results are tabulated in Table 5.1. To determine the capacitive values of the used GCE in the various electrolyte

solutions at pH 9, basic KOH solution was added until the desired pH was reached. The charging current was determined at an applied potential of 0.6 V at various scan rates, and the plots of which are illustrated in Figure 5.23.

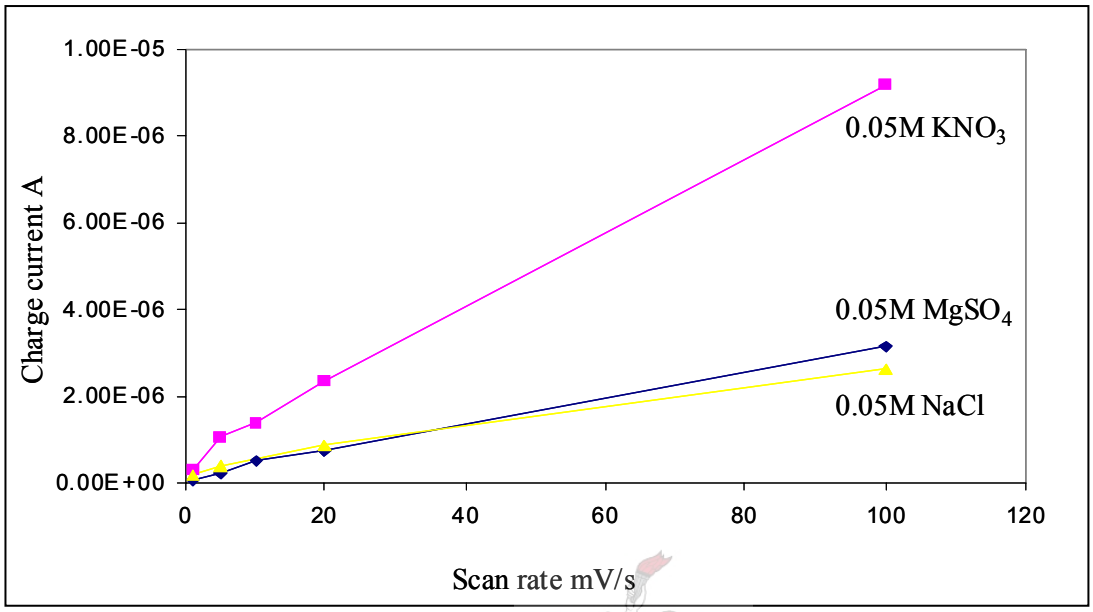

Figure 5.24: The charging current measured for various scan rates at an applied potential of 0.6 V in 0.05 M NaCl, KNO_3 and $MgSO_4$ at pH 9.

The slopes of the scan rates versus the charging current for the 0.05 M solutions at pH 9 were calculated to be:

NaCl = 23.5µF

$MgSO_4$ = 30.6 µF

KNO_3 = 87.3 µF

These capacitance values were also divided by the active surface area (0.283 cm^2) and results are tabulated in Table 5.1.

Table 5.1: Capacitance for the used GCE divided by the active surface area (0.283 cm^2) in various electrolyte solutions at various pH values

Electrolyte 0.05 M	Capacitance (µF/cm^2)		
	pH 2	pH 6.5	pH 9
Sulphate	1102.0	99.3	108 .1
Nitrate	508.8	5.1	308.4
Chloride	97.8	80.5	83.0

5.7.2 Effect of pH on the electrode reactions

pH plays a very important role in surface electrode reactions. Hydrogen adsorption at lower pH and the acceleration of water reduction at higher pH influence the electrode reactions by taking up active sites on the electrode surface.

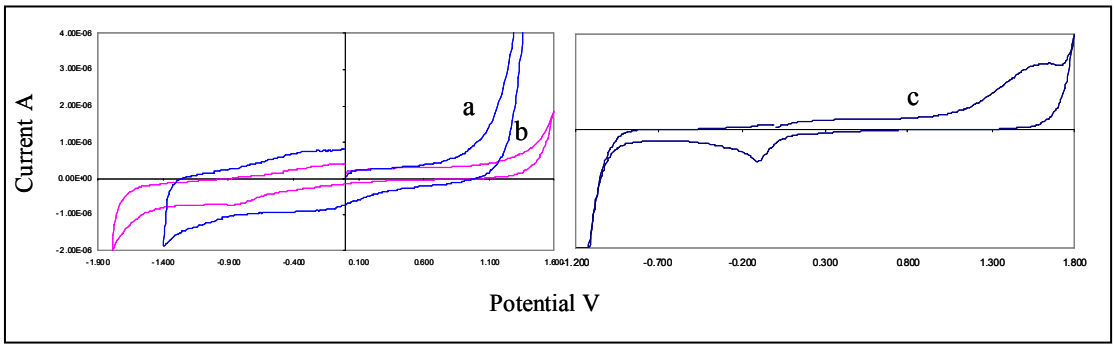

Figure 5.25: Cyclic voltammograms for the used GCE in 0.05 M sulphate solutions at a) pH 9, b) pH 6.5 and c) pH 2.

As discussed in Section 5.6.3, the reduction of sulphate at -0.6 V is attributed to the following electrode reaction:

$$SO_4^{2-} + 4H^+ + 4e^- \leftrightarrow H_2SO_3 + H_2O \qquad (5.10)$$

Due to the pH dependence of this reaction it is not a surprise that the reaction produces a higher current at lower pH. At lower pH the capacitance of the used GCE is considerable higher than for any other pH. Sulphate is therefore held in a much larger diffusion double layer and at an applied potential of 0.85V, the oxidation of sulphate to peroxydisulphate is accelerated:

$$2SO_4^{2-} \leftrightarrow S_2O_8^{2-} + 2e^- \qquad (5.2)$$

The effect of pH on the reduction of chlorine is clear from the plots in Figure 5.26. At a high pH the reduction of chlorine is not observed, whereas hydrogen adsorption to form hydrogen gas dominates at lower pH.

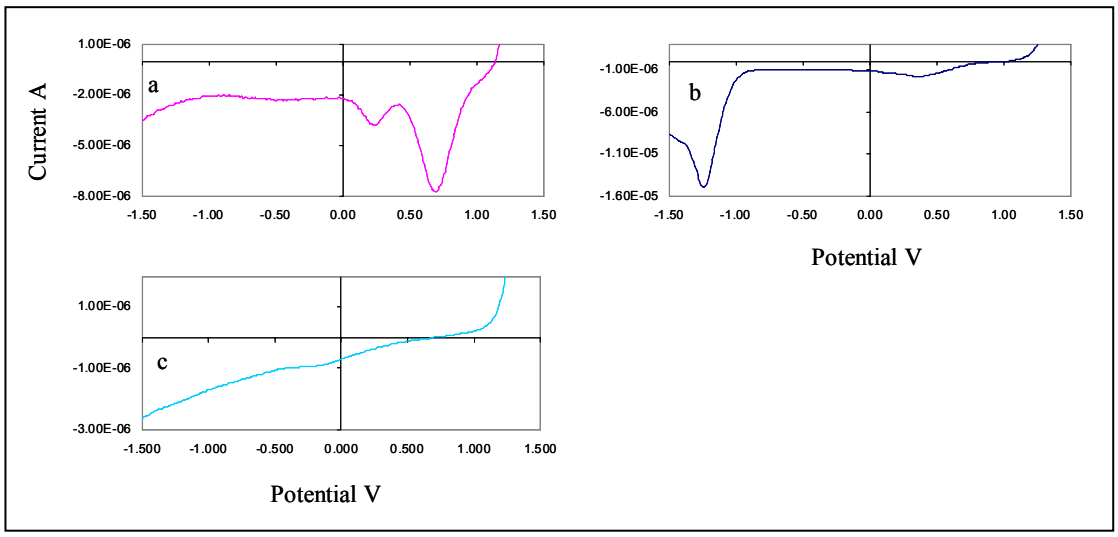

Figure 5.26: Cyclic voltammograms for the used GCE in 0.05 M chloride solutions at a) pH 6.5, b) pH 9 and c) pH 2.

The oxidation of nitrite to form nitrate is accelerated at higher pH, whereas surface redox reactions inhibit the oxidation at lower pH (figure 5.7.5).

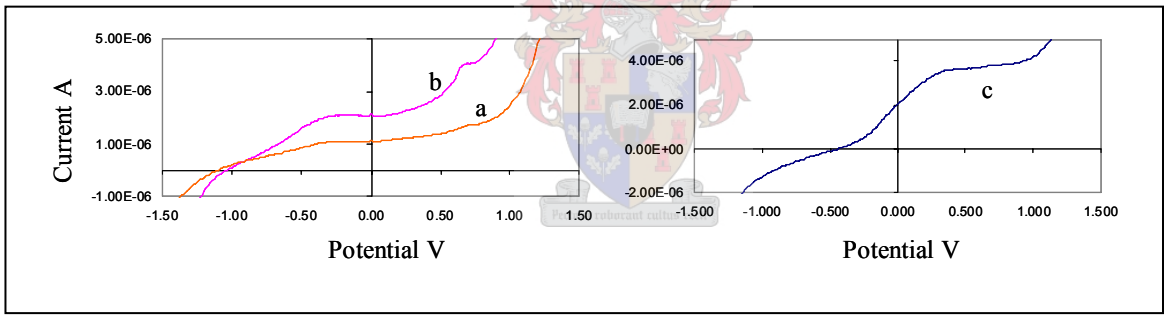

Figure 5.27: Cyclic voltammograms for the used GC in 0.05 M nitrate solutions at a) pH 6.5, b) pH 9 and c) pH 2.

5.8 Conclusions

The capacitances of the different carbon electrodes used were compared to that of commercial GCE. The area of the custom carbon electrode is 2.54 cm^2, 0.283 cm^2 for the commercial GCEs and 1.8 cm^2 for the carbon sheet. The $\mu F/cm^2$ for the custom electrode, the used and polished electrode and the carbon sheet are compared in Table 5.2.

Table 5.2: The capacitance ($\mu F/cm^2$) for the custom electrode, the used and polished GCE electrodes and the carbon sheet

Electrode	Capacitance ($\mu F/cm^2$)		
	0.05M $MgSO_4$	0.05M KNO_3	0.05M NaCl
Custom carbon	2.55E 04	3.22E 04	3.07E 04
Used GCE	99.3	5.12	80.5
Polished GCE	3.07	7.60	13.4
Carbon Sheet	6.56E 03	5.26E 03	4.93E 03

The size of the double layer is generally larger on the used GCE than on the polished GCE, due to the higher surface activity caused by the reduction of the surface functional groups on the GCE. These quinonic, ketonic and carboxylic functional groups are reduced to CO and CO_2, and this increases the surface porosity and hence the surface roughness.

The double layer capacity increases with increasing surface roughness [9]. SEM images were taken of the carbon sheet as well as the custom carbon electrode to validate the surface roughness, which increased the observed capacitance on the custom electrode and the carbon sheet. These images are shown in Figure 5.28.

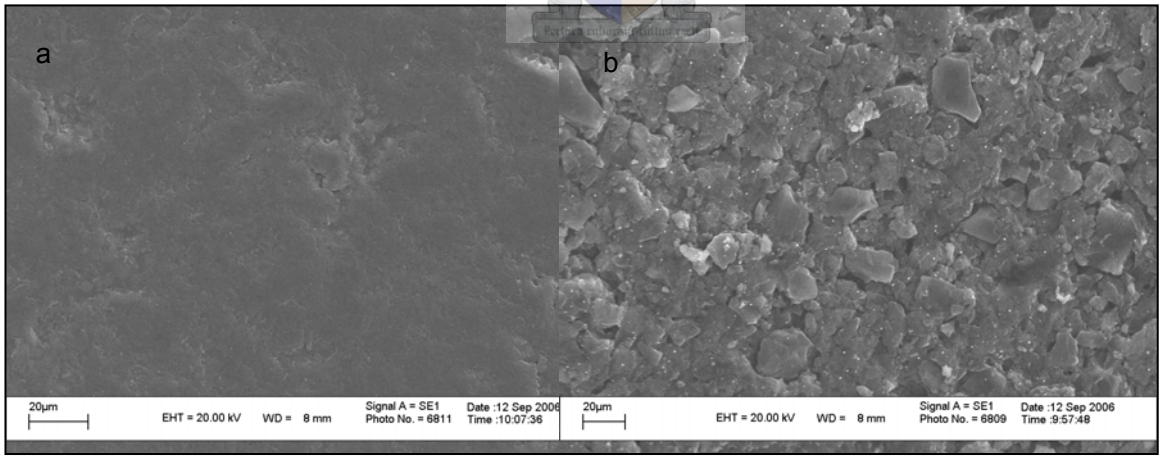

Figure 5.28: SEM images for the a) custom glassy carbon electrode and b) carbon sheet.

The porosity of the carbon sheet and the custom carbon electrode, together with impurities on the surface, add considerably to their capacitance. The active surface area used in these experiments also induced a much larger double layer.

The oxidation of nitrate and the reduction and oxidation of chlorine are only observed on the glassy carbon electrodes. These reactions are diffusion controlled and are irreversible. Surface redox reactions are observed on all the electrodes. On the polished GCE however the nature of the redox reaction is clearer than on the used GCE. This is because the functional groups on the surface of the used GCE have already been oxidized to form the oxide film layer on the surface. This also confirms that the surface reduction is an irreversible process.

The nature of the double layer and the possible electrode reactions in a desalination plant need to be considered for the following reasons:

1) The size of the double layer determines the capacitance of the electrode interface. The ions are attracted to the electrodes, which removes them from the effluent. With a larger double layer, less energy is required to remove these ions without too many electrode reactions occurring
2) The oxidation of chloride to chlorine is important. This is because Cl_2 is a strong oxidizing agent, and could compromise the electrode surface as well as degrade the ion-exchange resin or ion-exchange membrane in the desalination cell.
3) At an applied potential of 1.2 V, implemented by the prototype plant, electrode reactions could occur. The most prominent of all is the reduction of water to hydrogen gas, which is also a strong reducing agent. Therefore, pH control is also very necessary to inhibit the H_2 formations as far as possible. Plant effluents are generally kept at a pH 8.

5.9 References

1) Wang, J.*Analytical Electrochemistry*. Second Edition. John Wiley & Sons, Inc., 2000. Chapter 1
2) Application notes from Epsilon instruments, accessed July 2006 //C:\EpsilonEC\HTML\Techniques\CycVolt\cv_analysis.html
3) Bard, A.J.; Faulkner L. R.. Electrochemical Methods. Fundamentals and Applications. Second Edition. John Wiley & Sons. Chapter 1
4) Kim C. -H.; Pyun, S. -I. Journal of the Korean Ceramic Society. 2003, 40 (9), 819-826
5) Biniak, S.; Szymanski, G.; Siedlewski, J.; Swaitkowski, A. Carbon. 1977, 35 (12), 1799 -1810

6) Farmer, J.C.; Fix, D.V.; Mack, G.V; Pekala, R.W.; Poco, J.F. J. Electrochem. Soc. 1996, 143 (1), 159-169
7) Instrumental Methods in Electrochemistry. Southampton Electrochemistry Group; Horwoord publishing, Chichester. Chapter 2 and 6, p 178 -228
8) Hu, I.; Karweik, D. H.; Kuwana, T. J. Electroanal. Chem. **1985**, 188 59
9) Engstrom, R. C. Anal. Chem. **1982**, 54, 2310
10) Falat, L.; Cheng, H.Y. Anal. Chem. **1982**, 54, 2108
11) Gunasingham, H.; Fleet, B. Analyst (London) **1982**, 107, 896
12) Laser, D.; Ariel, M. J. Electroanal. Chem**. 1974**, 52, 291
13) Engstrom, R. C.; Strasser, V.A. Anal. Chem. **1984**, 56, 136
14) Blurton, K.F. Electrochim. Acta**, 1973**, 18, 869
15) Schreurs, J. Van Der Berg, A. Wonders, E. Barendrecht, J. R. Neth. Chem Soc. **1984**, 103, 251
16) Hine, F.; Yasuda, M.; Iwata, M. J. Electrochem. Soc. **1974**, 749
17) Lowe, E. R.; Banks, C. E.; Compton, R.G. Anal Bioanal Chem. **2005**, 382, 1169 – 1174
18) Novak, D. M.; Tilak, B. E.; Conway B. E. Modern Aspects of Electrochemistry No 14. Plenum Press, NY (1982) 195 -318
19) Janssen, L. J. J. Electrochim. Acta, **1974**, 19, 257 – 265
20) Janssen, L. J. J.; Hoogland, J. G. Electrochim. Acta, **1970**, 15, 941 – 951
21) Urushibata, H.;Uchida, I.,Toshima, S. J. Electroanal. Chem.,**1981**, 117, 43-52
22) Newbery, E.; Lopez de Haddad, M.P. Analyst. **1985**, 110, 81 –82
23) Kaminskaya, O.V.; Zakhaova, E. A.; Slepchenko, G. B. J. Anal. Chem. **2004**, 59 (11), 1091 – 1096
24) Jiang, R.; Wang, X.; Li, L.; Jiang, G. L. Electrochem. Comm. **2005**, 7, 597 – 601
25) Chebotareva, N.; Nyokong, T. J. Appl. Electrochem. **1997**, 27, 975-981

Chapter 6

Conductivity studies across composite carbon membranes

6.1 Summary

To determine the conductive properties of the ion-exchange membrane, a prototype cell was built to measure the ion-transport across the membrane. A model was chosen to describe the first 30 minutes of equilibrium in the solution compartments of the cell, which is under a concentration gradient with the deionised water compartment. Variances in the changes in the conductivity rates for the various solutions are discussed.

6.2 Introduction

Conductivity measurements were performed with a custom built cell schematically represented in Figure 3.2 in Chapter 3. There are two compartments in the custom cell, separated by an ion-exchange membrane. The membrane was equilibrated in the 0.05 M electrolyte solutions before being implemented in the cell. The one compartment was filled with 0.05M NaCl, $MgSO_4$ and KNO_3, respectively, and the other with deionised water. The purpose of these experiments was to investigate the selectivity of the ion-exchange membrane for the different anions. Figure 6.1 illustrates the ion exchange through the membrane in the custom cell. Anions in the electrolyte solutions are attracted to the anode through the membrane into the deionized water compartment. To keep neutrality in the membrane, H^+ moves through the membrane to the cathode.

The change in conductivity of the H_2O compartment is due to two possible gradients. The first is the diffusion of anions through the membrane from an area of high concentration to an area of much lower concentration; this is called the concentration gradient. The second is a much more complicated diffusion, which is caused by a potential gradient.

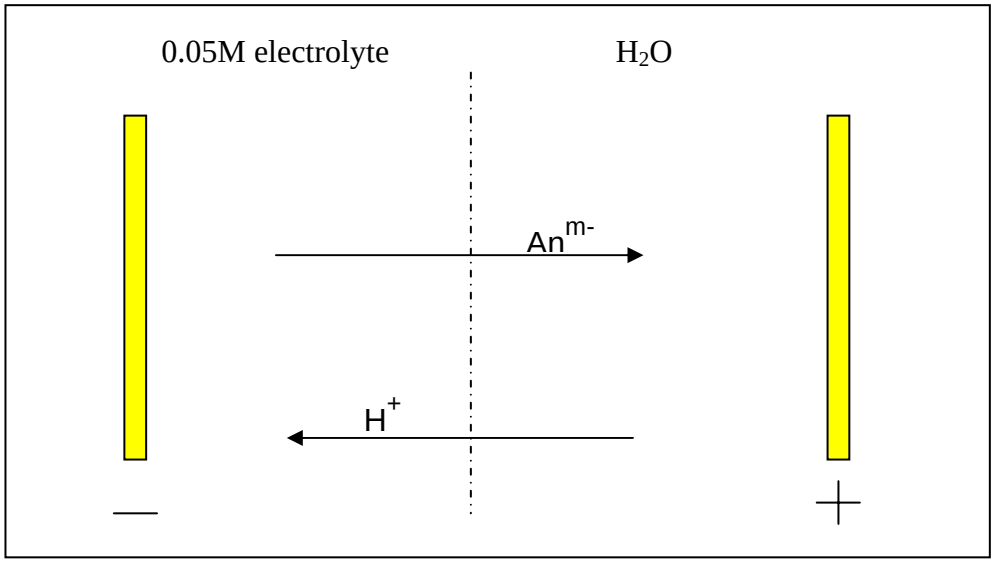

Figure 6.1: Ion exchange through the membrane in the custom cell.

According to Brüschke [1], mass transport through non-porous membranes can best be described by the so-called “solution-diffusion-model”. Figure 6.2 describes the overall mass transport in three consecutive steps:

a) Sorption of a component out of the solution in the membrane material
b) Transport through the membrane along a driving gradient
c) Desorption on the other side of the membrane

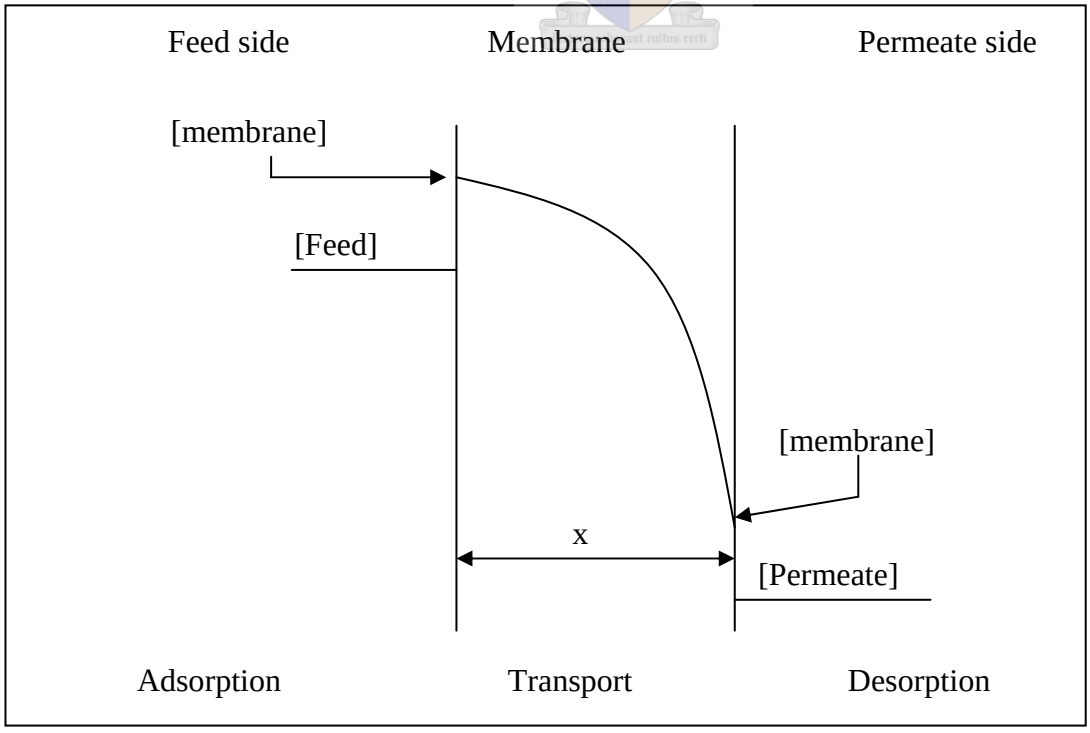

Figure 6.2: The solution-diffusion model.

Though even non-porous membranes may have pores whose diameter will be in the 5 to 10 Å range, they are still classified as non-porous and, to some degree, obey the "solution-diffusion" mechanism. After the compartments are filled, only one half of the cell is able to conduct the current through the solution. Deionised water will have a very high resistance to the flow of electrical current to complete the circuit; therefore, for the first stage of the experiment, ion transport will only occur via the concentration gradient. After a sufficient number of ions has been transported through the membrane to the opposite side of the cell, the circuit can be completed and the potential gradient will come into play. When a constant potential is applied ions are attracted to the oppositely charged electrodes. Therefore the ions are now drawn through the membrane to the opposite sides, and it is then expected that the conductivity of the water compartment will increase even more [2].

The kinetics of the ion exchange through the membrane for the concentration gradient could be described by a Michaelis-Menten type kinetics model [3]. This model is generally used to describe the enzymatic reaction on a substrate, but is also a simple transition state model to describe the transformation of a reactant via an intermediate:

$$E + S \underset{k_{-1}}{\overset{k_1}{\rightleftharpoons}} ES \xrightarrow{k_2} E + P$$

E = enzyme

S = substrate

P = product

Therefore the following model of the system is proposed:

$$M + I \underset{k_{-1}}{\overset{k_1}{\rightleftharpoons}} IM \xrightarrow{k_2} M + P$$

I = ions in solution

M = membrane

P = product

k_1, k_{-1} and k_2 are rate constants for the various reactions.

IM represents the complex formed inside the membrane. The exact nature of the intermediate is not known, but it is assumed that both physi-sorption and chemi-sorption occur.

A steady state approximation is made, therefore

$$\frac{d[IM]}{dt} = k_1[I][M] - k_{-1}[IM] - k_2[IM] = 0 \qquad (6.1)$$

$$[IM] = \frac{k_1[I][M]}{k_{-1} + k_2} \qquad (6.2)$$

$$K_m = \frac{k_{-1} + k_2}{k_1} \qquad (6.3)$$

K_m is the Michaelis constant. It represents the dissociation constant for the IM intermediate, or rather the affinity of the ion for the intermediate [4].

Therefore:

$$[IM] = \frac{[I][M]}{K_m} \qquad (6.4)$$

The rate of the reaction is:

$$\frac{d[P]}{dt} = k_2[IM] \qquad (6.5)$$

The concentration of the membrane remains constant throughout the experiment. Therefore:

$$[IM] = \frac{([M] - [IM])[I]}{K_m} \qquad (6.6)$$

Rearrangement gives:

$$[IM]\frac{K_m}{[I]} = [M] - [IM] \qquad (6.7)$$

$$[IM]\left(1 + \frac{K_m}{[I]}\right) = [M] \qquad (6.8)$$

$$[IM] = \frac{[M]}{1 + \frac{K_m}{[I]}} \tag{6.9}$$

Substituting (6.9) into (6.5) and multiply by [I]/[I] gives:

$$\frac{d[P]}{dt} = k_2[M]\frac{[I]}{K_m + [I]} \tag{6.10}$$

dP/dt is known at the reaction rate. If we take the reciprocal of (6.10) then:

$$1/\text{ rate} = \frac{K_m + [I]}{k_2[M][I]} \tag{6.11}$$

$$1/\text{rate} = \frac{K_m}{k_2[I][M]} + \frac{1}{k_2[M]} \tag{6.12}$$

In our experiments the change in concentration of the ions in solution were monitored by conductivity measurements and therefore the change in conductivity is related to the bulk change in ions (concentration), which includes H^+, OH^- as well as the ions in the 0.05M electrolyte solutions. To determine the K_m value for the various electrolyte solutions, the rate of change in the conductivity of the bulk solution is plotted against the change in conductivity of the solution.

6.3 Experimental

To determine the efficiency of the ion-exchange membrane a custom ED-cell was made. A full description of the cell was given in Section 3.4. Two compartments were separated by means of an ion-exchange membrane. The one compartment was filled with 0.05 M solutions of NaCl, $MgSO_4$ and KNO_3, the other was always filled with deionised water. The only change in conductivity of the water solution was due to anions permeating through the membrane either due to the concentration gradient or due to the applied potential. The membrane was equilibrated overnight in the respective salt solutions. A constant potential of 1.5V was applied to the cell. The change in conductivity was measured for 400 minutes for both compartments.

6.4 Results and discussion

The model described in Section 6.2 was used to evaluate the behaviour in the custom cell for the first 20 minutes. Thereafter the ion-transport was influenced primarily by the applied potential, due to there being a sufficient number of ions in the water compartment to carry the electrical current. The reciprocal of the conductivity rate change was plotted against the reciprocal of the conductivity at a certain time. The results are illustrated in Figure 6.3 for each electrolyte solution.

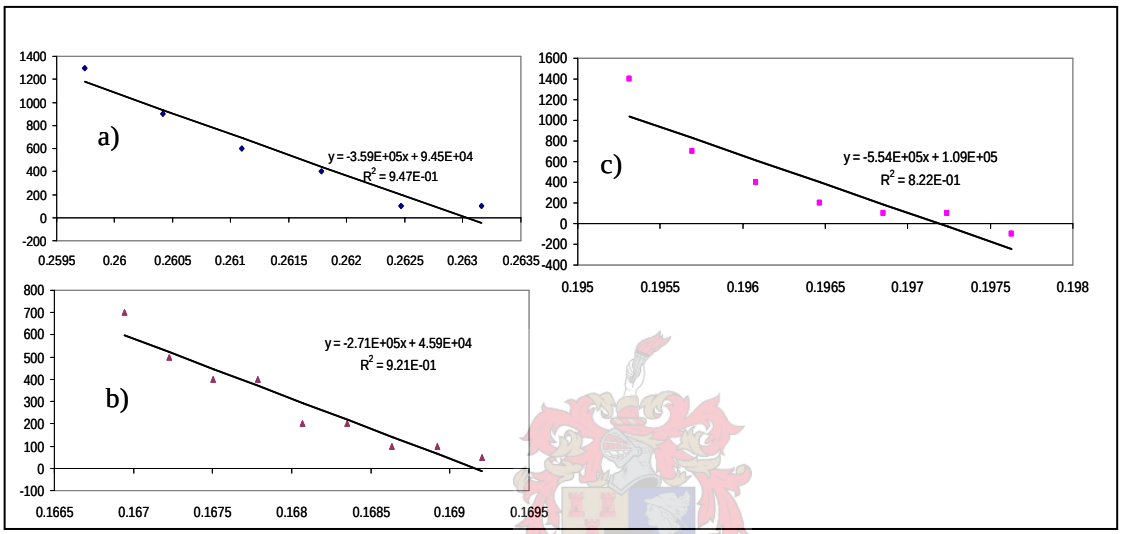

Figure 6.3: The reciprocal of the rate versus the reciprocal of the conductivity of the 0.05 M electrolyte solutions: a) $MgSO_4$, b) KNO_3 and c) NaCl.

To determine the affinity of the membrane for the various anions in solution, the K_m value for H^+ was determined in each of the 0.05 M solutions. Because the membrane has to remain neutral, we can then conclude the following:

rate of H^+ transport $\underset{\longleftarrow}{\overset{\text{membrane}}{\longrightarrow}}$ rate of anion transport

K_m was determined by dividing the slope by the y-intercept for each plot in Figure 6.3. The results for each anion solution are tabulated in Table 6.1.

Table 6.1: The slope, y-intercept and K_m (slope/y-intercept) value for each 0.05 M solution

	0.05 M $MgSO_4$	0.05 M NaCl	0.05 M KNO_3
Slope	3.59E+05	5.54E+05	2.71E+05
y- intercept	9.45E+04	1.09E+05	4.59E+04
K_m	3.802	5.071	5.912

If K_m is the affinity for the membrane towards the H^+ in the various solutions, then the intermediate inside the membrane has a much longer lifetime in the KNO_3 solution. The molar conductivities of the anions in aqueous solution are listed again (as in Table 2. 1) [5]:

SO_4^{2-} = 16.00 $S.m^2.mol^{-1}$

NO_3^- = 7.146 $S.m^2.mol^{-1}$

Cl^- = 7.632 $S.m^2.mol^{-1}$

K_m is related to the molar conductivities of the various anions in solution. This assumption can be made since 0.05 M solutions were used in all the experiments and in the same reservoirs. The conductivity of sulphate is much higher than that of nitrate and of chloride, and therefore the H^+ exchange over the membrane with SO_4^{2-} can occur more quickly. One also has to keep in mind that for membrane neutrality, two H^+ have to exchange for every one bivalent sulphate. The small K_m value for H^+ exchange in sulphate solutions indicates the lower affinity of the membrane for H^+, and therefore SO_4^{2-}. The difference in the K_m for exchange with nitrate and chloride solutions is also comparable with the difference in their molar conductivities.

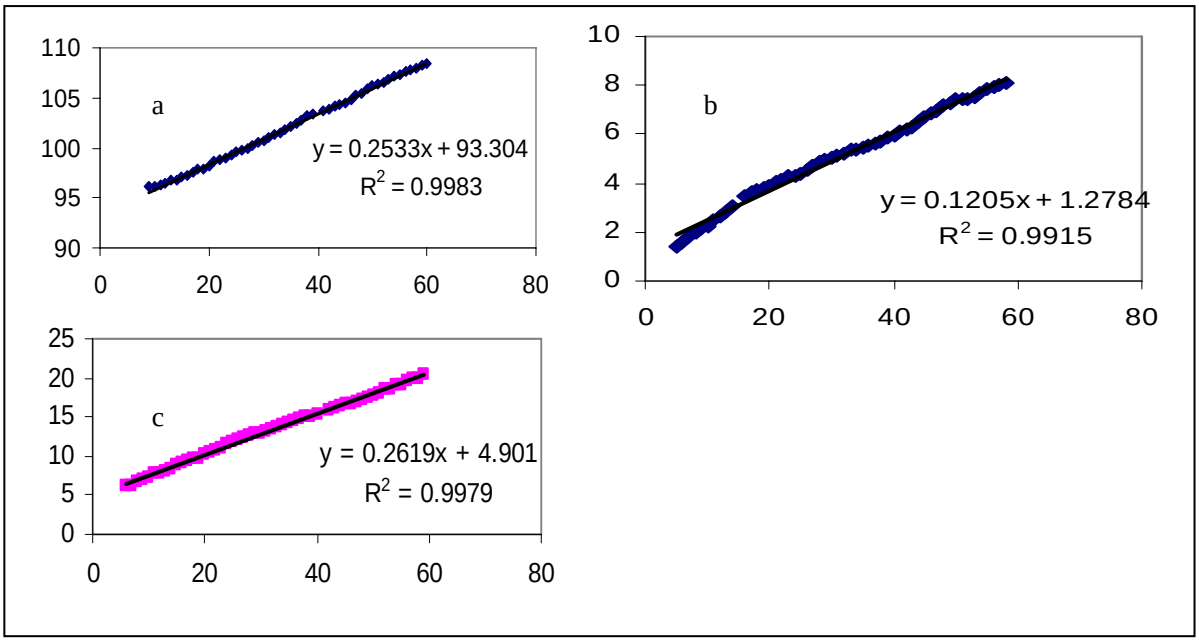

Figure 6.4: Change in conductivity measured for the first 60 min in the deionized water solutions separated from the a) KNO_3, b) NaCl and c) $MgSO_4$ solutions.

The conductivity of the deionized water cell was also monitored. The increase in conductivity is due to the anions exchanging through the membrane from the 0.05 M solution compartment. The change in the conductivity was measured for 400 min, but for the purposes of determining the concentration gradient only the first 60 min were investigated. The results are illustrated in Figure 6.4. The slope of the graph was used to determine the rate of conductivity (hence concentration) change. The cell with the 0.05 M $MgSO_4$ compartment indicated a higher increase. This was expected due to the high molar conductivity of SO_4^{2-} versus NO_3^- and Cl^- . The slope for the chloride cell had a much lower rate of increase. During the experiment for the sodium chloride cell a gas was observed in the water compartment. Even if the current could not be successfully carried through the water compartment, the chloride anions where attracted to the anode, adsorbed onto the surface and oxidized to chlorine gas. The reservoir in which the conductivity meters were set, was outside of the cell, therefore there was sufficient room for the chloride to be oxidised before being measured by the conductivity meters. Chloride ions which moved through the membrane could not be accurately measured, and therefore the slope for this anion is much lower than expected.

6.5 Conclusions

During the first 30 minutes of the experiment the Michaelis-Menten model describes the interaction of the membrane with the sulphate, nitrate and chloride solutions quite well. After the water compartment has sufficient anions to carry the potential through the cell, the potential gradient will force the anions through the membrane and the model becomes void. No significant change in the water compartment is observed to indicate when the applied potential may add to the rate of conductivity change. This is thought to be due to saturation of the membrane surface on the solution side of the cell. Because the compositional, functional and diffusional properties of the membrane materials are not known, it is difficult to understand the nature of the ion-exchange when the potential gradient comes into consideration. From Chapter 4, it could be assumed that the functional group responsible for the transport through the anion exchange membrane is in fact the alcohol group (-OH). Anions will exchange with the -OH group on the surface of the membrane, and then the anions will be attracted to the anode by the applied potential. When the anion is released, it is again exchanged for the -OH present in the aqueous solution.

6.5 References

1. Brüschke, H. Pure & Appl. Chem., **1995**, 67 (6), 993-1002
2. Ervan, Y.; Wenten, I.G. Songklanakarin J. Sci. Technol. **2002**, 24, 955-963
3. Wikipedia, the free encyclopedia, http://en.wikipedia.org/wiki/Michaelis-Menten_kinetics, updated 2005
4. Briggs, G.E.; Haldane, J. B .S. Biochem. J. **1925**, 19, 339
5. Atkins, P. W. Physical chemistry. Sixth edition 1998. Oxford University Press. Chapter 24

Chapter 7

Impedance studies of simple anions towards the carbon composite membrane

7.1. Summary

EIS was used to determine the electrical parameters of the electrode/ electrolyte/ membrane arrangement in the custom made cell. Quantitative analysis was done by fitting the data into an equivalent electrical circuit and increasing the potential from 0 V to 1.6 V. These results were used to explain the various anion (in the electrolyte) and electrode reactions as well as describe the adsorption, diffusion and charge transfer phenomena that may occur at the electrolyte and membrane interfaces.

7.2. Introduction

7.2.1 Data presentation

Electrochemical impedance is measured by applying an AC potential to an electrochemical cell and measuring the current through the cell.

The application of a sinusoidal voltage (excitation signal) at time t:

$$V(t) = V_o \sin \omega t \qquad (7.1)$$

V_o = the maximum amplitude

$\omega = 2\pi f$

= the frequency (rad s^{-1}) to an electrical circuit that contains a combination of resistances and capacitances which will adequately represent the electrochemical cell.

f = frequency in Hz

The current response is given by:

$$I = I_o \sin (\omega t + \varphi) \qquad (7.2)$$

I_0 = the maximum current response

φ = the phase angle between the perturbation and the response.

Therefore

$$Z = V(t)/I(t) = \frac{V_0 \cos(\omega t)}{I_0 \cos(\omega t - \varphi)} = \frac{Z_0 \cos(\omega t)}{\cos(\omega t - \varphi)} \quad (7.3)$$

with Z_o = the amplitude of the impedance

t he phase shift = $\frac{\cos(\omega t)}{\cos(\omega t - \varphi)}$

Impedance is presented by a complex plot using Eulers relationship:

$$\text{Exp}(j\varphi) = \cos\varphi + j\sin\varphi \quad (7.4)$$

Therefore

$$V(t) = V_0 \exp(j\omega t) \quad (7.5)$$

and

$$I(t) = I_0 \exp(j\omega t - j\varphi) \quad (7.6)$$

$$Z = V/I = Z_0 \exp(j\varphi) = Z_0 (\cos\varphi + j\sin\varphi) \quad (7.7)$$

This is represented in a Nyquist complex plot in Figure 7.1:

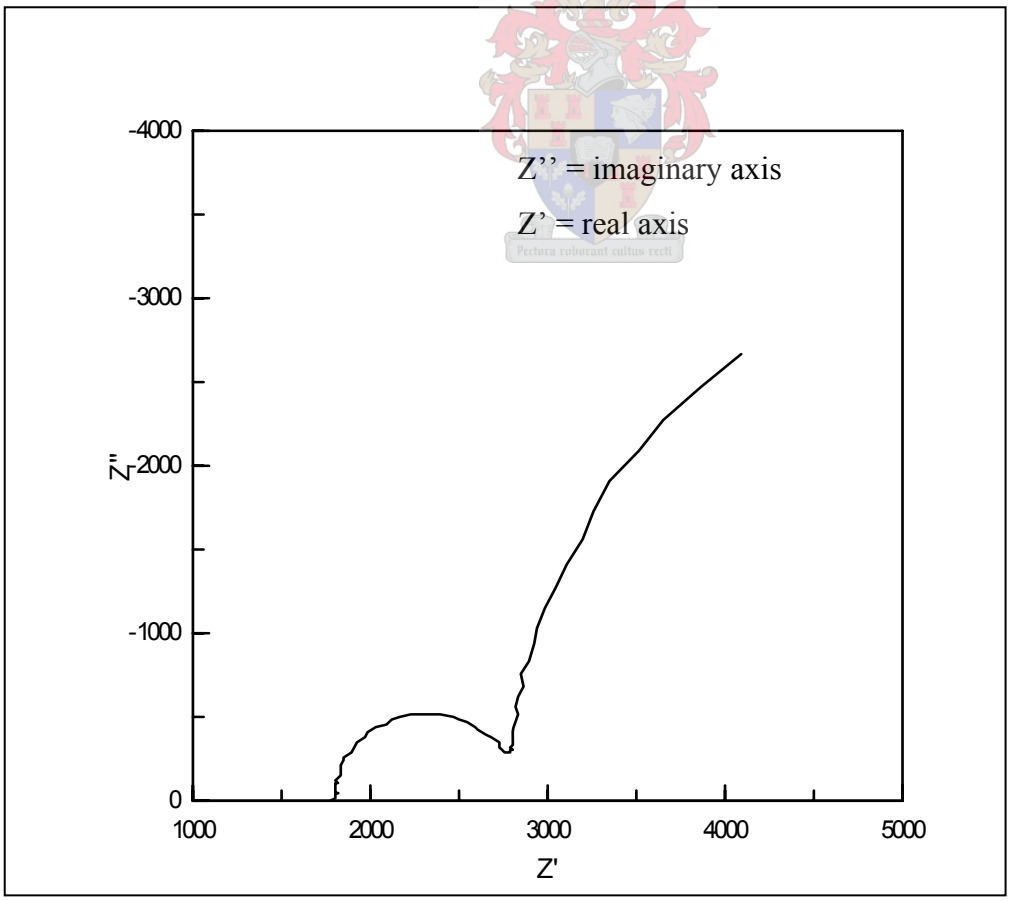

Figure 7.1: Complex plot of EIS data with an electron transfer reaction.

In the complex plot the semicircle at low values of Z' corresponds to the high frequency region. In EIS the high frequency region is usually interpreted as the electrical properties of the bulk electrode material under investigation. The low frequency region (high Z' value) provides information about the interfacial region in an electrical cell. The interfacial region in turn, provides information about the double layer (Helmholtz layer). The double layer exists on the interface between the electrode and its surrounding electrolyte. This layer is formed by ions of opposite charge adsorbing on the electrode surface. A major disadvantage of the Nyquist plot is the fact that you cannot tell what frequency was used to record the various data points in the plot. In the Bode plot, the magnitude (absolute value) of the impedance and the phase angle of the impedance vector can be plotted individually against the logarithm of the frequency [1, 2]. Warburg diffusion, for example, is observed between 10^3 and 10^{-5} Hz as a characteristic 45^0 slope.

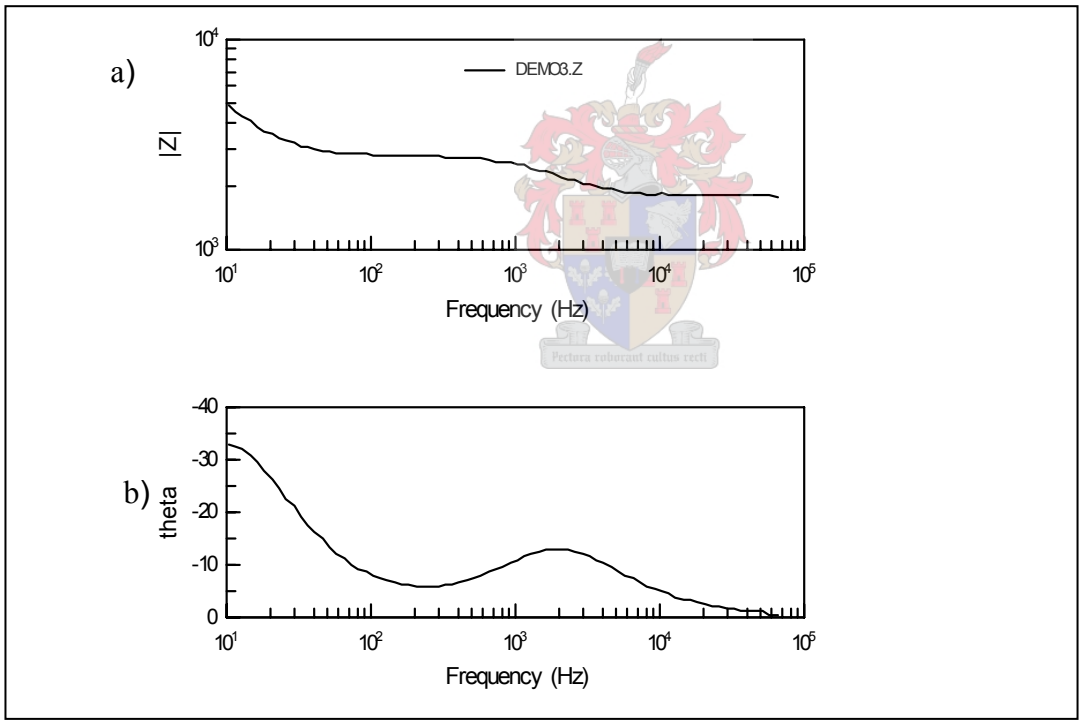

Figure 7.2: Bode plots: magnitude (a) and angle phase (b) change vs frequency [3].

Another popular presentation of the impedance on the Bode plots is to plot the log frequency on the x-axis and both the log of the absolute values of impedance and the phase shift on the y-axis [4, 5]. Figure 7.3 illustrates these Bode plots used to describe an electrical circuit with one time constant.

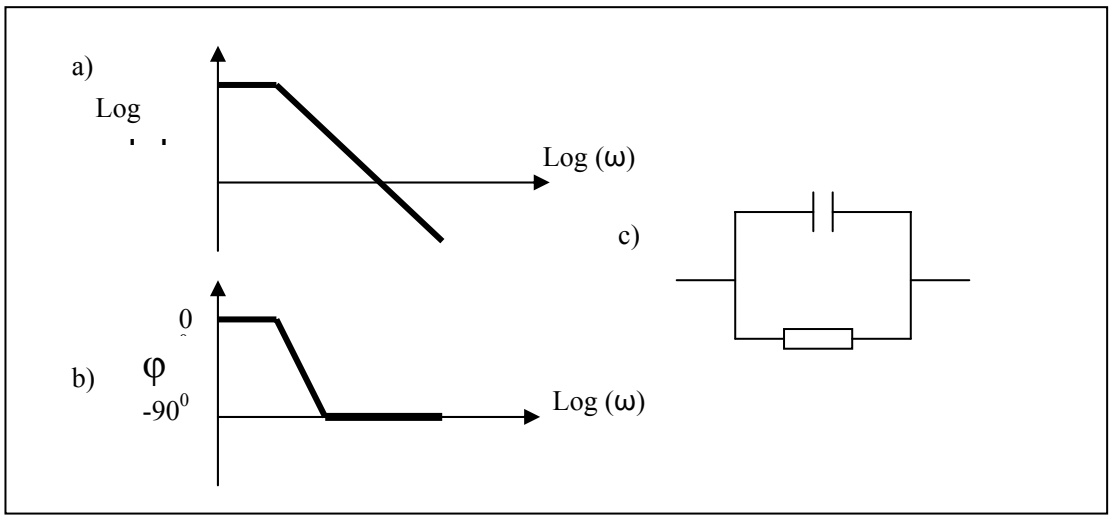

Figure 7.3: Bode plots: a) the log of the absolute value and b) the phase shift versus log frequency for the electrical circuit (c).

7.2.2 Common electrical circuits and circuit parameters

The most commonly used model for a simple electron transfer reaction includes the following:

- uncompensated solution resistance (R_s) in series with
- the double layer capacitance (Cd*l*)
- a charge transfer resistance (R_{ct}), and
- frequency dependent resistance, the Warburg impedance (Z_w).

The relative size between R_{ct} and Zw at any given frequency is a measure of the balance between kinetic and diffusion control. The simplified equivalent electrical circuit is called the Randles equivalent circuit.

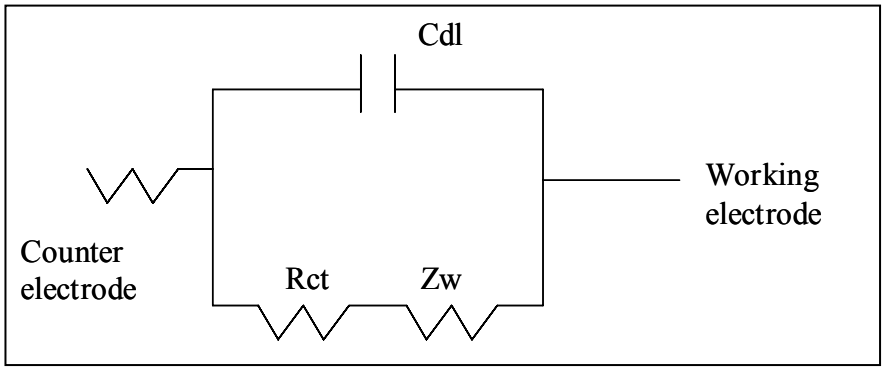

Figure 7.4: A Schematic diagram of the Randles equivalent circuit.

EIS is often analyzed by fitting it to an equivalent electrical circuit using common electrical elements such as resistors, capacitors and inductances.

Electrical element	Current vs voltage	Impedance
Resistor	E = I/R	Z = R
Inductor	E = L di/dt	Z = jωL
Capacitor	I = C dE/dt	Z = 1/jωC

Inductor impedances increase as the frequencies increase, whereas the impedance of capacitors decreases with increasing frequency. Capacitors have only an imaginary impedance component and the current through a capacitor is phase shifted 90 degrees with respect to the voltage [6, 7].

7.2.3 EIS for membranes

EIS has been used to determine the electrochemical characteristics of ion-exchange membrane (IEM) systems in order to understand the transport phenomena in these systems [8]. The functional groups on the membranes have fixed charges, which have a significant effect on the ion-exchange behaviour of the membranes. When an electric current passes through the membrane system, the current is carried by both positive and negative ions in the bulk solution phase, but mainly by the counterions in the IEMs due to Donnan exclusion. Moreover, the different transport numbers of the counterions in the bulk solution phase and the membrane leads to depletion in electrolyte concentration on the dilute solution side and to enrichment on the concentrated solution side [9]. As a result, concentration polarization occurs at the interface between the IEM and the electrolyte solutions, and polarized layers, i.e. the diffusion boundary layer (DBL), are finally formed on the membrane surface. Park et al [8] carried out impedance studies and found that the DBLs' conductivity is much lower that that of the ion-exchange membrane, which leads to higher impedance to current passing through the ion-exchange membrane. They inferred that at low frequencies the capacitive loop represents the electrical responses to interfacial phenomena (e.g., DBL, heterogeneous transport) originating from the IEM [10]. The impedance loops are affected by the concentration of the electrolyte and the distance between the two reference electrodes. The equivalent circuit for IEM systems is generally depicted as in Figure 7.5.

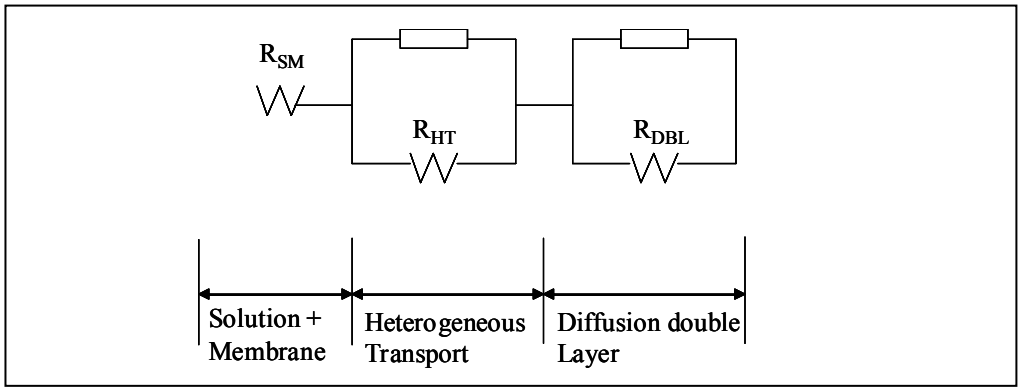

Figure 7.5: Representative equivalent circuit for the IEM system used in most systems, showing the effects of the membrane immersed in solution (SM), heterogeneous transport (HT), and the diffusion double layer (DBL).

In Figure 7.5 the IEM system is represented by a resistance and two parallel combinations of a resistance and a constant phase element.

EIS is also used to study fouling effects on membrane systems [10]. In general, the foulants present in natural streams are negatively charged and affect anion-exchange membranes containing fixed positive functional groups. The extent and nature of the fouling tendencies in ED are related to the electrochemical and physical properties of ion-exchange membranes and the foulants. EIS analysis done by Park et al [8, 10] proposed the following new equivalent circuit to illustrate the effect of fouling on the membrane (Figure 7.6).

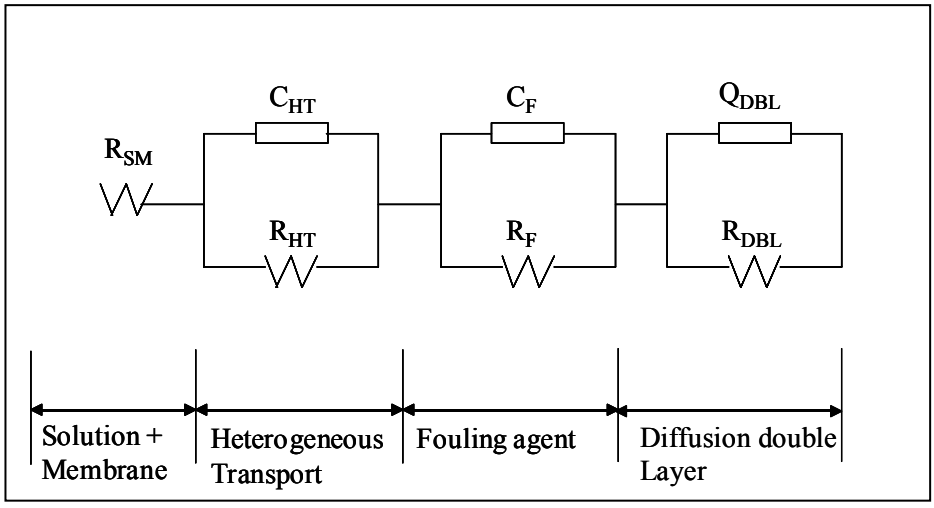

Figure 7.6: Equivalent circuit for an ion-exchange membrane system in the presence of a fouling agent. The system consist of the membrane immersed in solution (SM), heterogeneous ionic transport (HT), the fouling agent (F) and the diffusion boundary layer (DBL).

Lee et al [11] studied the electrical properties of composite RO membranes. They used an electrochemical cell with the following arrangement:

Electrode | NaCl solution | Membrane | NaCl solution | Electrode

The electrolyte and membrane were placed between two Pt electrodes. They analysed the above system with the following parameters; the capacitance and the resistance of the solution and membrane, and the interfacial properties between the solution and electrodes. At low frequency a Warburg impedance was introduced to analyse the electrical double layer and diffusivity of ions in solution. The equivalent circuit which illustrates all these phenomena is represented as shown in Figure 7.7.

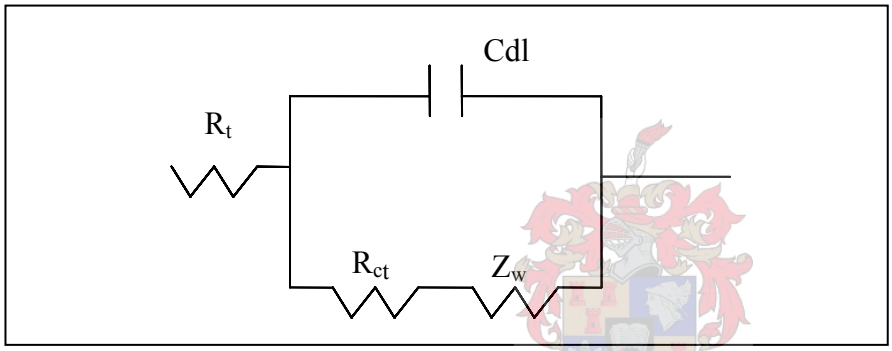

Figure 7.7: The equivalent circuit as suggested by Lee et al [11].

They also suggested the following equivalent circuit for a bathing solution membrane combination

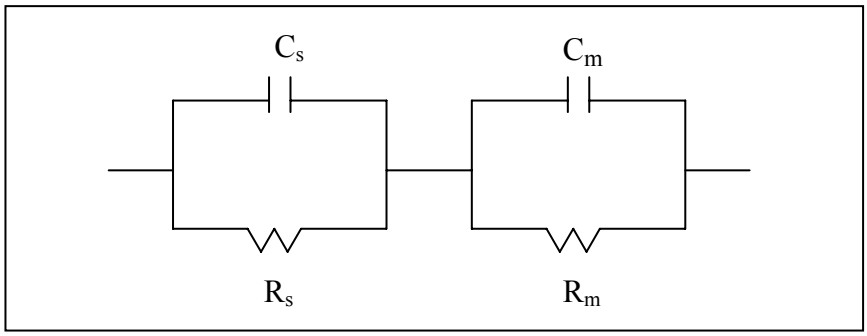

Figure 7.8: The equivalent circuit suggested by Lee et al [11] for a bathing solution membrane combination.

Here Rs and Cs are the total resistance and the capacitance of the solution, and Rm and Cm are the capacitance and the resistance for the membrane. They concluded that the

performance of RO membranes were improved by lower concentration of the electrolyte and less dipping in the aqueous phase, because this would then decrease the membrane resistance and increase the capacitance and dielectric constant. Acid dipping also decreased the membrane resistance.

7.3. Experimental

Experimental procedures for the EIS analysis containing the carbon composite membrane are outlined in Chapter 3.6. The response of the cell is measured over the higher frequency range and then analysed in the complex plane.

7.4 Results

Figure 7.9 and 7.10 illustrate typical results from the EIS runs over the potential range in the higher frequency region. For ZPLOT to fit the particular data, an equivalent circuit was chosen, which included the simple Randles equivalent circuit (for electrodes) and the equivalent circuit used by Part et al [10] to describe the parameters for ion-exchange membranes. All experiments were done at higher frequencies (10^5 to 10^{-1} Hz). The circuit for heterogeneous transport could then simply be included in the total resistance of the electrolyte.

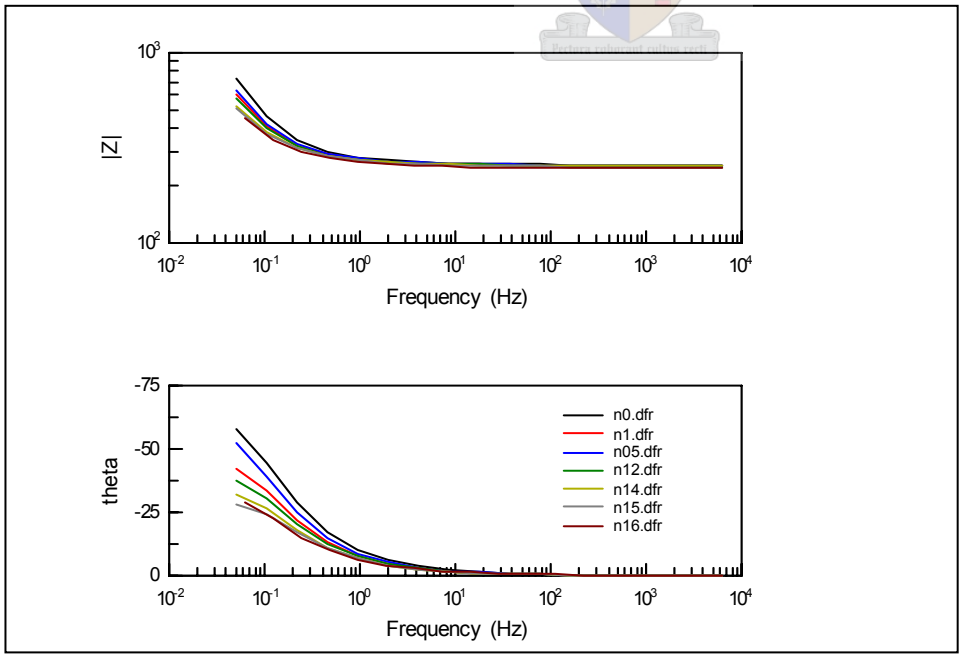

Figure 7.9: Bode plot: NaCl electrolyte solution in the high frequency region.

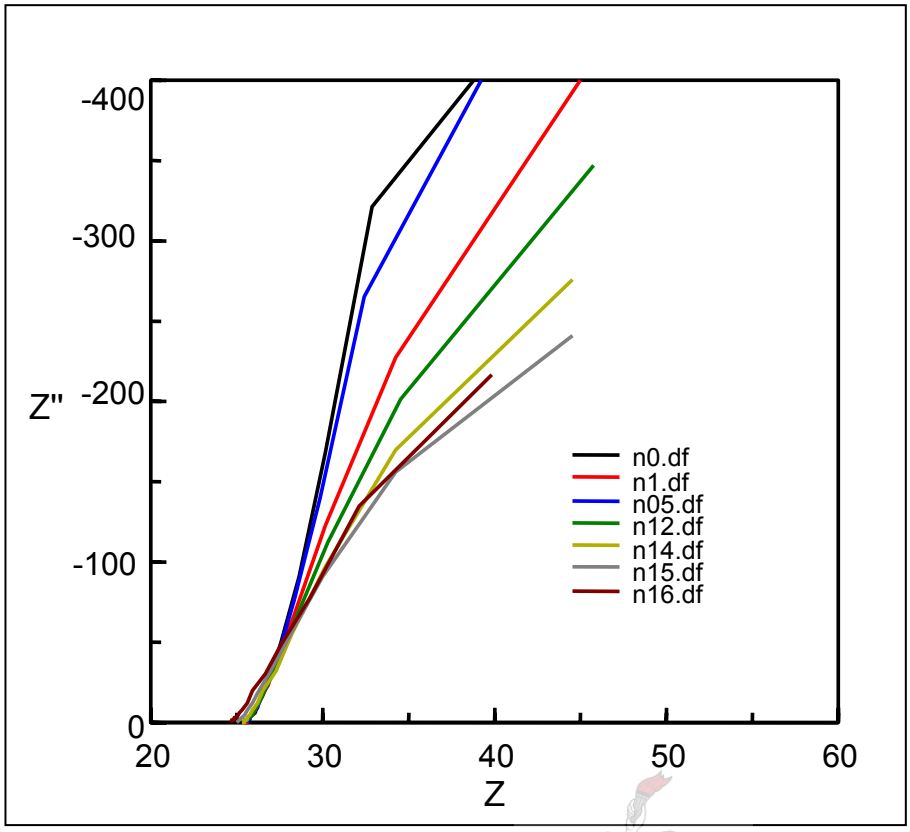

Figure 7.10: Complex plane for 0.05 M NaCl electrolyte solution for increasing applied potential.

The circuit used to describe the system with the best fit with Z-plot software is shown in Figure 7.11.

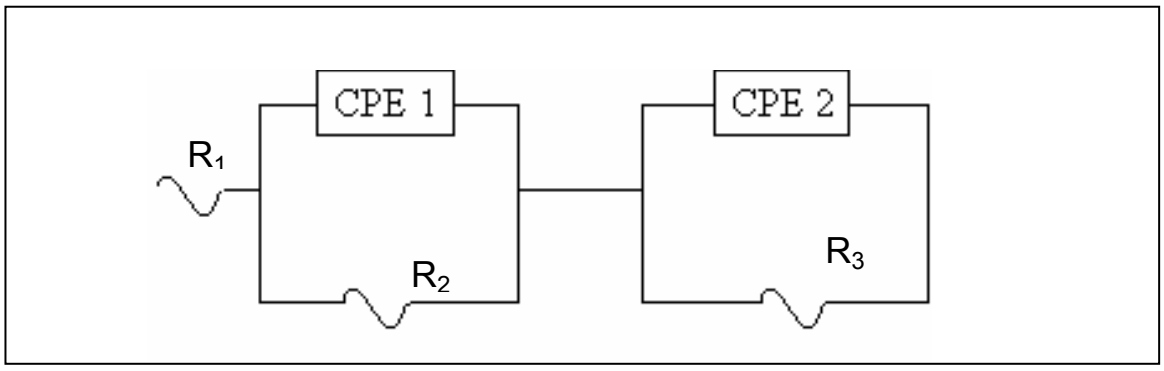

Figure 7.11: The electrical equivalent circuit depicting the results from the impedance studies done on the carbon composite membrane, in NaCl, $MgSO_4$, and KNO_3.

R_1 represents the resistance of the electrolyte solution. The constant phase element (CPE) is used in the model instead of a pure capacitor to compensate for non-homogeneity in the

system. For example, a rough or porous surface can cause a double layer capacitance to appear as a constant phase element, with a CPE-P between 0.9 and 1.

The CPE is defined by two values: CPE-T and CPE-P.

$$Z = 1/ [T (j\omega)^{P}] \qquad (7.8)$$

CPE-T is the capacitance associated with the constant phase elements. CPE-P is related to the capacitive or resistive nature of the constant phase element. If CPE-P is equal to 1 (in 7.8) then the equation is identical to that of the capacitor. When a CPE is placed in parallel to a resistor, a Cole-element (depressed semi-circle) is produced [12].

The CPE1 is associated with the behaviour at higher frequency and CPE2 accounts for the behaviour at lower frequency. CPE1 and R_2 describe the glassy carbon electrode in the cell. CPE1 is assumed to be the diffuse double layer for the electrode/electrolyte interface. To visualise the capacitance effect of the double layer, Figure 7.12 is an illustration of the double layer on the electrode interface, as described by the Stern model [13]. The double layer exits as a result of the alignment of ions (in solution) of opposite charge at the electrode surface. In the figure the effect of solvation has been ignored. The ions closest to the electrode are constrained into a rigid Helmholtz plane (OHP) while outside that plane the ions are dispersed as in the Gouy-Chapman model.

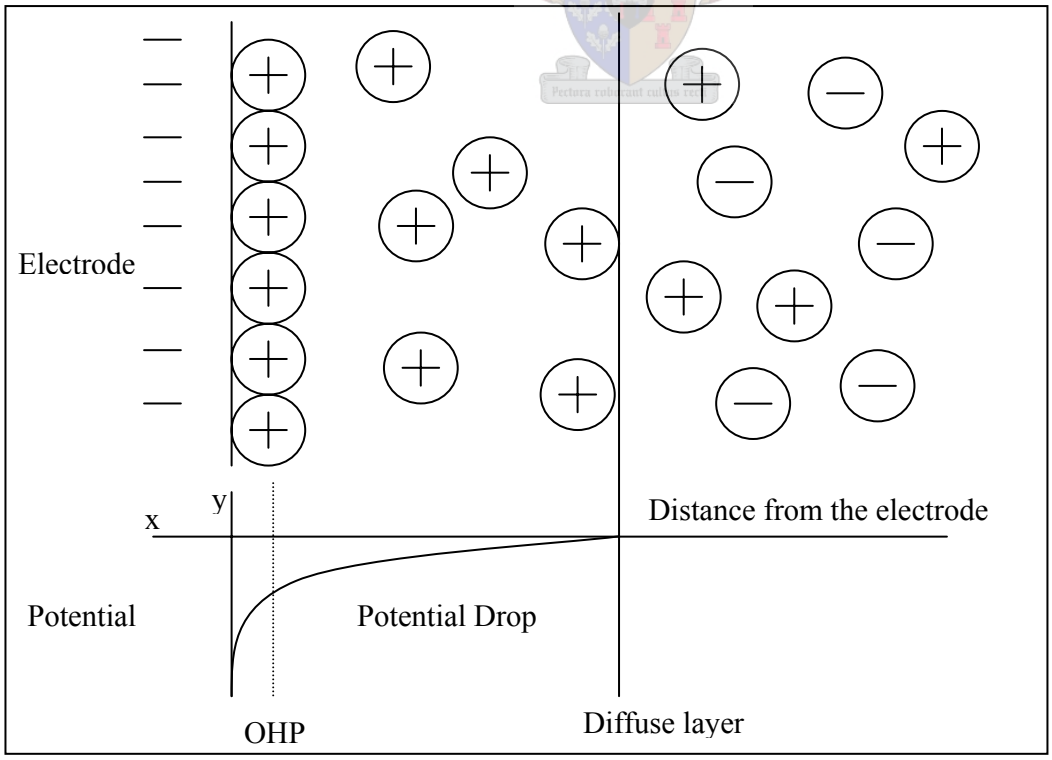

Figure 7.12: The Stern model for the electrical double layer, which includes the diffuse layer.

CPE2 and R_3 are the electrical properties of the composite carbon membrane. The qualitative results for the equivalent circuit with increasing applied potential, modelled in Figure 7.11, are tabulated for each electrolyte in Table 7.1.

Table 7.1: Equivalent circuit fitting results for the cell setup with 0.05 M NaCl as electrolyte

Potential V	R_1 (ohm)	CPE1-T Farads/cm^2	CPE1-P	R_2 (ohm)	CPE2-T Farads/cm^2	CPE2-P	R3 (ohm)
0	255.6	0.015294	0.49881	63.85	0.004806	0.94232	10964
0.5	255.3	0.016110	0.50522	55.84	0.005799	0.94343	4715.0
1	255.0	0.014540	0.52518	254.0	0.007958	1.00000	1215.0
1.2	254.2	0.014744	0.51168		0.010251	1.00000	680.30
1.4	253.5	0.014321	0.52774	291.1	0.011405	1.00000	552.20
1.5	250.1	0.013394	0.53932	195.4	0.011962	1.00000	452.30
1.6	246.9	0.010567	0.59655	64.89	0.010000	1.00000	506.00

Table 7.2: Equivalent circuit fitting results for the cell setup with 0.05 M KNO_3 as electrolyte

Potential V	R_1 (ohm)	CPE1-T Farads/cm^2	CPE1-P	R_2 (ohm)	CPE2-T Farads/cm^2	CPE2-P	R_3 (ohm)
0	228.8	0.013149	0.55549	29.24	0.004741	0.93421	off scale
0.5	221.9	0.011726	0.59641	20.17	0.004737	0.92387	34219
1.0	220.6	0.017341	0.50425	66.74	0.005795	0.95636	4318.0
1.2	218.3	0.017216	0.50248	95.27	0.006624	0.96482	1755.0
1.4	218.5	0.019637	0.49121	46.59	0.006920	0.91951	850.8.0
1.5	216.9	0.022547	0.47509	29.18	0.007124	0.88542	693.80
1.6	216.8	0.020231	0.50853	95.56	0.009050	0.93674	469.70

Table 7.3: Equivalent circuit fitting results for the cell setup with 0.05 M $MgSO_4$ as electrolyte

Potential V	R_1 (ohm)	CPE1-T Farads/cm^2	CPE1 –P	R_2 (ohm)	CPE2-T Farads/cm^2	CPE2-P	R_3 (ohm)
0	387.5	0.00958	0.55409	49.03	0.004434	0.92537	off scale
0.5	387	0.009451	0.55243	40.51	0.004682	0.90327	off scale
1	386.8	0.009719	0.53868	169	0.006226	1	2903
1.2	386	0.009857	0.54221	208.9	0.006844	1	1597
1.4	385.2	0.009827	0.55451	2495	0.009953	1	517.1
1.5	377.6	0.0923	0.56167	633.7	0.010557	1	460.4
1.6	373.2	0.010248	0.54243	377.9	0.00937	1	494.4

7.5 Discussion

The resistance of the electrolyte solutions, R_1, remains relatively constant with an increase in potential, decreasing very slowly from 1.4 V. CPE1-T values for the various electrolyte solutions are compared in Figure 7.13.

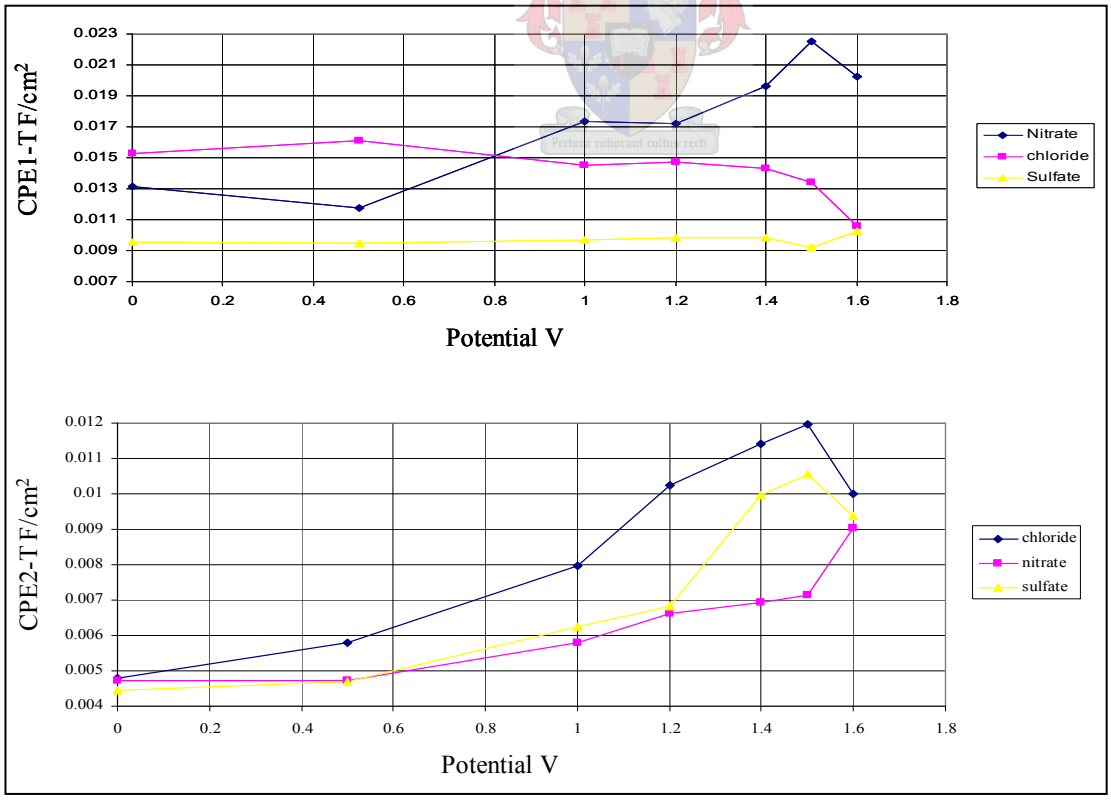

Figure 7.13: Changes in CPE with an increase in potential in 0.05 M solutions of $MgSO_4$, NaCl and KNO_3.

The double layer is formed when the potential is applied and ions of opposite charge are attracted to the electrode surface. Until 0.5 V the capacitance of the electrode in the solutions remain relatively constant, thereafter the capacitance of the nitrate solution increases sharply with potential, implicating an increase in the thickness of the diffusion layer. The chloride solution capacitance on the electrode decreases steadily and that of the sulphate solution remains constant. The decrease in the chloride solution is due to oxidation of Cl^- to chlorine gas above 0.75 V. This oxidation reaction is confirmed in CV and LSV. Consequently, depletion of chloride in the vicinity of the electrode occurs, therefore decreasing the thickness of the electrical double layer. Chloride is the only anion (of the three) that absorbs to the surface of the electrode and absorption increase with the formation of the surface oxide on the carbon electrode. Therefore the reduction of chlorine is accelerated and CPE1-T decreases.

Sulphate does not adsorb onto the surface of the electrode, but forms a diffusion double layer, which remains constant. The slight decrease in the CPE1-T value of the nitrate solution until 0.6 V is associated with the oxidation of nitrite to nitrate (depletion in nitrites next to the electrode surface). Nitrate is a larger molecule with a higher electronegativity, therefore the diffusion layer increases with increasing concentration of nitrate, adding to the capacitor effect. This oxidation reaction is also described in Section 5.2.2.

The CPE1-P value for all electrolyte solutions is relatively constant over all applied potentials. The Warburg impedance is assumed for nonhomogeneous surfaces and non-uniform diffusion layers when CPE-P is equal to 0.5 [14, 15]. This implies that the electrochemical reaction is under partial or complete mass transport diffusion control. This confirms that CPE1 is representative of the carbon electrode and that CPE1-T describes the diffusion layer on the electrode surface.

R_2 is the electrode resistance to charge transfer. Until an applied potential of 0.5 V the resistance of the electrode remains constant for all electrolyte solutions. Thereafter the increase in resistance is related to the formation of the surface oxide layer described in Section 2.2.1. Chlorine gas kinetics are strongly dependent on the surface of the anode material. In the case of glassy carbon, the surface quinonic groups accelerate the reduction of chloride to Cl_2. This is confirmed by the decrease in resistance to the electron transfer to

chlorine after 1.4 V. The large increase in the R_2 resistance in the sulphate electrolyte solution could be ascribed to the sheer size and hydration volume of the sulphate ion. After an applied potential of 1.5 V, water itself is oxidised to oxygen, and therefore the resistance R_2 for all electrolyte solutions decreases.

CPE2-T for the electrolyte solutions forms a thicker diffusion double layer with increasing applied potential. As the applied potential increases, the membrane itself is polarised. The fluctuational increase of CPE2-T in the nitrate solution observed in Figure 7.13 is ascribed to the possible electron transfer that can occur on the surface of the membrane to oxidize nitrite to form nitrate. CPE2-P remains in the area 0.9 -1 Farads/cm^2, confirming the capacitance behaviour of the non-homogeneous or porous surface.

R_3, which relates to the resistance of the membrane itself, decreases exponentially with applied potential for all the electrolyte solutions. This is due to the formation of the diffusion double layer, which grows thicker with increasing applied potential, and then offers a lower resistance to charge transfer. Therefore the conductivity of the membrane increases with applied potential; it has a thicker diffusion layer, but lower resistance to charge transfer (diffusion through the membrane).

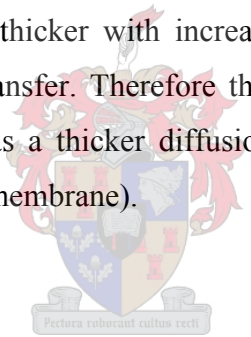

7.6 Conclusions

The equivalent circuit used to fit the impedance results is the same model suggested by Park et al [10] for IEM systems. The resulting complex plots will differ however because in this study different membranes were investigated and studies were carried out at high frequencies.

The SEM images included in Section 4.4 confirm the high surface roughness described by the near pure capacitor behaviour of the composite membrane. Figure 7.14 shows a SEM image of the custom carbon electrode used inside the cell. The rough and non-homogeneous surface confirms the Warburg experienced by the electrode surface.

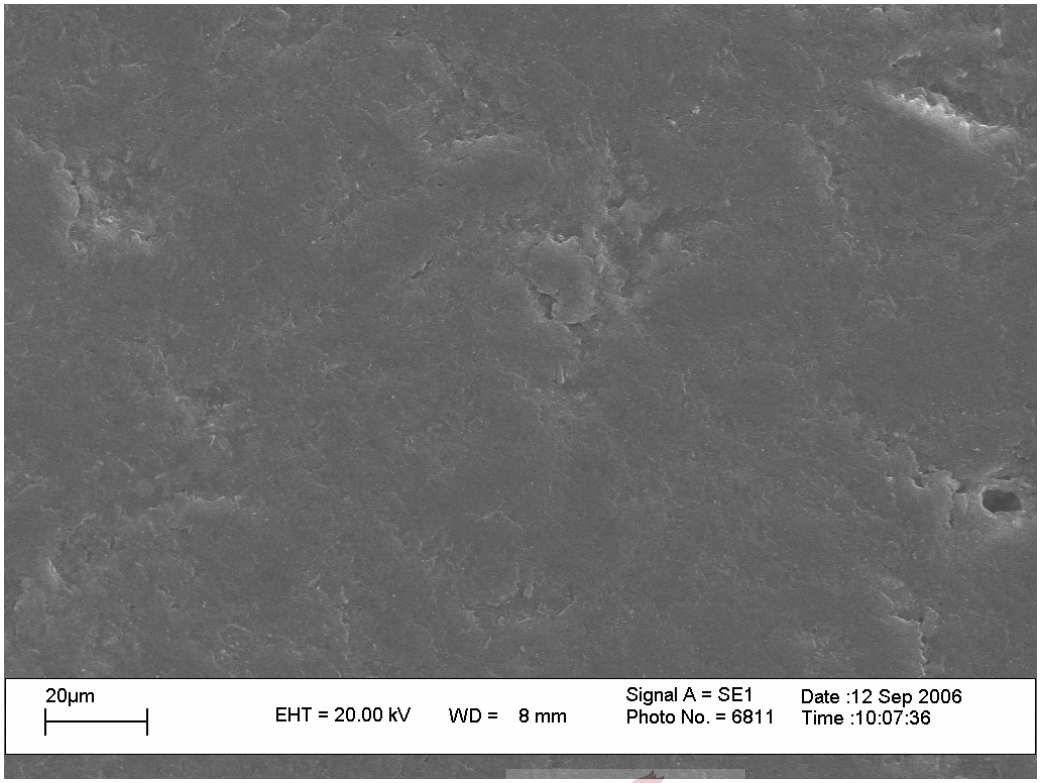

Figure 7.14: SEM image of the custom carbon electrode showing a rough and non-homogeneous surface.

To compare the capacitance observed on the custom electrode during the voltammetry studies (Section 5.5) and the impedance studies in this Chapter, the following must be taken into consideration:

- During the voltammetry studies the potential was swept over a whole potential window in one run, whereas the potential was kept constant for each measurement during the impedance studies.
- The capacitance measured in voltammetry is a pure capacitance, whereas a CPE, constant phase element, was used to describe the behaviour on the electrode surface in the impedance studies.

The capacitance observed for each anion in impedance increased as follows for a constant potential of 0 to 0.8 V:

$$SO_4^{2-} < NO_3^- < Cl^-$$

and for the potentials 0.8 to 1.6 V:

$$SO_4^{2-} < Cl^- < NO_3^-$$

The same order was observed for the voltammetry studies as in the latter impedance potential window. This selectivity differs from the other commercially available electrodes, due to the major differences in surface morphology and impurities on the surfaces.

The observed increase of the diffusion layer after 1.4 V for nitrate and the decrease for chlorine is confirmed by voltammetry studies. Nitrite is oxidised to nitrate at 0.9 V:

$$NO_2^- + 2H_2O \rightarrow NO_3^- + 2H^+ + 2e^- \quad (5.12)$$

Nitrate is a larger anion and increases the size of the diffuse layer, so increasing the capacitance. Chloride is oxidised to chlorine gas at 1.2 V:

$$Cl^- + e^- \rightarrow Cl_2 \quad (5.8 \text{ and } 5.9)$$

This reduces the amount of chloride in the area of the electrode and decreases the diffuse layer. No sulphate reactions were observed on the surface of the custom electrode therefore the diffusion layer remained relatively constant throughout the impedance studies.

Conductivity studies have shown that the composite membrane will have an affinity for the anions in the following order:

$$SO_4^{2-} < Cl^- < NO_3^-$$

Therefore the membrane "holds" onto nitrate the strongest, and transports sulphate much faster. The diffusion layers observed during the studies indicate that chloride forms a larger layer than sulphate does. The smaller diffusion layer could be described by the transport of ions through the membrane. The high affinity (Km) of the membrane for nitrate and the smaller diffusion layer could possible be a result of ion-exchange occurring between the anion and a surface functional group in the membrane.

Chilcott et al [16] have shown that the conductances of systems at lower frequencies are especially sensitive to the porosity inside the membrane. This, and the highly corrugated surface of the membrane, makes it necessary to consider more layers in the diffusion layer than the Helmholtz and Gouy-Chapman diffusion layers. Therefore a direct correlation between the conductance and capacitance on the membrane surface is still under investigation.

7.7 References

1. Priscilla G.L. Baker. PhD thesis. Sol-Gel Preparation, characterization and electrochemistry of mixed metal tin oxide electrodes. Chapter six. University of Stellenbosch. (2004) 76 – 113
2. Textbook of Electrochemistry. G. Kortüm, JO' M Bockris, volume 1951
3. Zplot online software manual: Bode and complex plots
4. Application notes from Gamry instruments, http://www.gamry.com, accessed July 2006
5. Application note BL8 from Princeton Applied Research, http://new.ametek.com, accesses July 2006
6. Brett, C. M. A; Brett, A. M. O. Electrochemistry. Principles, methods and applications. Oxford Univerity Press. (1996) Chapter 11, 224 – 251
7. . McDonald, J. R. Impedance Spectroscopy. John Wiley and Sons.(1995) 12-20
8. Park, J-S.; Choi, J-H.; Woo, J-J.; Moon, S-H. J. Colloid and Interface Sci. **2006**, 300, 2, 655-662
9. Barrangán, V. M.; Ruíz-Bauzá, C. J.Colloid Interface Sci. **1998**, 205 365
10. Park, J.-S.; Choi, J-H.; Yeon, K.-H.; Moon, S-H. J. Colloid and Interface Sci. **2006**, 294 129
11. D.-J. Lee, Y.-K. Choi, S.-B. Lee, K.-H. Ahn, B.-R. Min. Journal of Membrane Science. **1998**,150, 9-21
12. ZVIEW online software manual: Distributed circuit elements
13. Atkins, P.W. Physical Chemistry. Sixth Edition. 1998. Oxford University Press. Chapter 29
14. Park, S.-M.; Yoo, J.-S. Anal. Chem. **2000**, 75, 455A
15. Park, S-M.; Yoo, J.-S.; Chang B.-Y.; Ahn, E.-S. *Pure Appl. Chem*. **2006**, 78, 1069
16. Chilcott, T.C.; Chan, M.; Gaedt, L.; Nantawisarakul, T.; Fane, A.G.; Coster, H. G. L. J. Memb. Sci. **2002**, 195, 153-167

Chapter 8

Conclusions and recommendations for further studies

8.1 Conclusions

The primary task of the project was to characterize a patented composite carbon ion-exchange membrane. From elemental analysis done with EDX and PIXE it was established that the primary elements in the membrane were chloride, fluoride, oxygen, carbon and possibly hydrogen. With LC-MS and IR it was established that the membranes consisted of two polymers, with no carbonyl or aromatic functional groups. The molecular ion separations in the LC-MS spectra are similar to the molecular mass units in PEG and PEO. Thermal analysis indicated melting peaks corresponding to PEG and PEO (52^0C), propylene hexafluoropropylene tetrafluoroethylene copolymer (276^0C) and PCTFE (Kel-f, 138^0C).

After functional and elemental analysis the following possibilities remained: hexafluoropropylene tetrafluoroethylene copolymer, polychlorotrifluoroethylene (PCTFE), polyoxyethylene oxide (PEO) and polyethylene glycol (PEG).

The membranes investigated where made from the same materials, due to the fact that they had approximately the same elemental analysis, the same IR spectra and the same thermogram results. The presence of a cross-linked polymer is strongly suggested due to the early thermal degradation of the polymer and low solubility in concentrated sulphuric acid.

The carbon electrode used in the custom-made cell was electrochemically evaluated with CV, LSV and EIS. The capacitances measured during the voltammetry experiments of the custom carbon electrode, the used commercial carbon electrode and the carbon sheet were compared to that of commercial GCE

These electrodes were subjected to LSV and CV experiments in the same 0.05M sulphate, nitrate and chloride electrolyte solutions.

Reduction of the surface functional groups influenced the size of the double layers observed on the used and polished GCE. The reduction of the surface increases the surface porosity and surface roughness, which adds to the higher surface area.

The porosity and the impurities on the surface of the carbon sheet and the custom carbon electrode add considerably to their capacitance. The larger active surface area used in these experiments also induces a much larger double layer.

The oxidation of nitrate and the reduction and oxidation of chlorine were only observed on the glassy carbon electrodes. These reactions are diffusion controlled and are irreversible. Surface redox reactions were observed on all the electrodes. These surface reductions were also found to be highly irreversible. The oxidation of sulphate was observed on the polished GCE and the reduction of sulphate was observed only on the commercial GCEs. At lower and higher pH the reduction of hydrogen and the adsorption of oxygen inhibited all redox reactions.

The Michealis-Menten model was used to describe the first 30 min of the conductivity experiments. After sufficient ions have been transported across the membrane the electrolyte can carry a potential difference and a potential gradient is then applied, and then the Michealis-Menten model no longer applies. It is suggested that the ion-exchange membrane is basic and has a stronger affinity for SO_4^-. The possible ion exchange that occurs on the surface of the membrane is between the anions in solution and the alcohol group (observed in the IR-spectra).

EIS were carried out at high frequencies to determine the electrical properties of the membrane-electrode-electrolyte cell design. The high surface roughness of the membrane caused its almost pure capacitor behaviour. The behaviour of the electrode was described by a Warburg impedance for non-homogeneous surfaces.

The capacitance observed for each anion on the custom made electrode in impedance increased as follows for a constant potential of 0 to 0.8 V:

$SO_4^{2-} < NO_3^- < Cl^-$

and for potentials 0.8 to 1.6 V:

$SO_4^{2-} < Cl^- < NO_3^-$

The same order was observed in the voltammetry studies as in the latter impedance potential window. Conductivity studies have shown that the composite membrane will have an affinity for the anions in the following order:

$SO_4^{2-} < Cl^- < NO_3^-$

Therefore the membrane “holds” onto nitrate the strongest, and transports sulphate much faster. The diffusion layers observed in the studies indicate that chloride has a larger diffusion layer than sulphate. The smaller diffusion layer could be described by the transport of ions through the membrane. The high affinity (Km) of the membrane for nitrate and the smaller diffusion layer could be a possible ion-exchange occurring between the anion and a surface functional group in the membrane.

This selectivity of the custom made electrode, the used GCE and polished GCE differs from each other, and this is due to the major differences in their surface morphology and impurities on their surfaces.

The observed increase of the diffusion layer after 1.4V for nitrate and the decrease for chlorine seen the impedance studies, is confirmed by voltammetry studies.
Nitrate is a bigger anion and increases the size of the diffuse layer increasing the capacitance. The diffuse layer on the electrode increases with increasing potential in the nitrate solution, due to the oxidation of nitrite to larger nitrate ions. The larger nitrate increases the diffuse layer and therefore the capacitance on the electrode surface.
The amount of chloride in the area of the electrode is reduced due to the oxidation of chloride to chlorine gas which decreases the diffuse layer on the carbon electrode. The diffusion layer of sulphate ions remained relatively constant throughout the impedance studies because no sulphate reactions occurred on the electrode surface.

8.2 Recommendations for further study

I recommend that impedance studies be done at lower frequencies to investigate the possibility of diffusional layers other than the Helmholtz and Gouy-Chapman diffusion layer. The cell design could be idealised and the electrode/ electrolyte/ membrane setup brought closer together, to mimic the design used in the electrodialysis prototype plant in Tswane. Conductivity studies and EIS can then be repeated and a model can be constructed for the potential gradient.